PLASMA INTERACTION PROCESSES THAT LEAD TO VISCOUS FORCES IN THE SOLAR WIND

H. Pérez de Tejada;
Instituto de Geofísica, UNAM
México, D. F.

ISEST workshop

(26-30 October 2015)

CONTENTS

Shefer et al., 1979

(Mariner 5 Measurements)

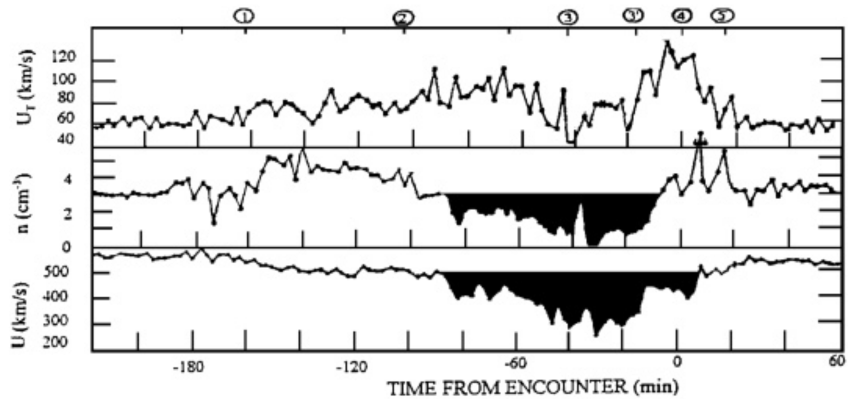

(Mariner 5 Measurements)

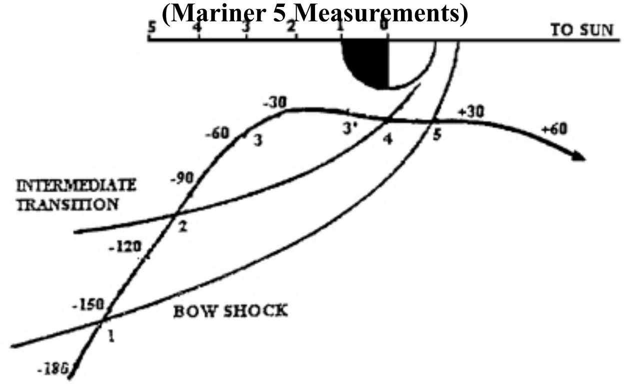

Knudsen et al., 1981

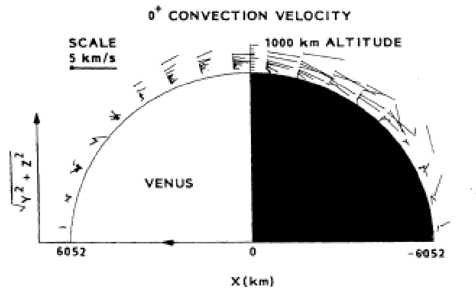

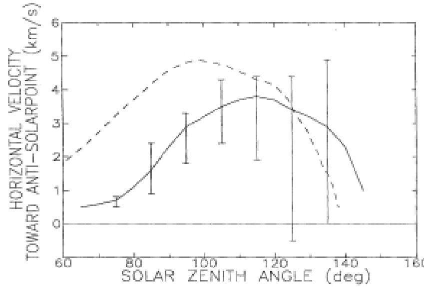

Pérez-de-Tejada, H., 1986

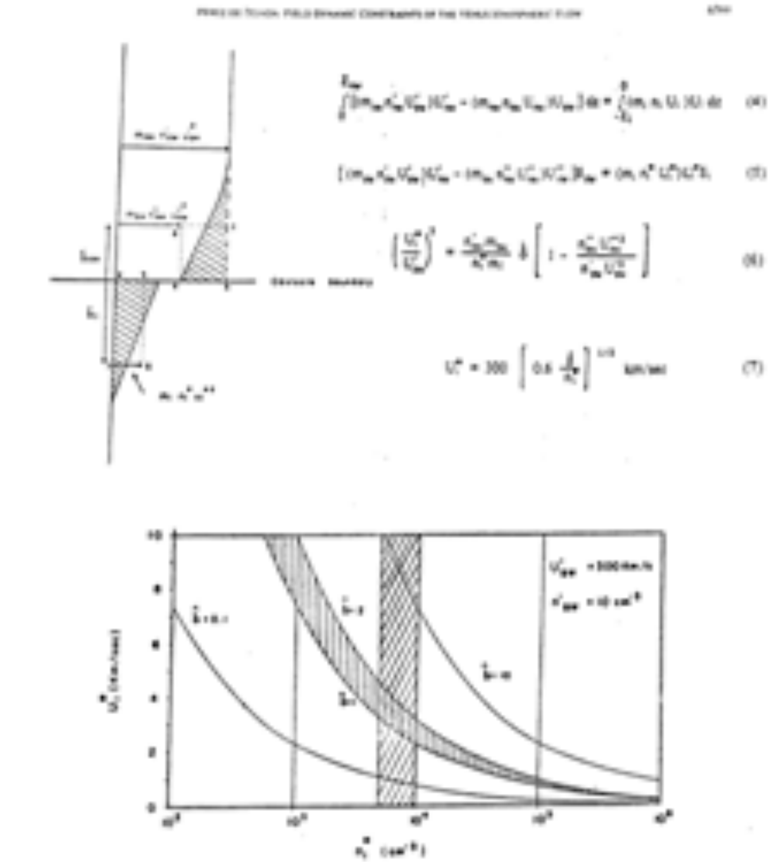

Fig. 2. Ionospheric flow velocities calculated from (7) as a function of the effective topside ionospheric density n_i^* at the terminator and for various values of the thickness parameter δ. The intersection of both shaded areas depicts the region where the calculated velocities best represent those suitable to the problem. U_{sw}' and n_{sw}' are, respectively, the velocity and density of the shocked, re-expanded, solar wind in the outer ionosheath outside the boundary layer at the terminator.

Entry and distribution of solar wind momentum in the upper ionosphere

Momentum transport processes in the solar wind and in the Venus upper ionosphere are different. For the high (~ 10^3 cm^{-3}) local plasma density measured in the upper ionosphere the momentum transport can occur through particle-particle (coulombian) collisions, On the other hand, momentum transport in the solar wind (ionosheath) may occur through magnetic turbulent conditions where hydromagnetic instabilities (Shapiro et al., 1995) lead to wave-particle interactions. Despite their different physical process it is possible to carry out a comparative calculation of the parameters that are involved. For each case we will assume in the plasma momentum equation that the inertial force is equal to the viscous force and neglect other forces.

For the trans-terminator flow in the Venus upper ionosphere the momentum equation is:

$$\rho_i v_i \partial v_i/\partial x = \mu_i \partial^2 v_i/\partial y^2$$

where ρ_i v_i and μ_i are the density, speed, and viscosity coefficient of the trans-terminator flow which moves in the x-direction.

In the ionosheath flow the inertial force of the solar wind is also assumed to be equal to the viscous force applied at the ionopause. The mom**en**tum equation is:

$$\rho_{sw} v_{sw} \partial v_{sw}/\partial x = \mu_{sw} \partial^2 v_{sw}/\partial y^2$$

where ρ_{sw}, v_{sw}, and μ_{sw} are the density, speed, and viscosity coefficient of the solar wind that streams in the x-direction. From this latter equation we will consider that the inertial force in the solar wind can be replaced by the viscous force so that the solar wind momentum is used to produce the trans-terminator flow.

Values of the viscosity and kinematic viscosity coefficients (Pérez-de-Tejada, 2009)

Using scale values (upper case) and assuming constant density values both momentum equations become

$$\rho_i V_i^{2}/L_i = \mu_i V_i/\delta_i^2$$
$$\rho_{sw} V^2_{sw}/L_{sw} = \mu_{sw} V_{sw}/\delta^2_{\mathbf{sw}}$$

where L_i, L_{sw}, and δ_i, $\delta_{\mathbf{sw}}$ are the length and the width of the region where the viscous forces apply in both plasmas. From these equations the ratio of the viscosity coefficients is:

$$\mu_i/\mu_{sw} = (\rho_i/\rho_{sw})(V_i/V_{sw})(L_i/L_{sw})(\delta_i/\delta_{\mathbf{sw}})^2$$

which can be estimated by taking typical values, that is:

$\rho_i/\rho_{sw} \sim 16\ 10^2$ ($n_{sw} \sim 10\ cm^{-3}$ and $n_i \sim 10^3\ cm^{-3}$ for the O+ ions at high altitudes
$V_i/V_{sw} \sim 10^{-2}$ ($V_{sw} \sim 300$ km/s and $V_i \sim 3$ km/s)
$(\delta_i/\delta_{sw})^2 \sim 10^{-1}$ ($L_{sw} \sim 1800$ km, $\delta_i \sim 600$ km)

Since $L_{sw}/L_i \sim 1$ we obtain: $\boldsymbol{\mu_i/\mu_{sw} = 1.6}$ implying that the viscosity coefficient, **which is an indicator of the ability of the flow to modify a velocity shear** (Batchelor et al. 1979), may not be very different in the solar wind and in the upper ionosphere. This result implies that the solar wind momentum that is applied to the Venus ionosphere and its distribution through the trans-terminator flow proceed at a comparable rate.

Different constraints are applicable to the kinematic viscosity coefficient **$\nu = \mu/\rho$ which gives a measure of the particles of the flow for transport momentum** (Batchelor et al. 1979). In this case the large mass density values of the O+ ions lead to $\boldsymbol{\nu_i}$ values that are up to three orders of magnitude larger than those in the solar wind. Under such conditions the relative value of the Reynolds number $R = VL/\nu$ in both regions using $\nu_i/\nu_{sw} \sim 10^{-3}$ and $V_i/V_{sw} \sim 10^{-2}$ is $R_i/R_{sw} \sim 10$ for equal L values.

Mean free path values in the ionosheath flow and in the Venus ionosphere

An analysis is required to examine the way in which wave-particle interactions in the ionosheath provide a mechanism whose effect is communicated and later handled by particle-particle (coulombian) collisions in the Venus upper ionosphere. This analysis can be conducted by examining the mean free path λ corresponding to both situations.

For particle-particle collisions the mean free path λ_i is given by:

$\lambda_i = 16\pi\varepsilon_o(KT)^2/(Z^2 n_i e^4)$ (Beizer, 1980)

where $n_i \sim 10^3$ cm^{-3} is the O+ ion density, T = 2 10^3 °K, and Z = 8 with K being the Boltzmann constant. With such numbers we obtain $\lambda_i \sim 50$ km for the O+ ions in the upper ionosphere.

For wave-particle interactions in the ionosheath flow we can use:

$\nu = u_i\, \lambda/2$

which relates λ and the thermal speed u_i of a gas to its kinematic viscosity coefficient ν (Liepmann and Roshko, 1957). By using $u_i \sim 100$ km/s and $\nu \sim 6\ 10^3$ km^2/s from the Mariner 5 measurements we obtain: $\lambda_{sw} \sim 100$ km, which is comparable to the λ_i value.

If wave-particle interactions are responsible for the manner in which the solar wind momentum is delivered to the upper ionosphere where particle-particle collisions are applicable it is significant that the effective mean free path in both regions are comparable.

A possible implication of this view is that the population mixing that occurs across the region of interaction between the solar wind and the ionospheric plasma takes place under conditions in which there is also a gradual change in the physical processes that produce the transport of momentum.

CONCLUSSIONS

1 - Viscous transport of solar wind momentum to the Venus upper ionosphere is adequate to account the momentum flux of the night-ward directed ionospheric flow.

2 – Comparable values of the viscosity coefficient of the solar wind with that in the Venus upper ionosphere can be derived by assuming particle-particle (coulombian) collisions and wave-particle (magnetic turbulent) interactions. This result may imply that viscosity could be an inherent property of the solar wind derived from either process.

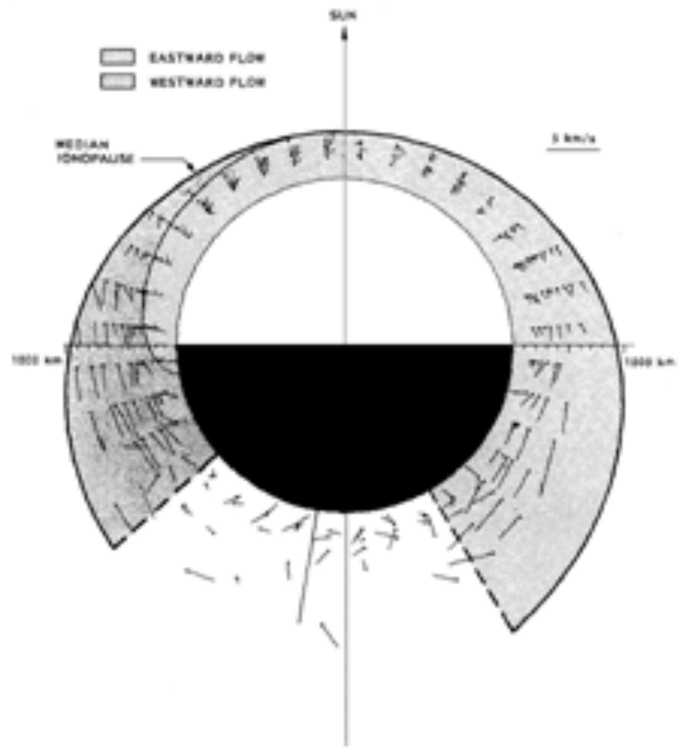
SUN
EASTWARD FLOW
WESTWARD FLOW
MEDIAN
IONOPAUSE
5 km/s
1000 km
1000 km

Interacción del viento solar con la ionosfera de Venus

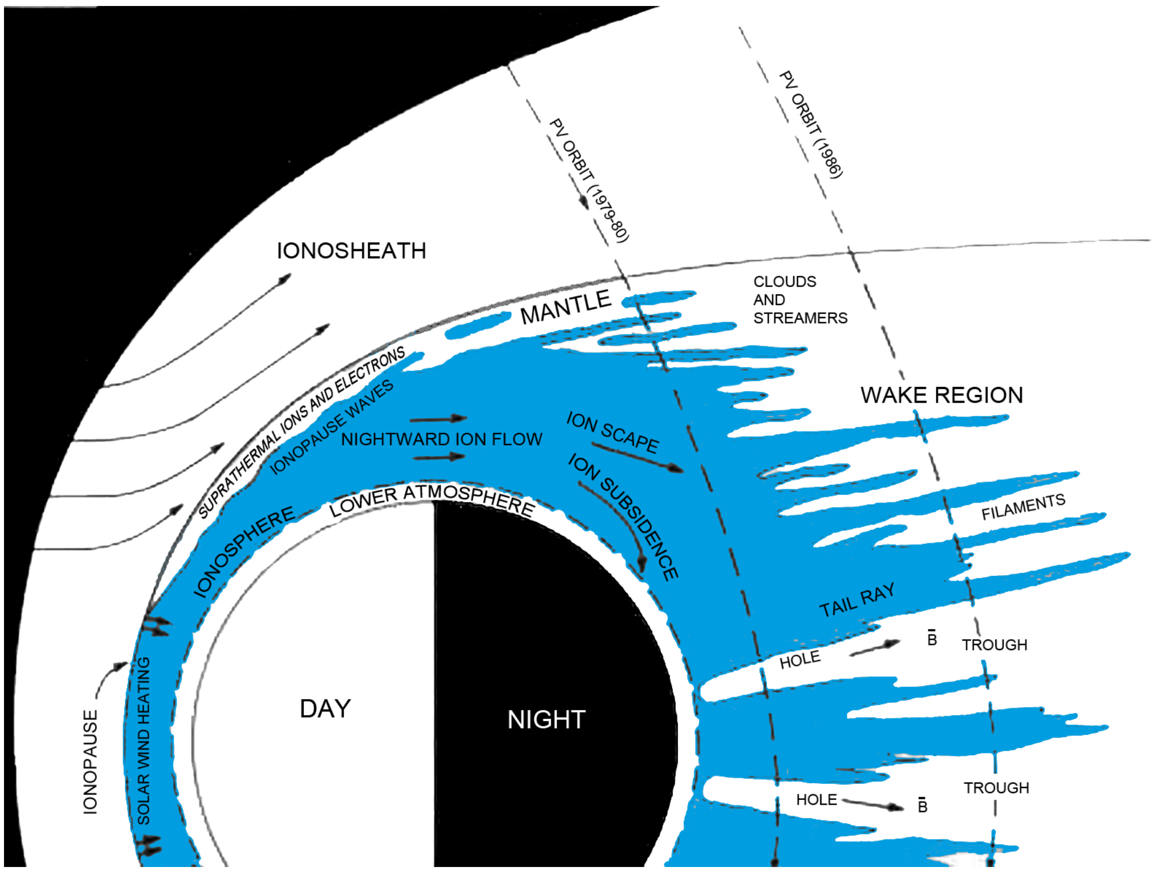

Flujo ionosférico de Venus

ION DYNAMICS IN THE VENUS IONOSPHERE

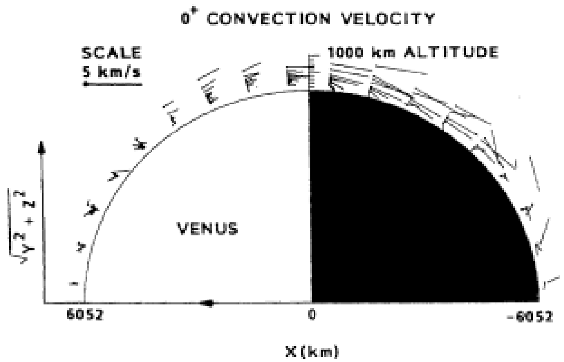

K. L. MILLER AND R. C. WHITTEN

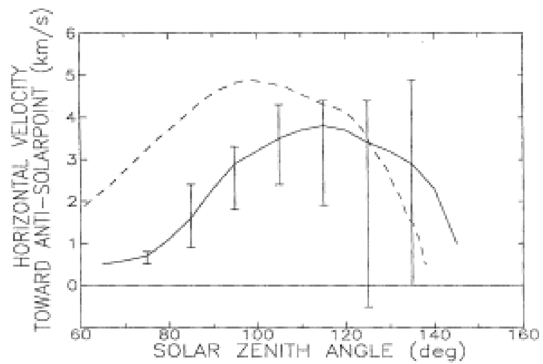

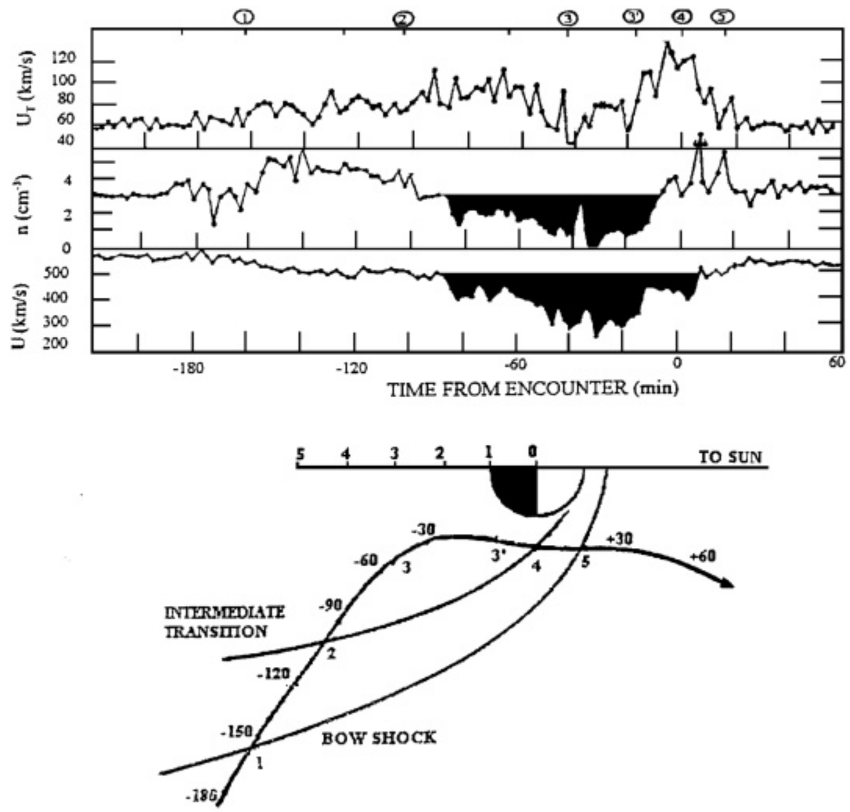

Figure 7 – Thermal speed, density, and bulk speed of the solar wind measured with the Mariner 5 spacecraft (its trajectory projected in cylindrical coordinates is shown in the lower panel). The labels 1 through 5 along the trajectory and at the top of the upper panel mark important events in the plasma properties (bow shock, intermediate plasma transition) (after Bridge et al..1967).

Transferencia de momento cinético

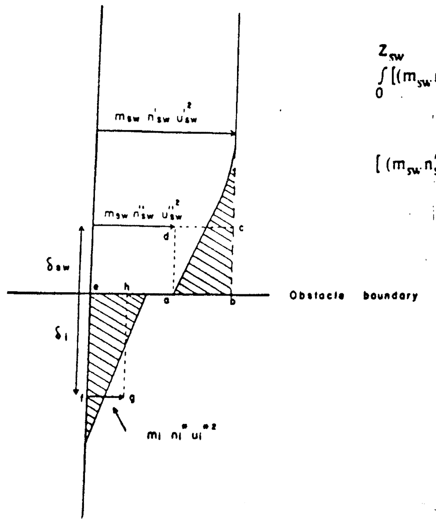

$$\int_0^{Z_{sw}} [(m_{sw} n'_{sw} U'_{sw}) U'_{sw} - (m_{sw} n_{sw} U_{sw}) U_{sw}]\, dz = \int_{-Z_i}^{0} (m_i\, n_i\, U_i) U_i\, dz \tag{4}$$

$$[(m_{sw} n'_{sw} U'_{sw}) U'_{sw} - (m_{sw} n''_{sw} U''_{sw}) U''_{sw}]\delta_{sw} = (m_i\, n_i^*\, U_i^*) U_i^* \delta_i \tag{5}$$

$$\left(\frac{U_i^*}{U'_{sw}}\right)^2 = \frac{n'_{sw} m_{sw}}{n_i^* m_i}\, \hat{\delta} \left[1 - \frac{n''_{sw} U''^2_{sw}}{n'_{sw} U'^2_{sw}} \right] \tag{6}$$

$$U_i^* = 300 \left[0.6 \frac{\hat{\delta}}{n_i^*} \right]^{1/2} \text{km/sec} \tag{7}$$

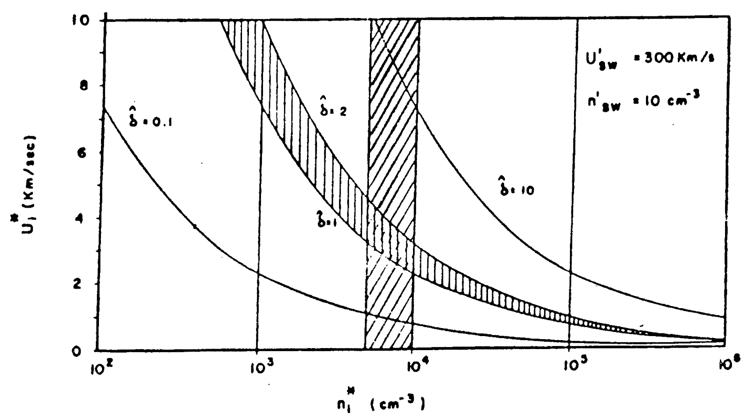

Fig. 2. Ionospheric flow velocities calculated from (7) as a function of the effective topside ionospheric density n_i^* at the terminator and for various values of the thickness parameter $\hat{\delta}$. The intersection of both shaded areas depicts the region where the calculated velocities best represent those suitable to the problem. U'_{sw} and n'_{sw} are, respectively, the velocity and density of the shocked, re-expanded, solar wind in the outer ionosheath outside the boundary layer at the terminator.

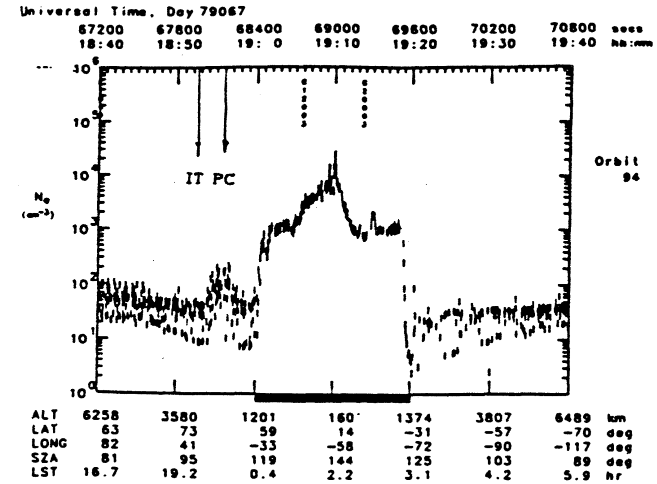

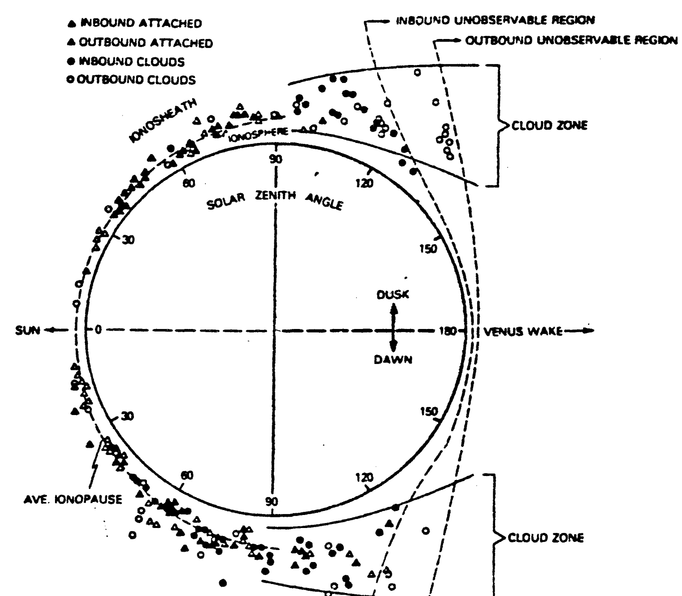

FIG. 4. THE SZA DISTRIBUTION OF WAVELIKE ATTACHED PLASMAS AND CLOUDS OBSERVED DURING THE FIRST 600 ORBITS.

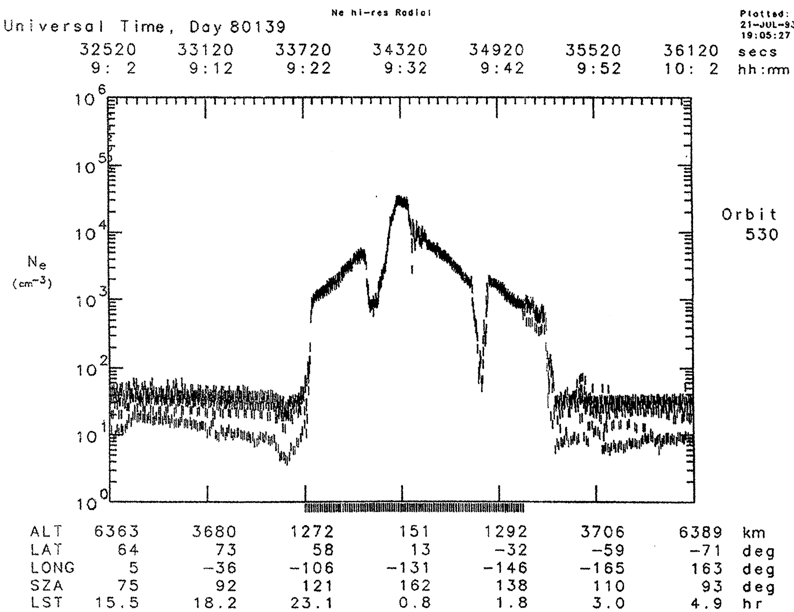

Brace et al.: Holes in the Nightside Ionosphere of Venus

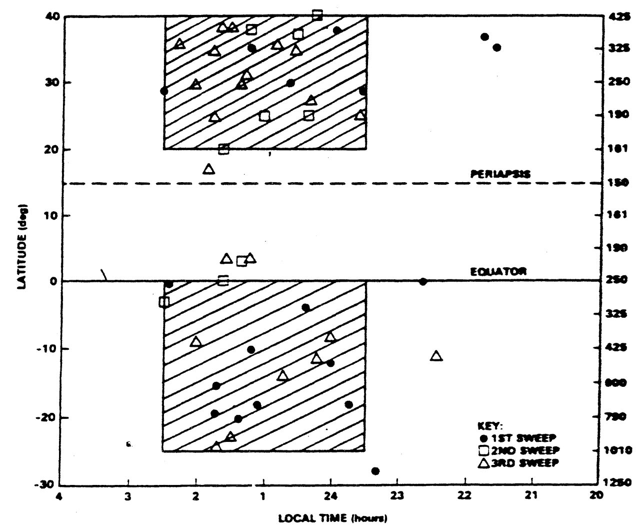

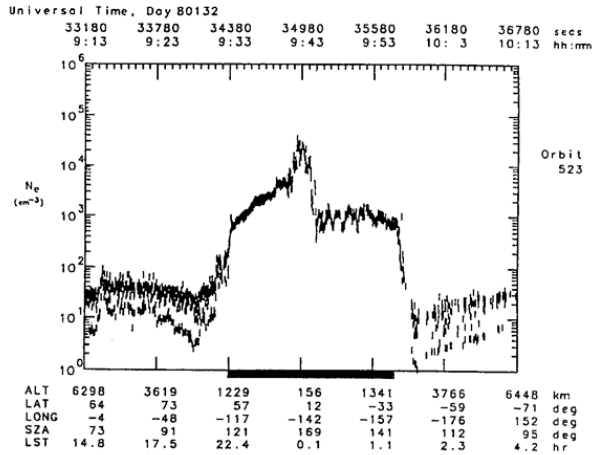

Universal Time, Day 80132
33180 33780 34380 34980 35580 36180 36780 secs
9:13 9:23 9:33 9:43 9:53 10: 3 10:13 hh:mm
Ne (cm-3)
Orbit 523
ALT 6298 3619 1229 156 1341 3766 6448 km
LAT 64 73 57 12 -33 -59 -71 deg
LONG -4 -48 -117 -142 -157 -176 152 deg
SZA 73 91 121 169 141 112 95 deg
LST 14.8 17.5 22.4 0.1 1.1 2.3 4.2 hr

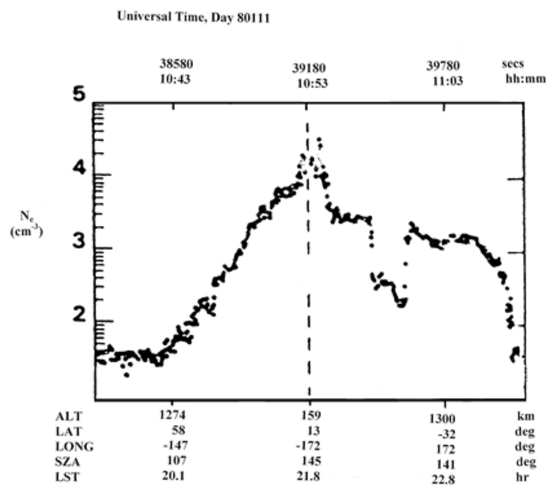

Universal Time, Day 80111
38580 10:43
39180 10:53
39780 11:03
secs hh:mm
Ne (cm-3)
ORBIT 502
ALT 1274 159 1300 km
LAT 58 13 -32 deg
LONG -147 -172 172 deg
SZA 107 145 141 deg
LST 20.1 21.8 22.8 hr

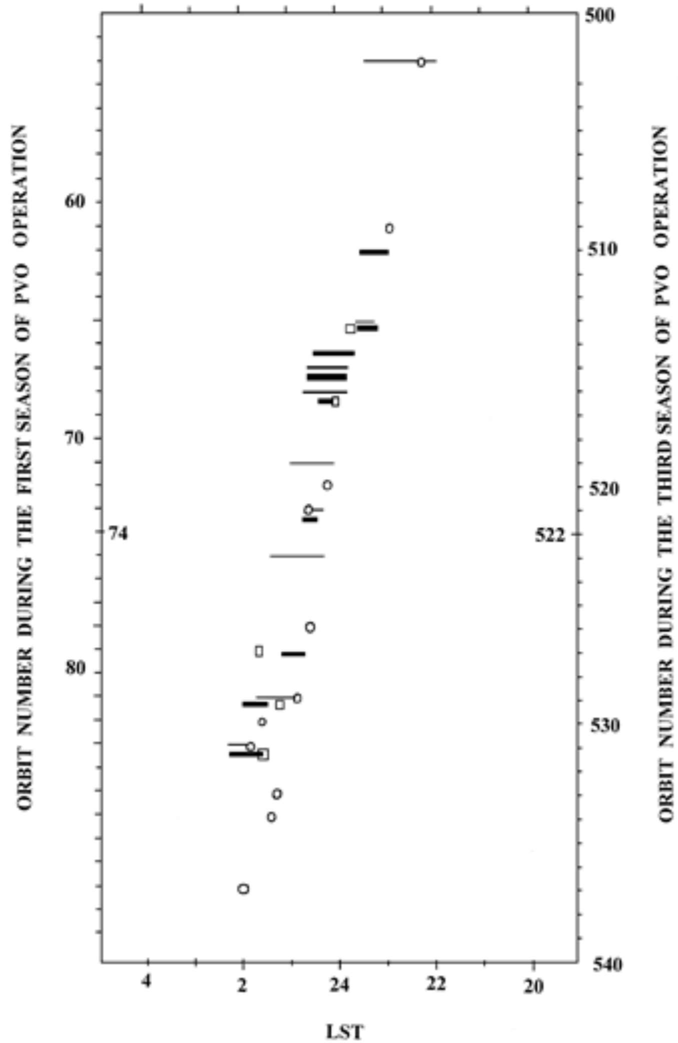

ORBIT NUMBER DURING THE FIRST SEASON OF PVO OPERATION
ORBIT NUMBER DURING THE THIRD SEASON OF PVO OPERATION
60
70
74
80
500
510
520
522
530
540
4
2
24
22
20
LST

PLASMA CHANNELS

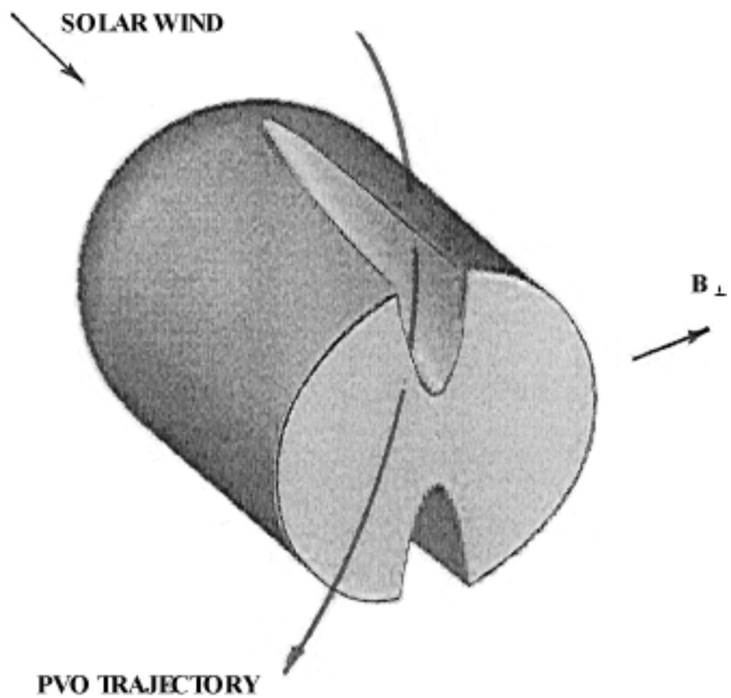

Schematic of the Venus nightside ionosphere with plasma channels that extend downstream from the magnetic polar regions. The trajectory of the PVO is traced for a situation in which the spacecraft traverses a plasma Channel across the nightside ionosphere (Pérez-de-Tejada, 2001).

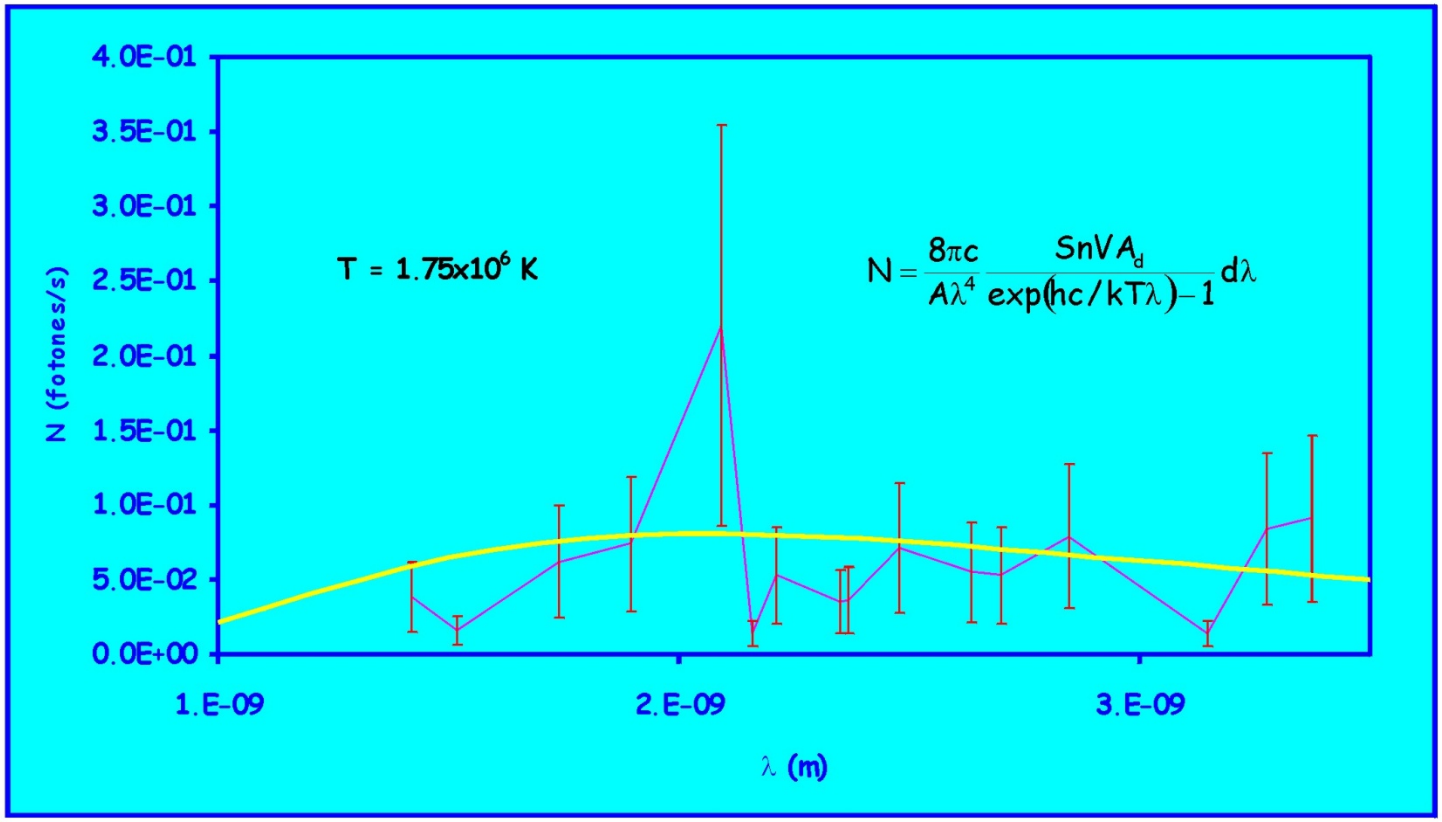

Line spectrum of the Mars halo measured with the reflecting gratingspectrometer (RGS) of the XMM Newton satellite at X-ray wav elengths [Dennerl et al., 2006]. The continuous curve represents the black body emission expected at the T ~ 1.75 106 °K that is inferred by fitting to the intensity of the dominant emission lines of the spectrum.

Miller and Whitten, 1991

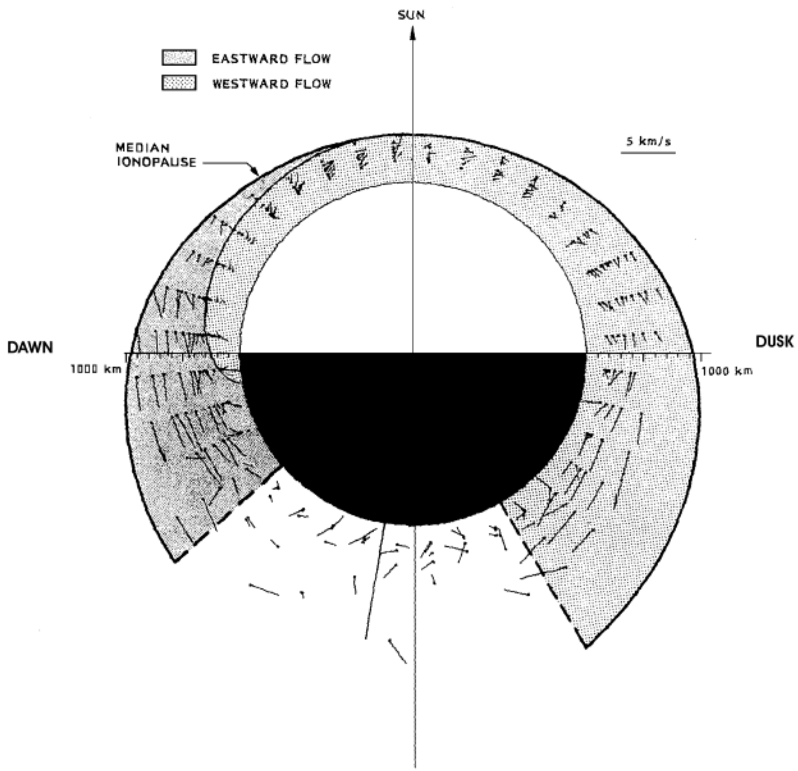

Pérez-de-Tejada, 2006

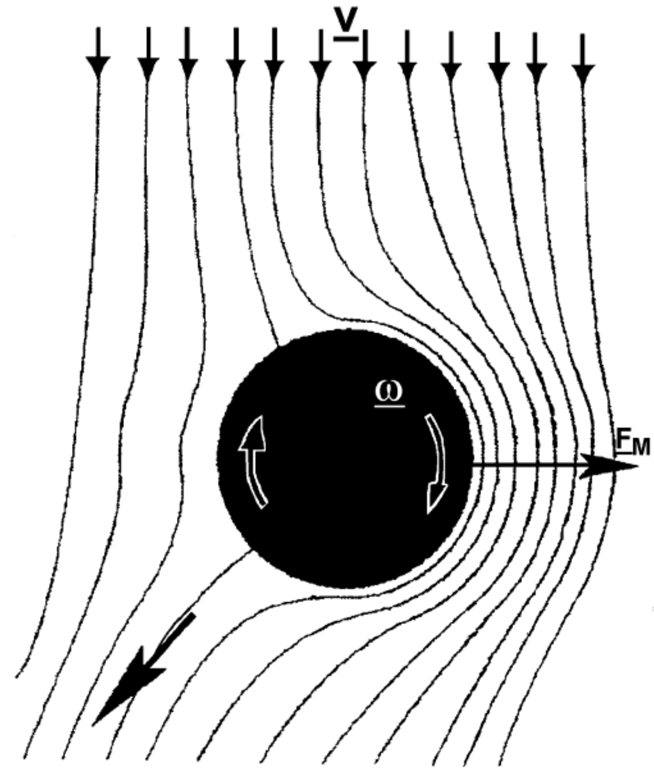

Magnus Force Eq: $F_M = C_M (r_2{}^3 - r_1{}^3)\, \rho\, V_i\, \omega$ **Bernoulli´s Eq:** $P + \rho V^2/2 = cst$

Dawn-Dusk Displacement: $D = A\, \zeta^2/2 = (F_M/M)[\pi\, r^2/2\, /V_i]^2/2$

VENUS EXPRESS (LUNDIN ET AL., 2011)

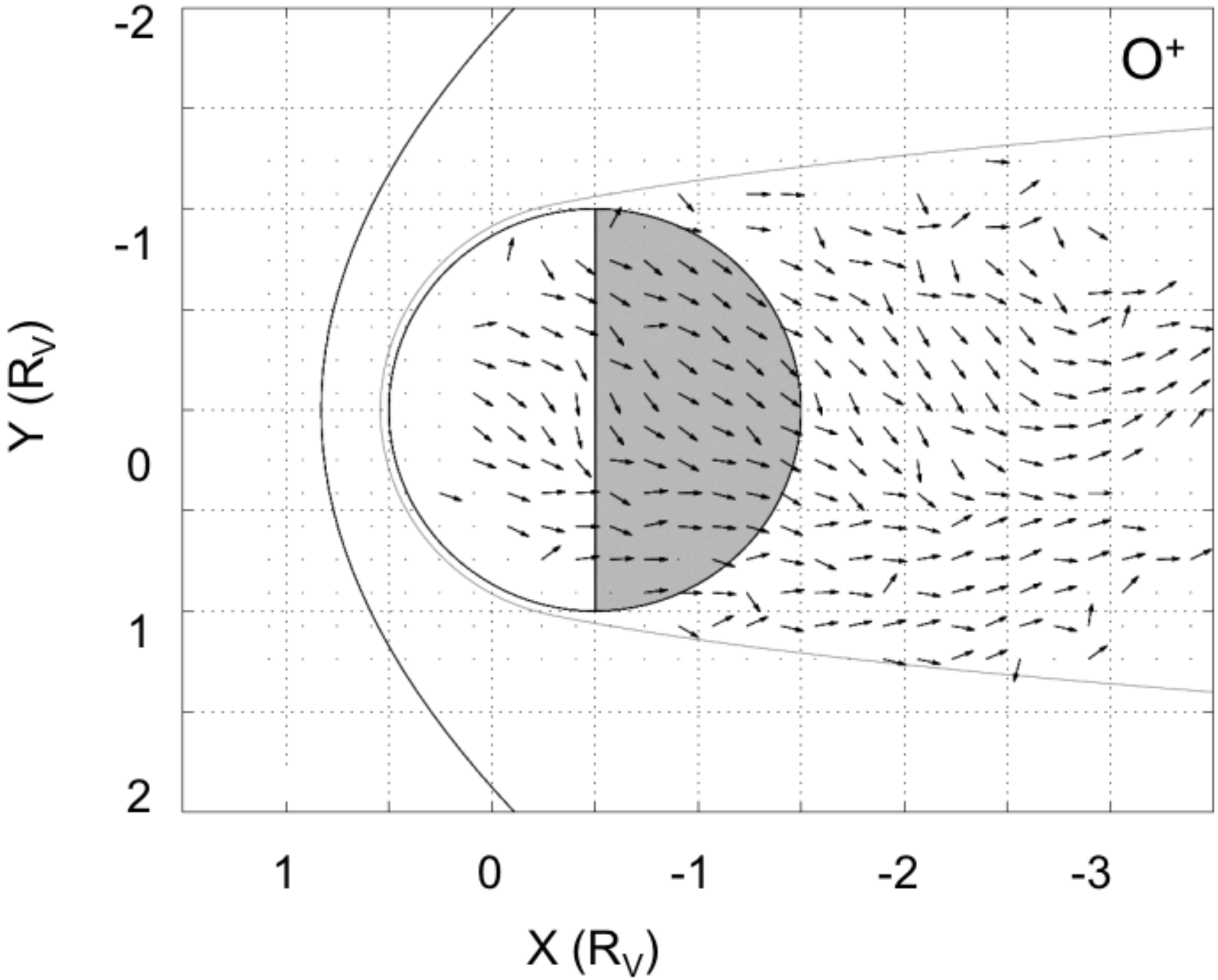

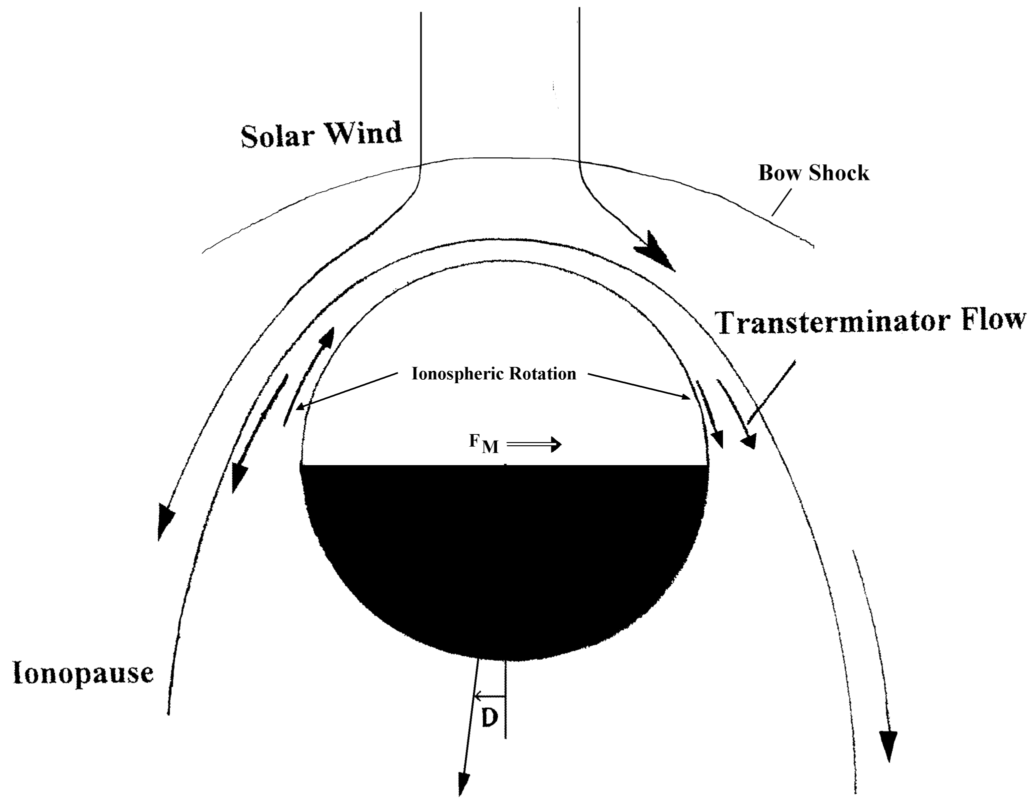
Solar Wind
Bow Shock
Transterminator Flow
Ionospheric Rotation
F_M
Ionopause
D

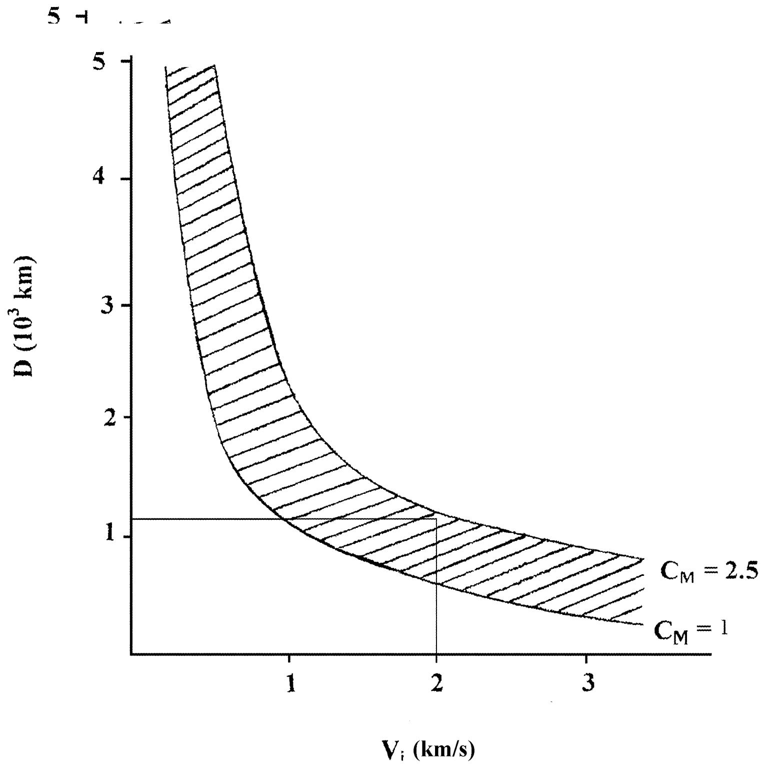

East-West Displacement: $D = A\zeta^2/2 = (F_M/M)\,(N_i\,\pi r^2/2)^2/2$

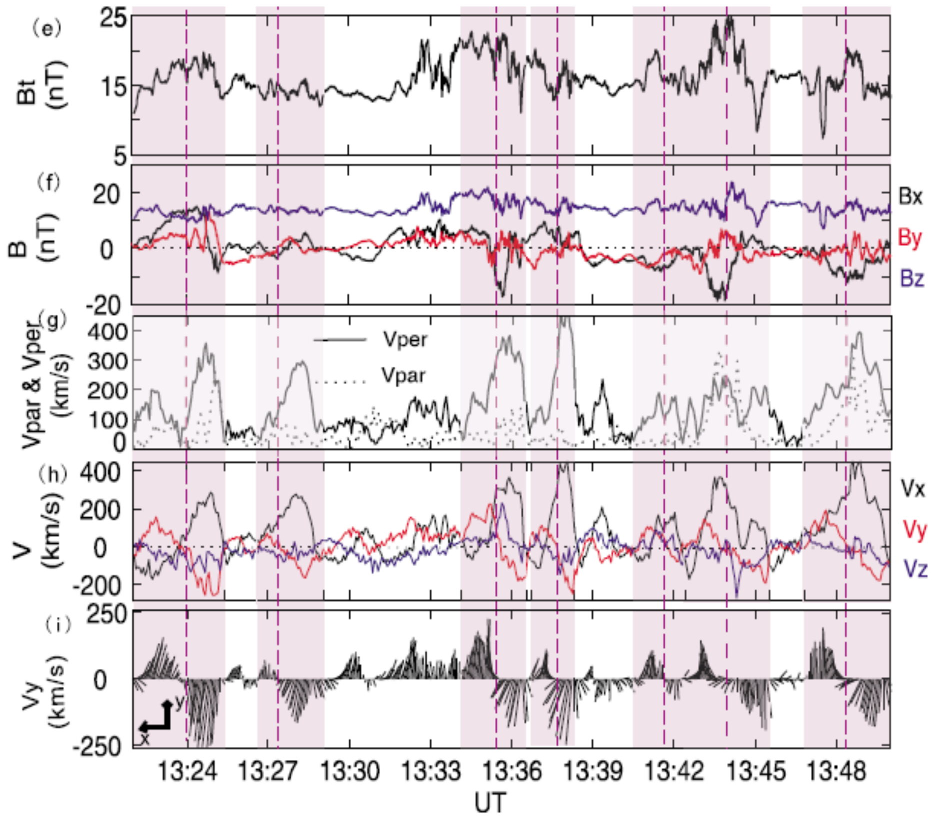

A series of flow vortices in the earth´s magnetosphere observed by a Cluster spacecraft on July 6, 2003. The magnetic field and its components are indicated in the top two panels and the ion velocity and its components in the two lower panels (the velocity components in a reference frame in which the z and the x axes are parallel and perpendicular to the average magnetic field are in the middle panel). The profiles were selected from those presented in Figure 7 of Tian et al., (2010).

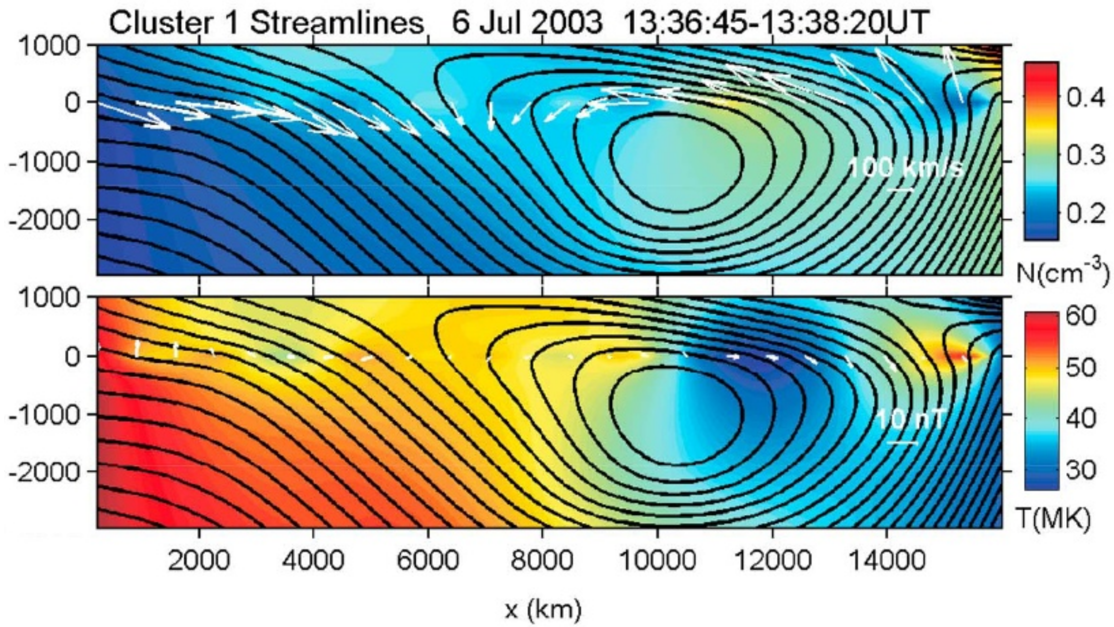

Map of flow streamlines projected on the xy plane derived from the velocity rotation measured in the 13:36:45 UT – 13:38:20 UT time interval of July 6, 2003 . The streamlines are traced on the ion density (top panel) and on the ion temperature (lower panel) distributions (the white arrows in the top panel represent the measured velocity vector direction, and those in the lower panel the direction of the magnetic field). The streamlines describe conditions from the inner plasma sheet ac ross the dawn side of the magnetosphere and were selected from those presented in Figure 11 of Tian et al., (2010).

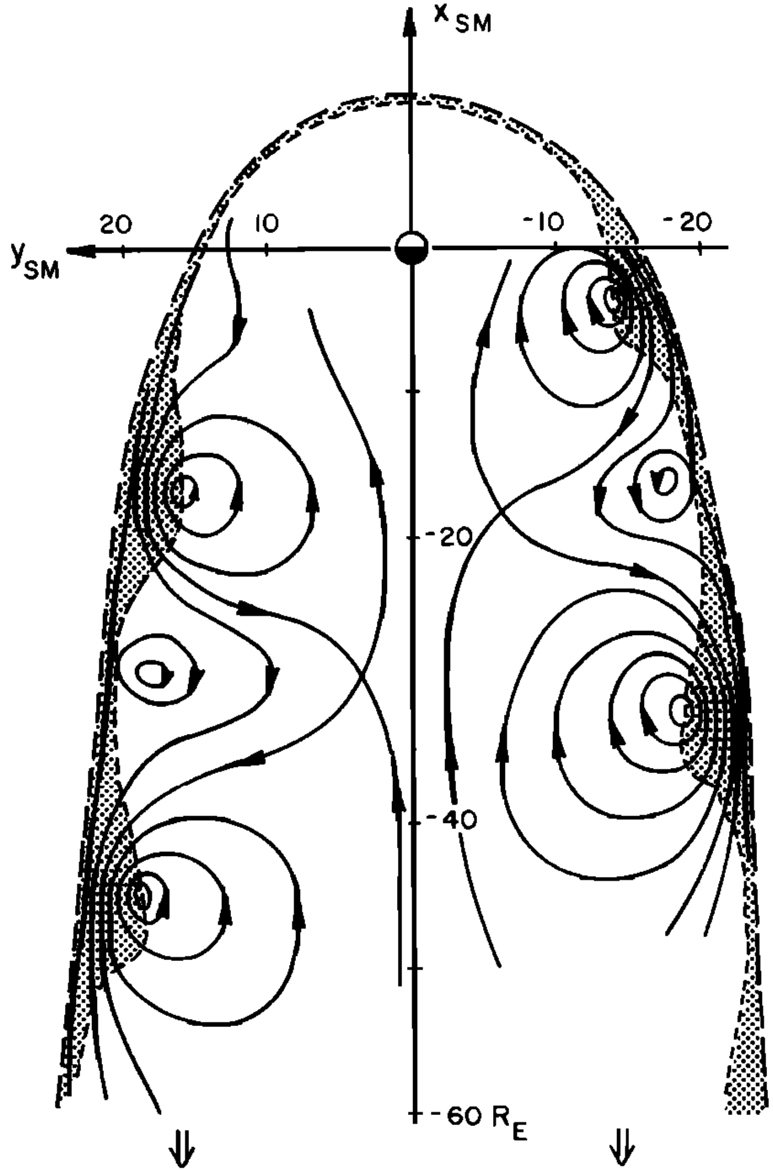

Schematic description of plasma vortices within the earth´s magnetosphere inferred from the ISEE measurements. The flow pattern represented by the solid lines is itailward through the magnetosphere as it is indicated by he white arrows at the bottom (Hones et al., 1981).

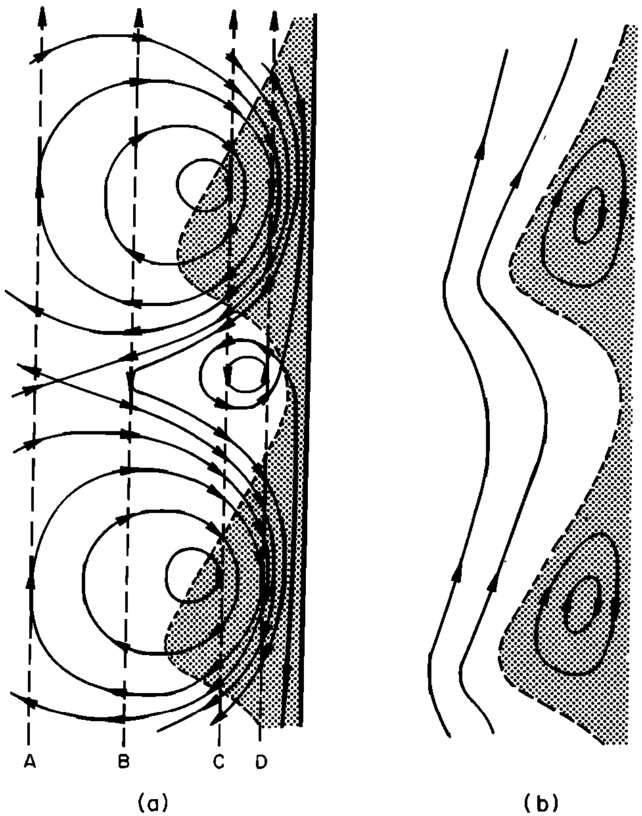

(left panel) Dawn sector of the flow pattern depicting the sequence of flow vectors observed at four different distances from the magnetopause. (right panel) Flow in the rest frame of the tailward moving wave (Hones et al., 1981).

PIONEER VENUS (Pérez-de-Tejada et al., 1982)

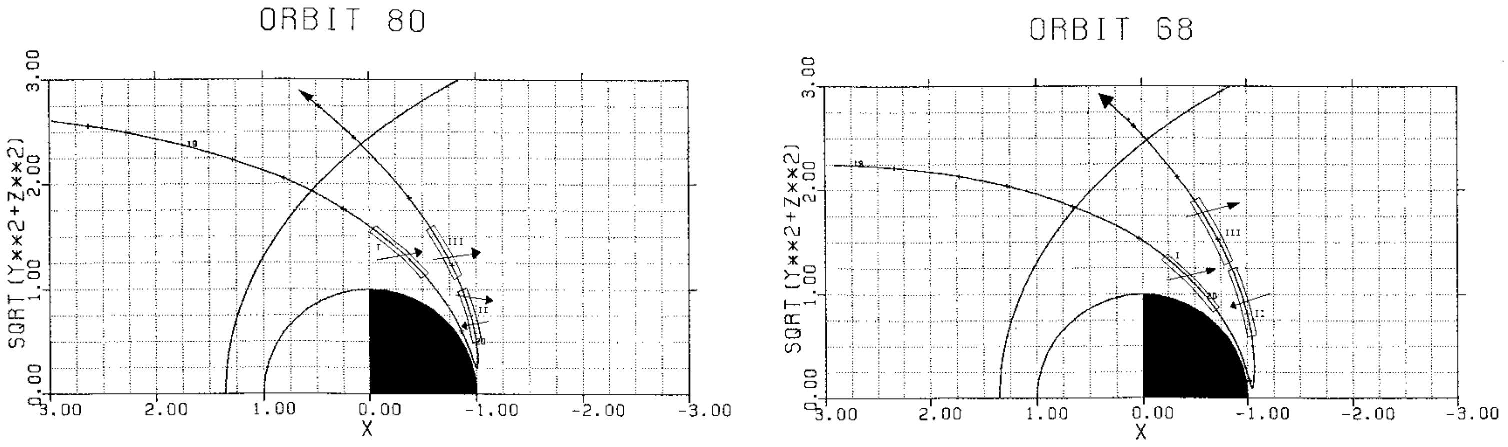

(Representative position of energy cycles (rectangular shapes) where measurements were made along the trajectory of the PVO in orbit 80 (left panel) and in orbit 68 (right panel) projected on a quadrant in cylindrical coordinates. The arrows show schematically the (latitudinal) velocity direction of ion fluxes detected at different energy steps within each cycle.

VENUS EXPRESS (LUNDIN ET AL., 2011)

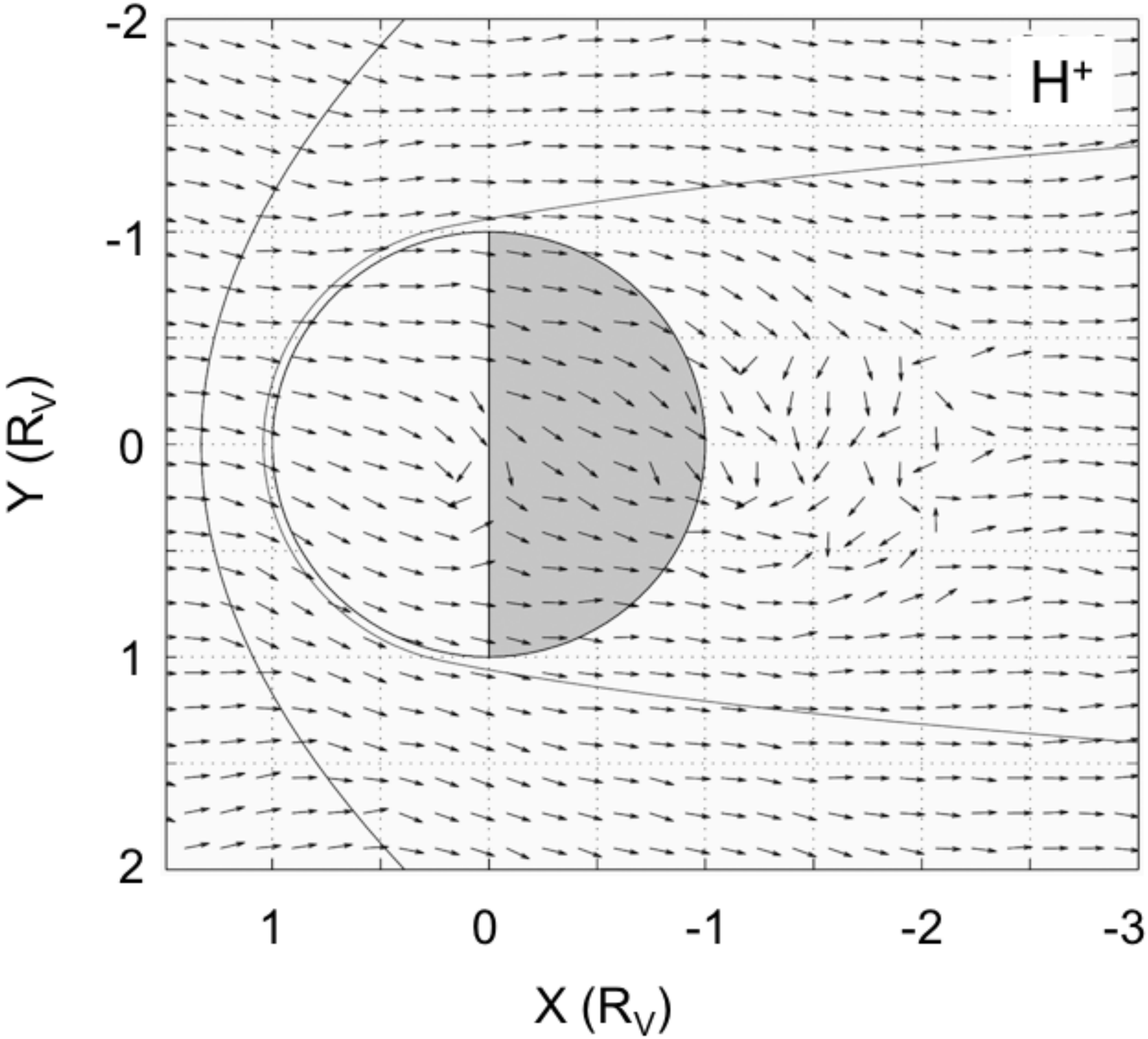

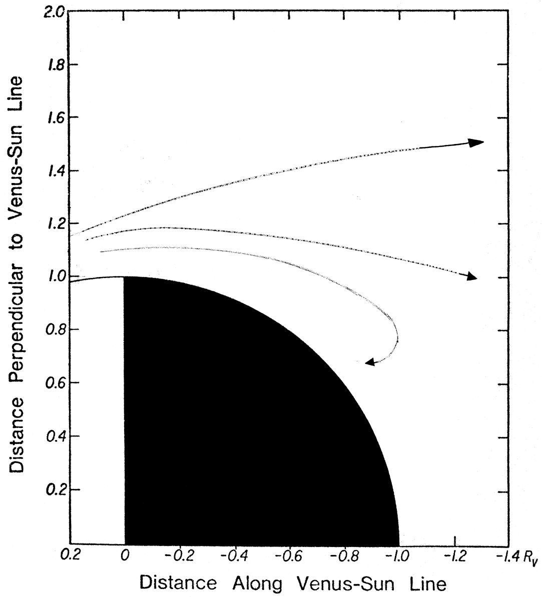

2.0
1.8
1.6
1.4
1.2
1.0
0.8
0.6
0.4
0.2
Distance Perpendicular to Venus-Sun Line
0.2
0
-0.2
-0.4
-0.6
-0.8
-1.0
-1.2
-1.4 R_V
Distance Along Venus-Sun Line

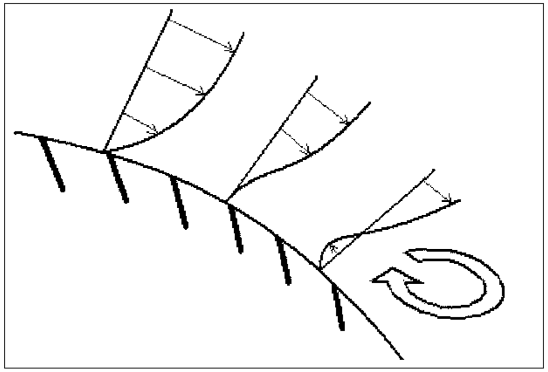

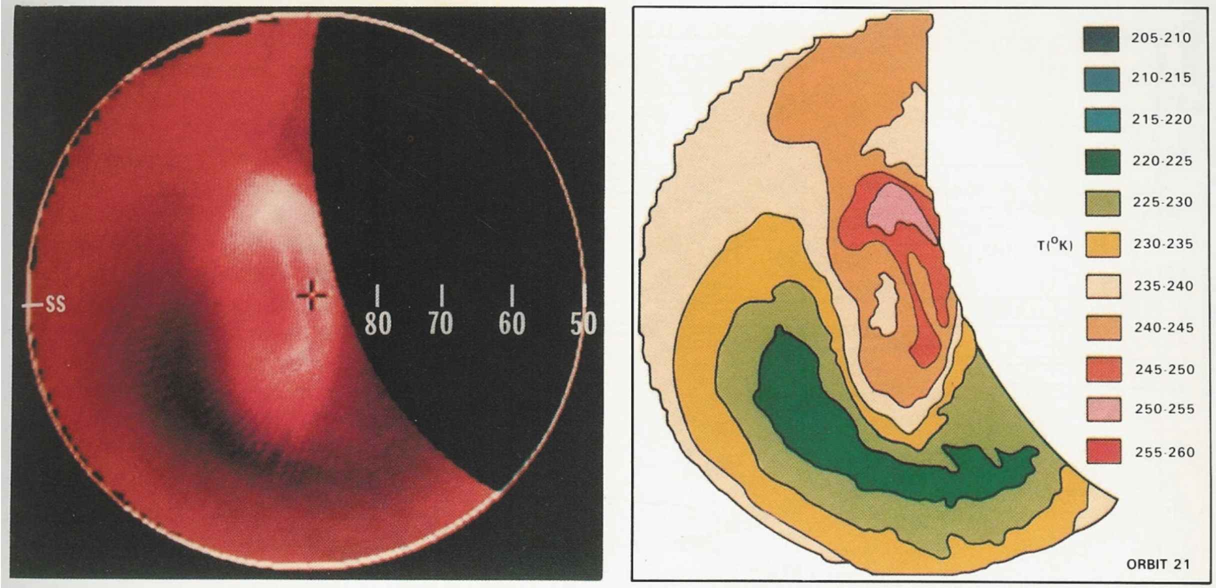

Figure 6-19(a). North polar infrared image and plot showing the temperatures. The north pole is in the center, the outer boundary is 50° north latitude, the noon point at SS at the left. The blacked out area is the region from which no data were obtained because of the geometry of the spacecraft's orbit. This image was obtained on December 26, 1978 during orbit 21.

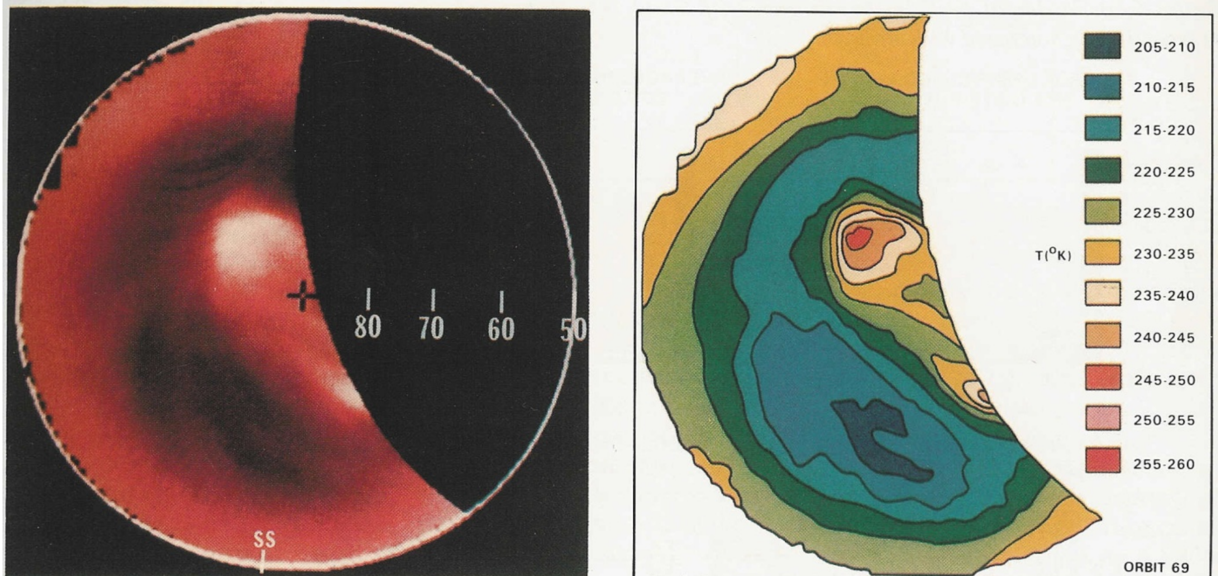

Figure 6-19(b). A similar image to (a) obtained February 11, 1979 on orbit 69.

Figure 6-18. Eight consecutive polar stereographs of Venus' northern hemisphere taken at 11.5 µm. These images were taken one each day on orbits 32 through 39 (January 5 through 12, 1979). The north pole is at the center of each image and the equator is the outer boundary with the noon point at the bottom. Note that the polar dipole returns to approximately the same position in a period of three days.

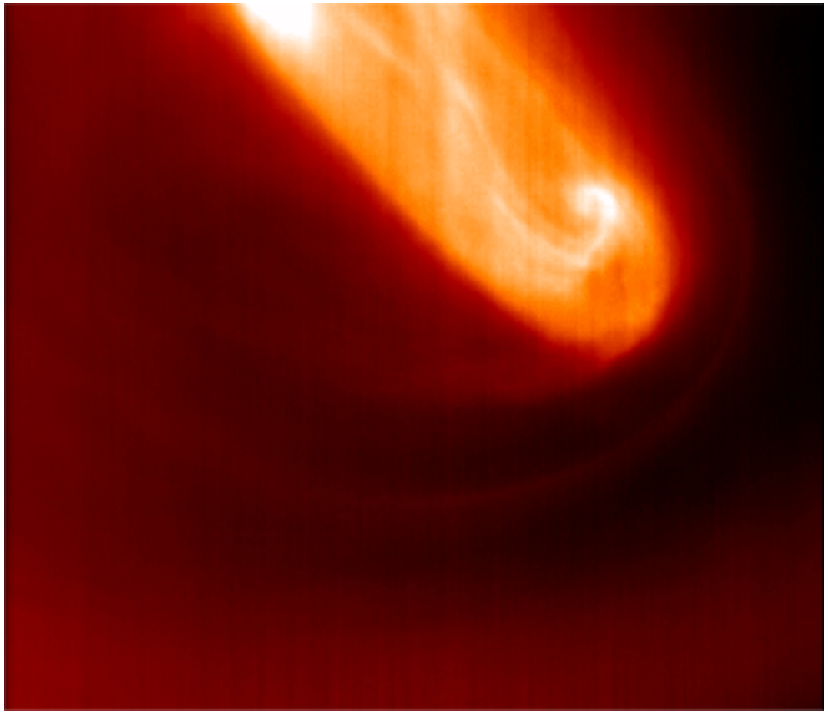

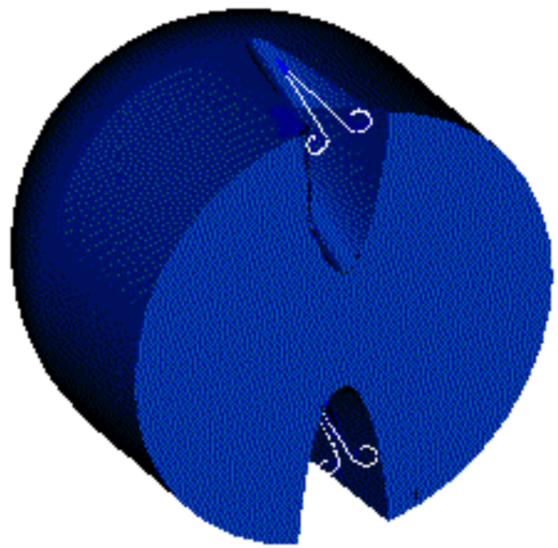

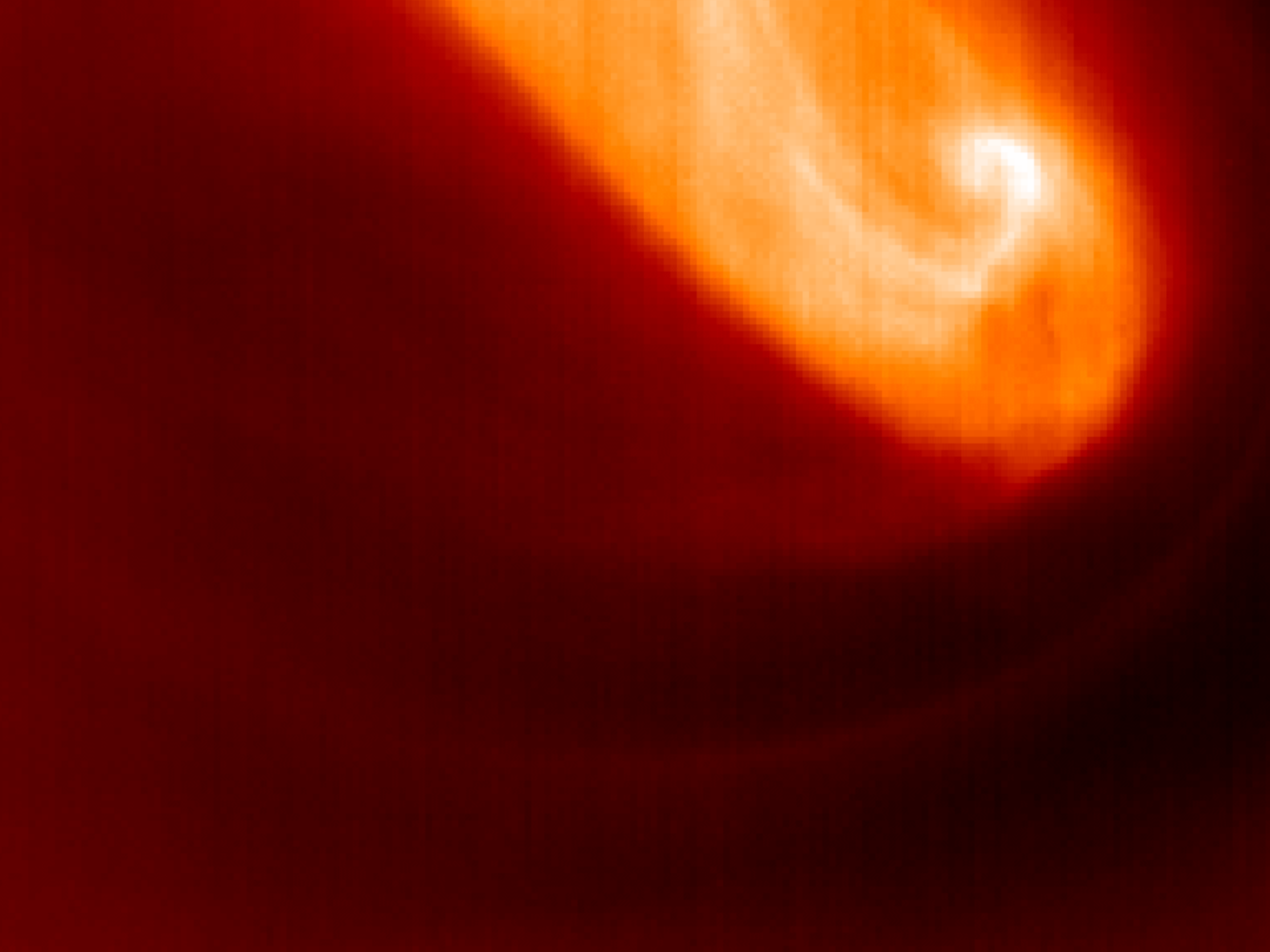

13-May-2007 17:36:16

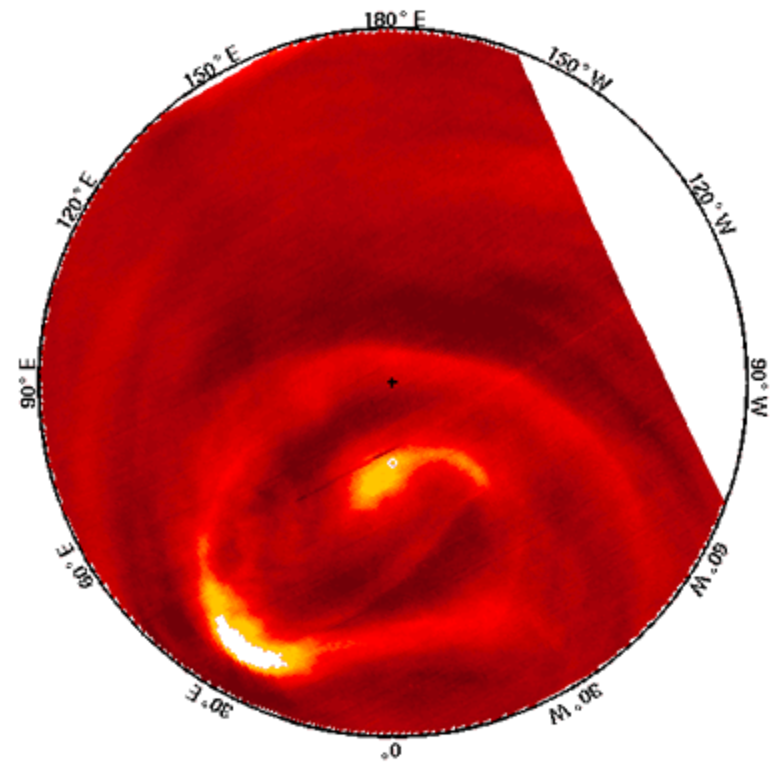

DESPLAZAMIENTO DE LAS NUBES DE PLASMA

(Fuerzas de presión magnética y presión cinética)

Ec. de momento: $\rho_{sw}(U_{sw} \cdot \nabla)\ U_{sw} = (B_{sw} \cdot \nabla)\ B_{sw}/\mu_e - \nabla(B_{sw}^2/2\mu_e) + \rho_{sw}\ \nu\ \nabla^2\ U_{sw}$

Ec. de momento en forma no-dimensional: $\rho_{sw}\ U_{sw}^2 \sim \rho_{sw}\ U_{sw}^2\ [(V_A/U_{sw})^2/2 + (L/\delta)^2/R]$

$U_{sw}/V_A = M_A$ es el número de Mach de Alfven [$V_A = B_{sw}/(\mu_e\ \rho_{sw})^{1/2}$ es la velocidad de Alfven]
(M_A es el cociente de la densidad de energía cinética a la densidad de energía magnética)

$R = U_{sw}L/\nu$ es el número de Reynolds (L es la distancia efectiva de la región de flujo viscoso)
δ es el ancho de la capa límite de velocidad

Usando: 300 km/s $< U_{sw} <$ 500 km/s $n_{sw} \sim 2\ cm^{-3}$ $B_{sw} \cong 10$ nT

Se encuentra: $1 < M_A < 3$ (densidad de energía magnética < densidad de energía cinética)

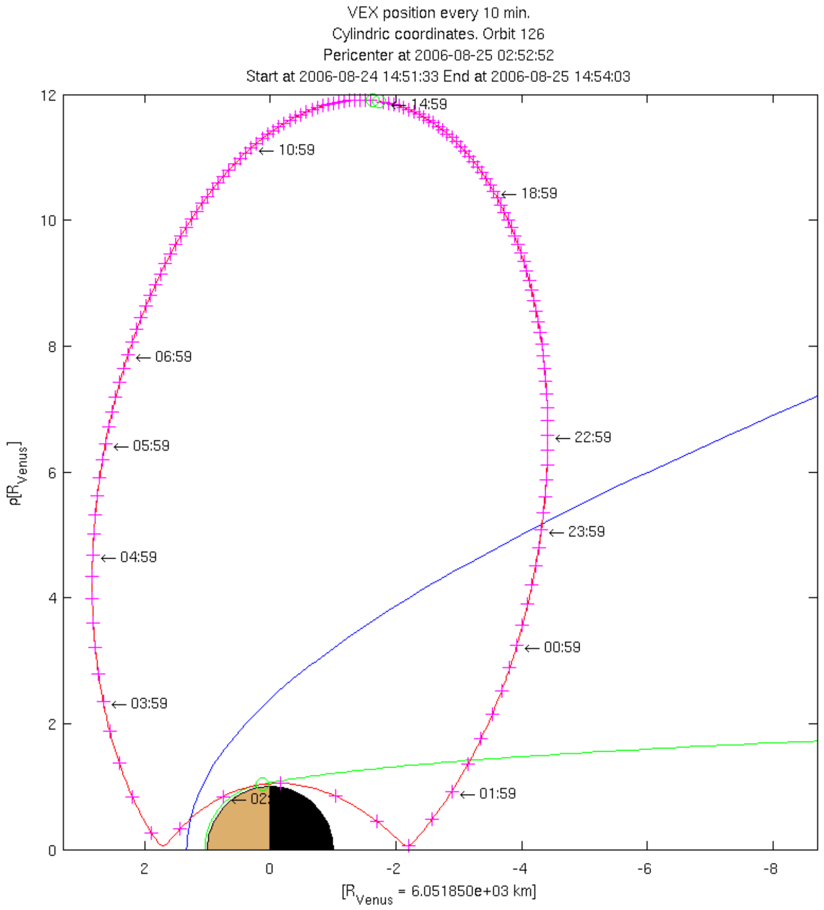
VEX position every 10 min.
Cylindric coordinates. Orbit 126
Pericenter at 2006-08-25 02:52:52
Start at 2006-08-24 14:51:33 End at 2006-08-25 14:54:03
ρ[R_Venus]
[R_Venus = 6.051850e+03 km]
14:59
10:59
18:59
06:59
05:59
22:59
04:59
23:59
00:59
03:59
01:59

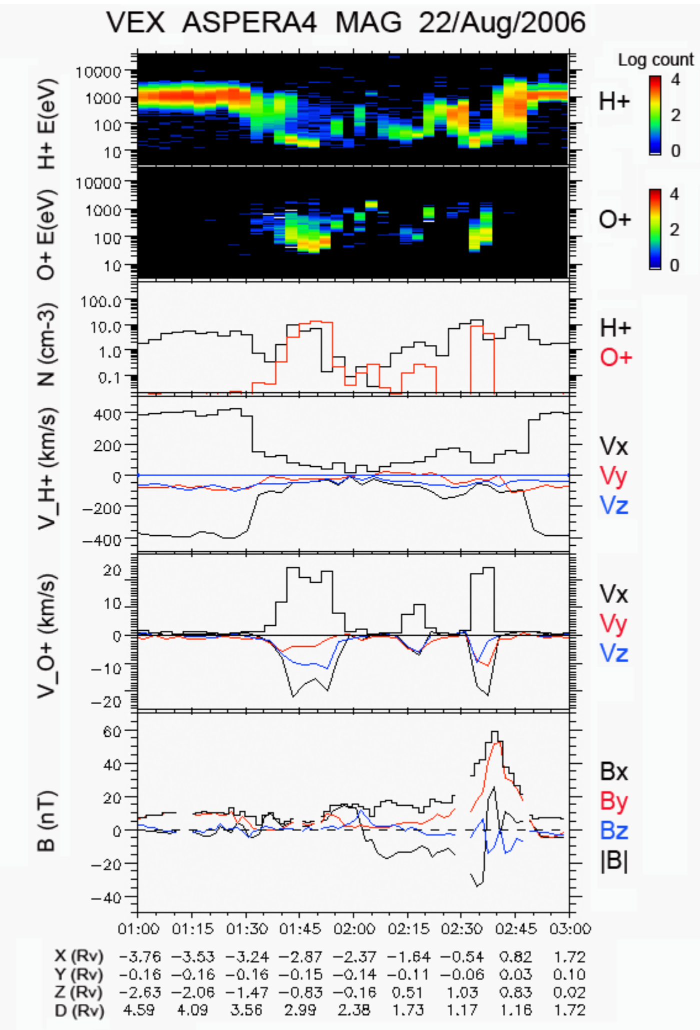
VEX ASPERA4 MAG 22/Aug/2006
H+ E(eV)
10000
1000
100
10
Log count
H+
4
2
0
O+ E(eV)
O+
N (cm-3)
100.0
10.0
1.0
0.1
H+
O+
V_H+ (km/s)
400
200
0
−200
−400
Vx
Vy
Vz
V_O+ (km/s)
20
10
0
−10
−20
Vx
Vy
Vz
B (nT)
60
40
20
0
−20
−40
Bx
By
Bz
|B|
01:00 01:15 01:30 01:45 02:00 02:15 02:30 02:45 03:00
X (Rv) −3.76 −3.53 −3.24 −2.87 −2.37 −1.64 −0.54 0.82 1.72
Y (Rv) −0.16 −0.16 −0.16 −0.15 −0.14 −0.11 −0.06 0.03 0.10
Z (Rv) −2.63 −2.06 −1.47 −0.83 −0.16 0.51 1.03 0.83 0.02
D (Rv) 4.59 4.09 3.56 2.99 2.38 1.73 1.17 1.16 1.72

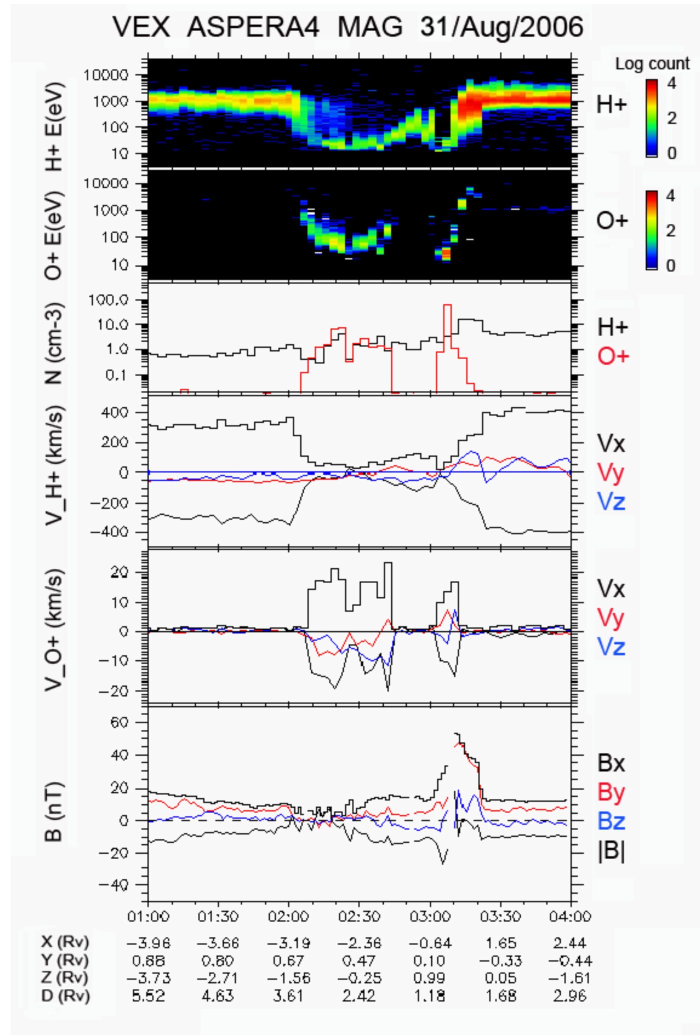
VEX ASPERA4 MAG 31/Aug/2006
H+ E(eV)
10000
1000
100
10
Log count
H+
4
2
0
O+ E(eV)
O+
N (cm-3)
100.0
10.0
1.0
0.1
H+
O+
V_H+ (km/s)
400
200
0
−200
−400
Vx
Vy
Vz
V_O+ (km/s)
20
10
0
−10
−20
Vx
Vy
Vz
B (nT)
60
40
20
0
−20
−40
Bx
By
Bz
|B|
01:00 01:30 02:00 02:30 03:00 03:30 04:00
X (Rv) −3.96 −3.66 −3.19 −2.36 −0.64 1.65 2.44
Y (Rv) 0.88 0.80 0.67 0.47 0.10 −0.33 −0.44
Z (Rv) −3.73 −2.71 −1.56 −0.25 0.99 0.05 −1.61
D (Rv) 5.52 4.63 3.61 2.42 1.18 1.68 2.96

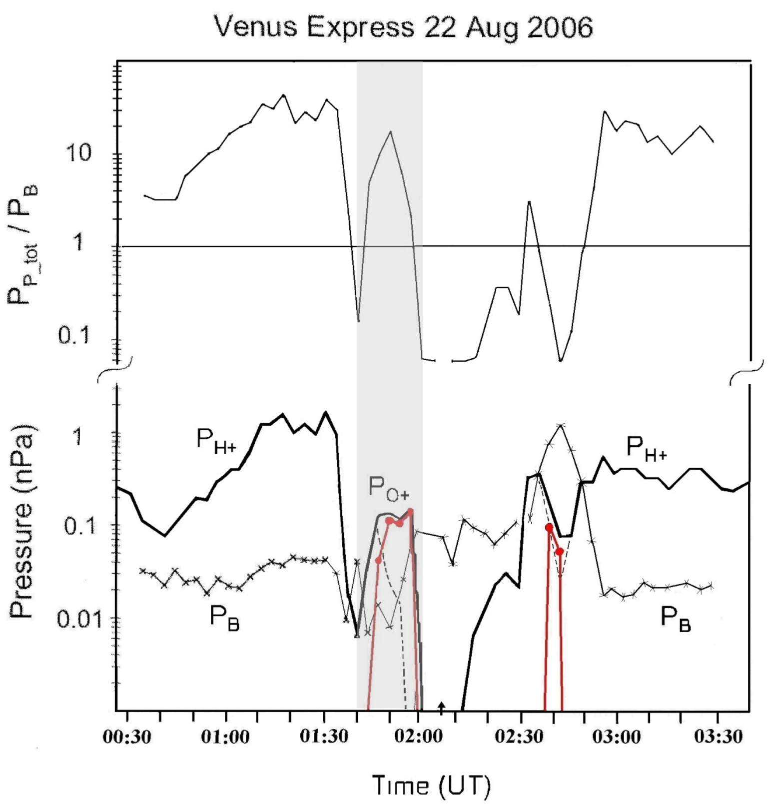

Venus Express 22 Aug 2006
P_{P_tot} / P_B
10
1
0.1
Pressure (nPa)
1
0.1
0.01
P_{H+}
P_{O+}
P_B
00:30
01:00
01:30
02:00
02:30
03:00
03:30
Time (UT)

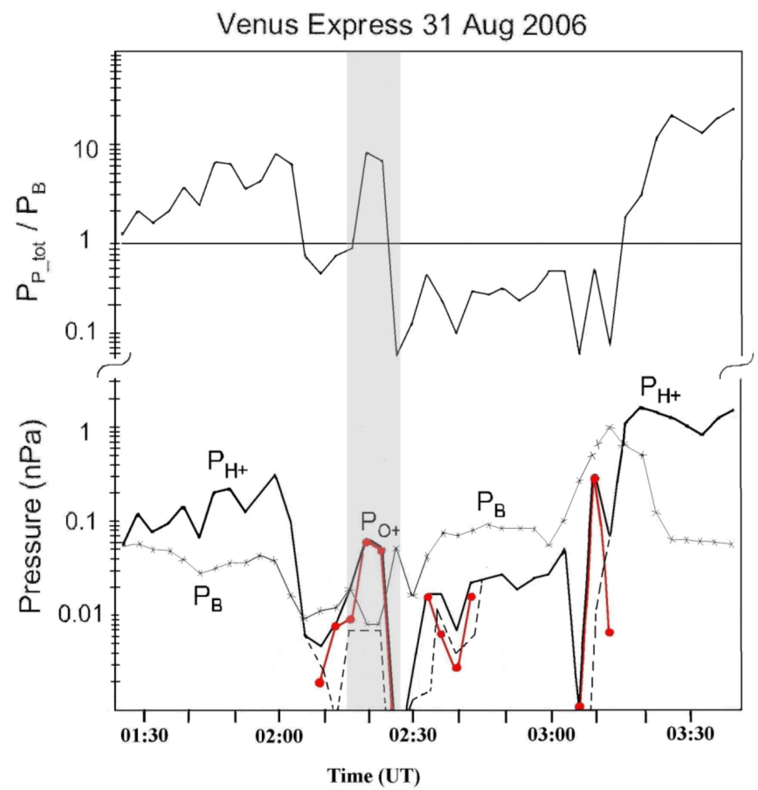

Venus Express 31 Aug 2006
P_{P_tot} / P_B
10
1
0.1
Pressure (nPa)
1
0.1
0.01
P_{H+}
P_{O+}
P_B
01:30
02:00
02:30
03:00
03:30
Time (UT)

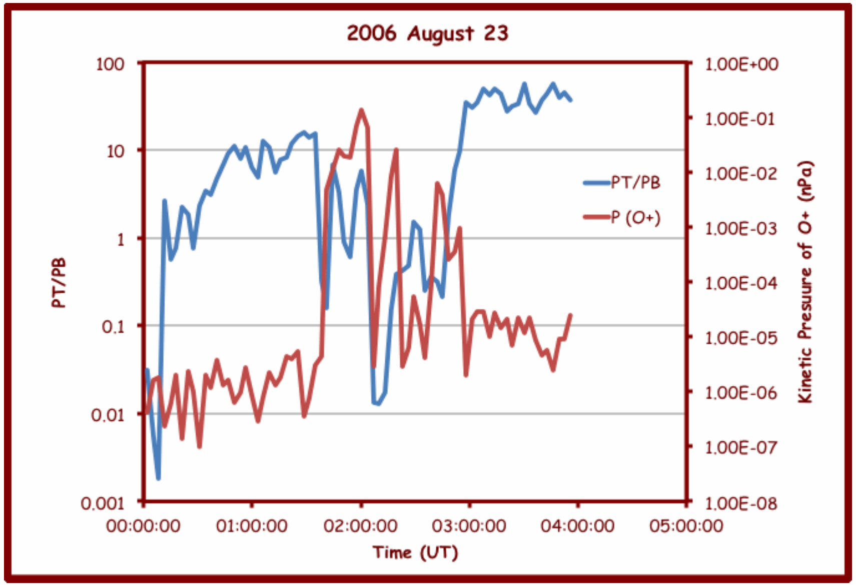
2006 August 23
PT/PB
Kinetic Presuure of O+ (nPa)
Time (UT)
PT/PB
P (O+)
100
10
1
0.1
0.01
0.001
1.00E+00
1.00E-01
1.00E-02
1.00E-03
1.00E-04
1.00E-05
1.00E-06
1.00E-07
1.00E-08
00:00:00
01:00:00
02:00:00
03:00:00
04:00:00
05:00:00

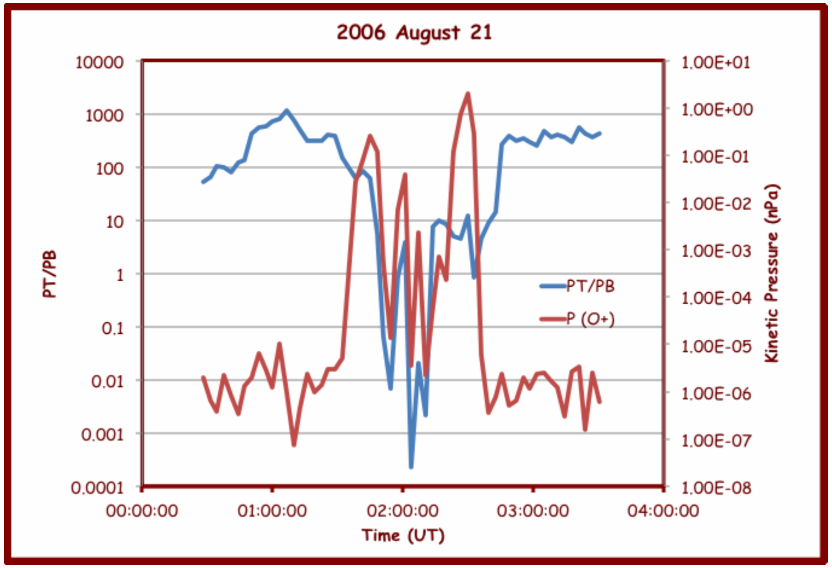
2006 August 21
PT/PB
Kinetic Pressure (nPa)
Time (UT)
PT/PB
P (O+)
10000
1000
100
10
1
0.1
0.01
0.001
0.0001
1.00E+01
1.00E+00
1.00E-01
1.00E-02
1.00E-03
1.00E-04
1.00E-05
1.00E-06
1.00E-07
1.00E-08
00:00:00
01:00:00
02:00:00
03:00:00
04:00:00

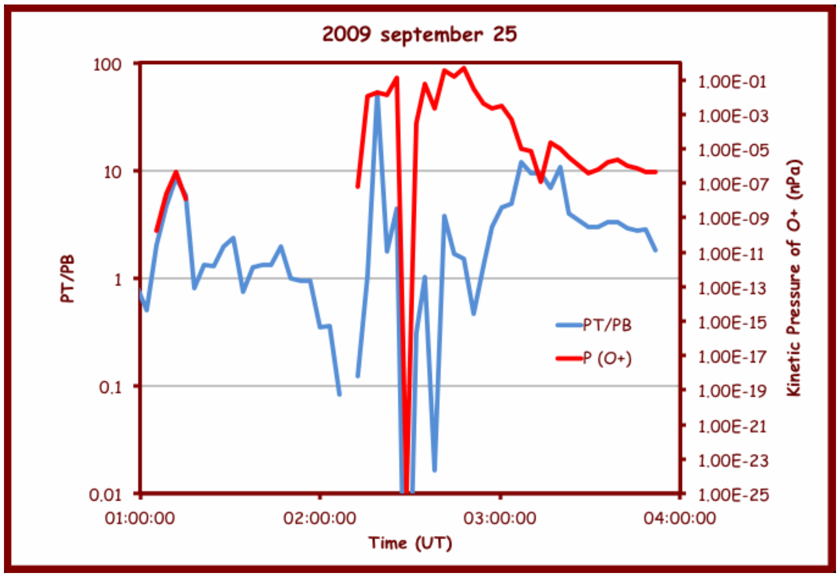

2009 september 25
PT/PB
Kinetic Pressure of O+ (nPa)
Time (UT)
PT/PB
P (O+)
100
10
1
0.1
0.01
1.00E-01
1.00E-03
1.00E-05
1.00E-07
1.00E-09
1.00E-11
1.00E-13
1.00E-15
1.00E-17
1.00E-19
1.00E-21
1.00E-23
1.00E-25
01:00:00
02:00:00
03:00:00
04:00:00

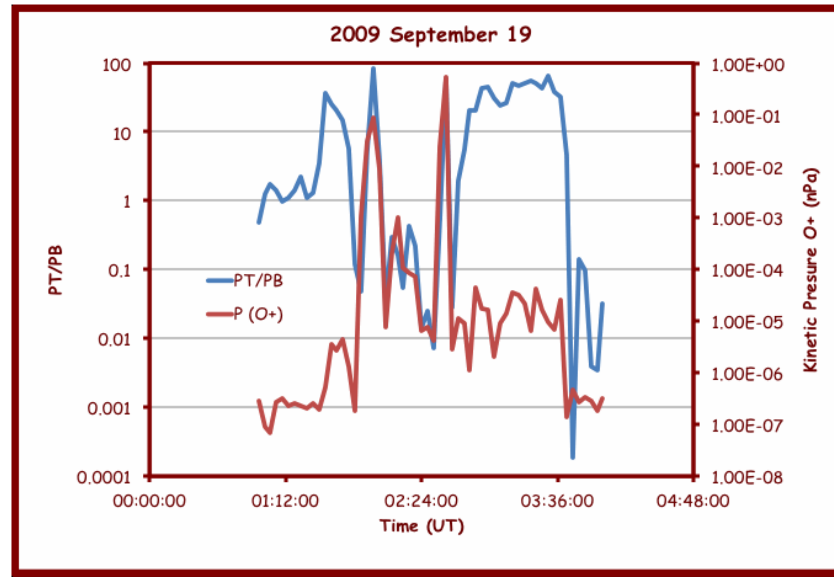

2009 September 19
PT/PB
Kinetic Presure O+ (nPa)
Time (UT)
PT/PB
P (O+)
100
10
1
0.1
0.01
0.001
0.0001
1.00E+00
1.00E-01
1.00E-02
1.00E-03
1.00E-04
1.00E-05
1.00E-06
1.00E-07
1.00E-08
00:00:00
01:12:00
02:24:00
03:36:00
04:48:00

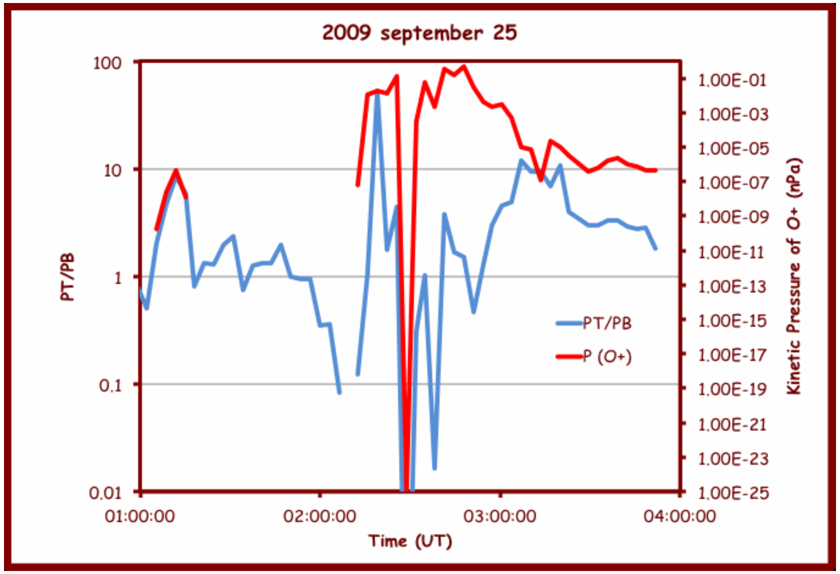

2009 september 25
PT/PB
Kinetic Pressure of O+ (nPa)
Time (UT)
PT/PB
P (O+)
100
10
1
0.1
0.01
1.00E-01
1.00E-03
1.00E-05
1.00E-07
1.00E-09
1.00E-11
1.00E-13
1.00E-15
1.00E-17
1.00E-19
1.00E-21
1.00E-23
1.00E-25
01:00:00
02:00:00
03:00:00
04:00:00

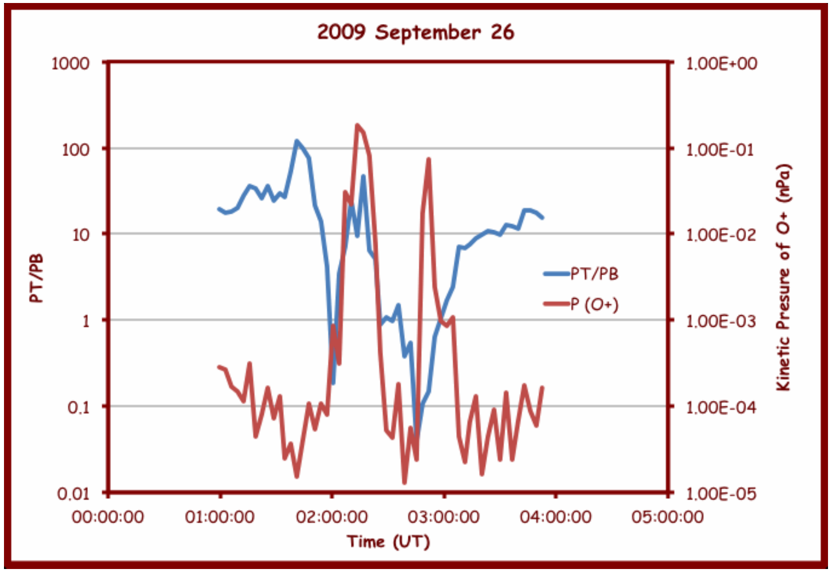

2009 September 26
PT/PB
Kinetic Presure of O+ (nPa)
Time (UT)
PT/PB
P (O+)
1000
100
10
1
0.1
0.01
1.00E+00
1.00E-01
1.00E-02
1.00E-03
1.00E-04
1.00E-05
00:00:00
01:00:00
02:00:00
03:00:00
04:00:00
05:00:00

Orbit date	O+ fluxes (UT)	PT	PB	PT/PB
21-08-06	01:45 UT	0.41 nPa	0.007 nPa	60
22-08-06	01:50 UT	0.18 nPa	0.026 nPa	8
23-08-06	02:00 UT	0.14 nPa	0.024 nPa	6
24-08-06	02:18 UT	0.27 nPa	0.065 nPa	4
31-08-06	02:20 UT	0.08 nPa	0.006 nPa	13
19-09-09	02:58 UT	0.09 nPa	0.001 nPa	83
22-09-09	02:13 UT	0.52 nPa	0.056 nPa	9
23-09-09	02:15 UT	0.04 nPa	0.022 nPa	2
25-09-09	02:20 UT	0.12 nPa	0.028 nPa	50
26-09-09	02:18 UT	0.19 nPa	0.021 nPa	40

Table I. VEX orbits selected to show the total plasma pressure PT and the magnetic field pressure PB that were measured at the time when peak values of the kinetic pressure of O+ ion fluxes were detected as the spacecraft moved through the southern hemisphere in the Venus wake (second column). The ratio of both quantities is given in the right side column (the pressure values are given in nanopascals).

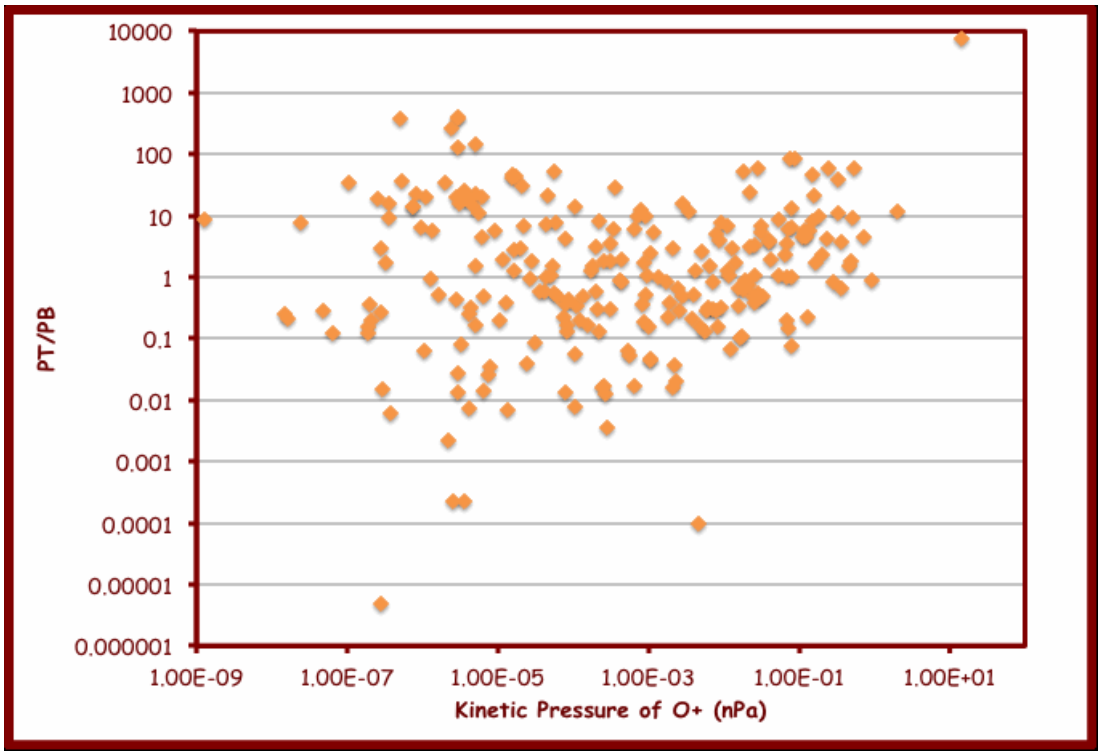
10000
1000
100
10
1
0,1
0,01
0,001
0,0001
0,00001
0,000001
PT/PB
1,00E-09
1,00E-07
1,00E-05
1,00E-03
1,00E-01
1,00E+01
Kinetic Pressure of O+ (nPa)

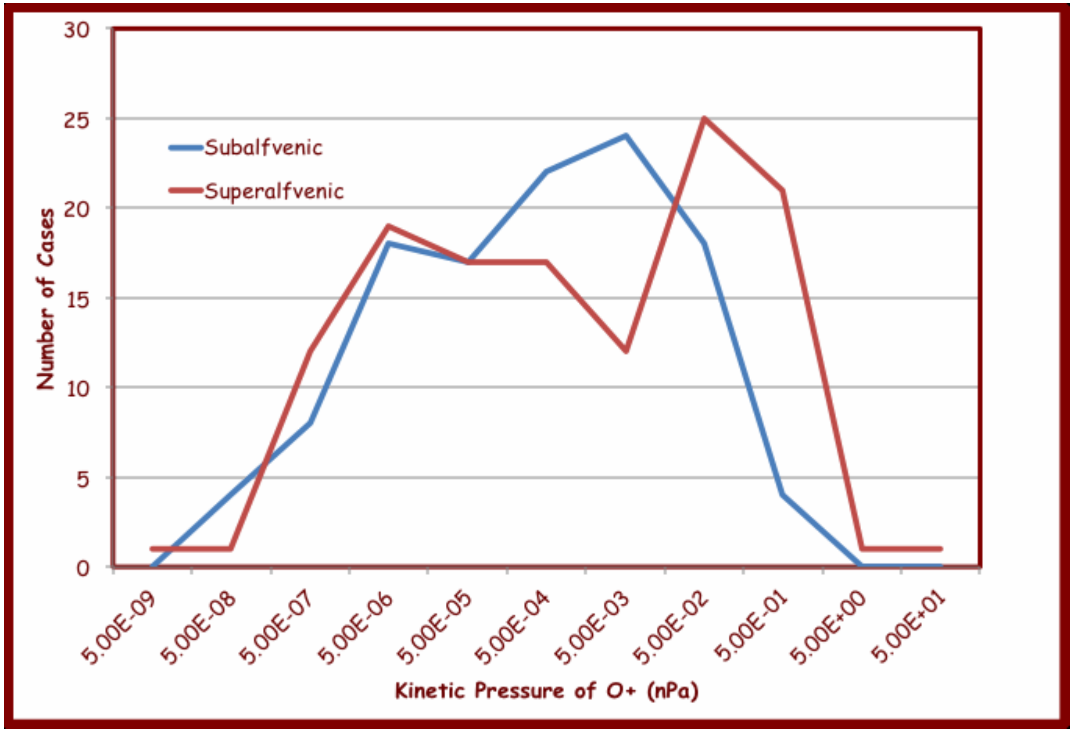

Subalfvenic
Superalfvenic
Number of Cases
30
25
20
15
10
5
0
5.00E-09
5.00E-08
5.00E-07
5.00E-06
5.00E-05
5.00E-04
5.00E-03
5.00E-02
5.00E-01
5.00E+00
5.00E+01
Kinetic Pressure of O+ (nPa)

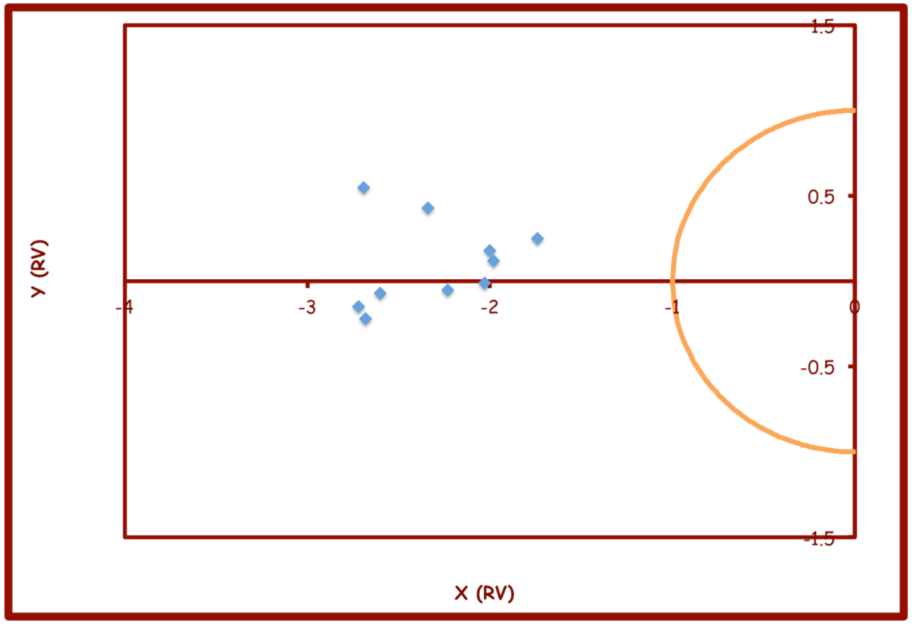

1.5
0.5
-0.5
-1.5
-4
-3
-2
-1
0
Y (RV)
X (RV)

VENERA DATA (Romanov et al., 1979)

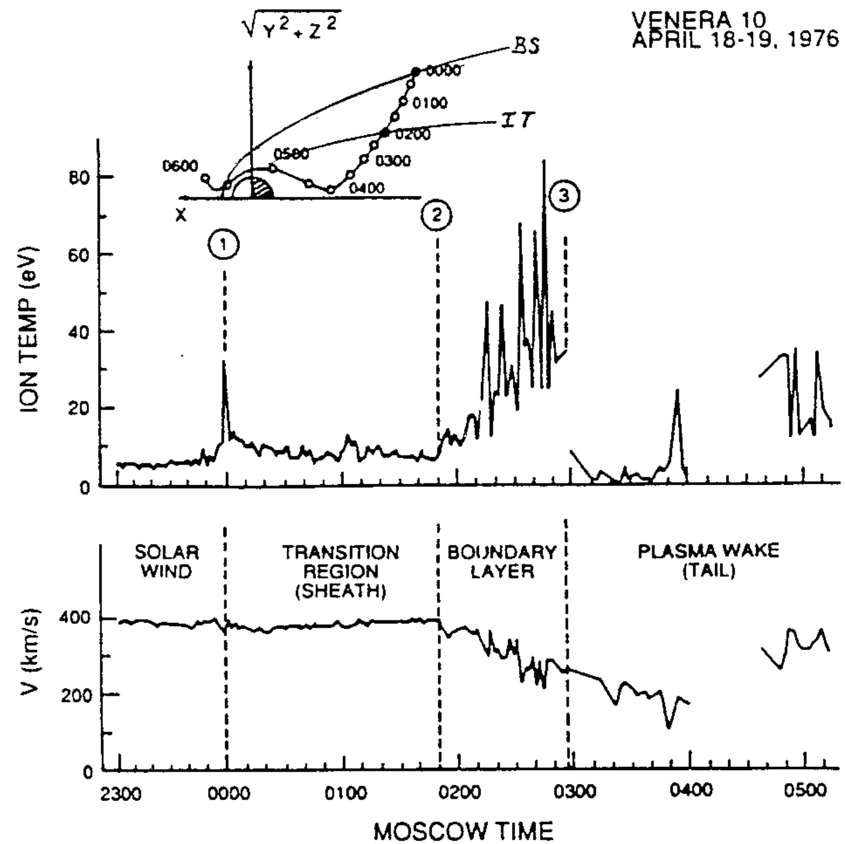

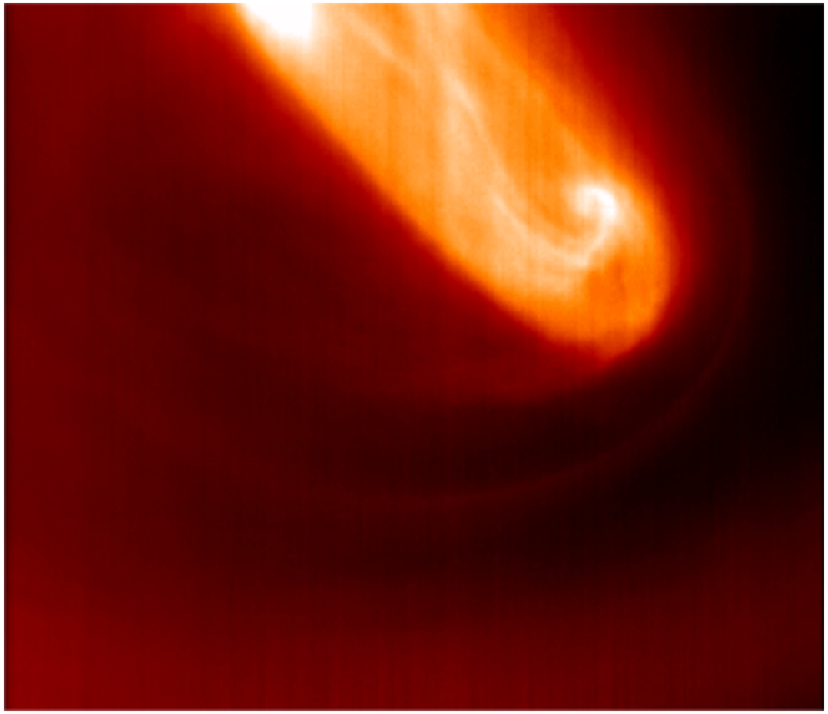

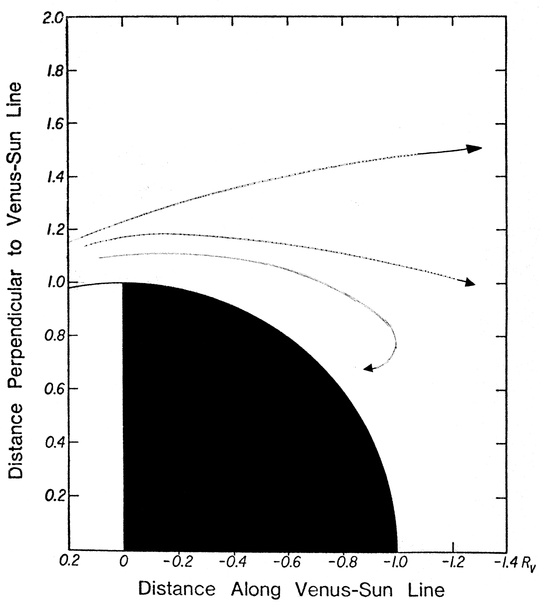
2.0
1.8
1.6
1.4
1.2
1.0
0.8
0.6
0.4
0.2
Distance Perpendicular to Venus-Sun Line
0.2
0
-0.2
-0.4
-0.6
-0.8
-1.0
-1.2
-1.4 R_V
Distance Along Venus-Sun Line

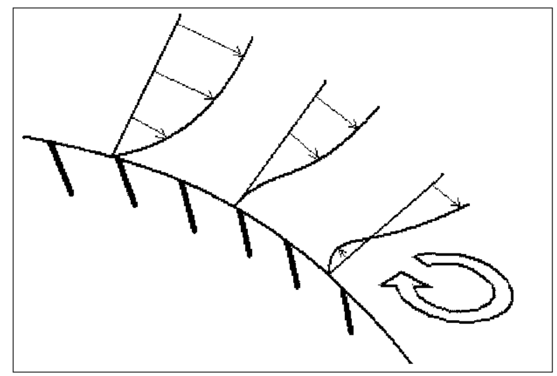

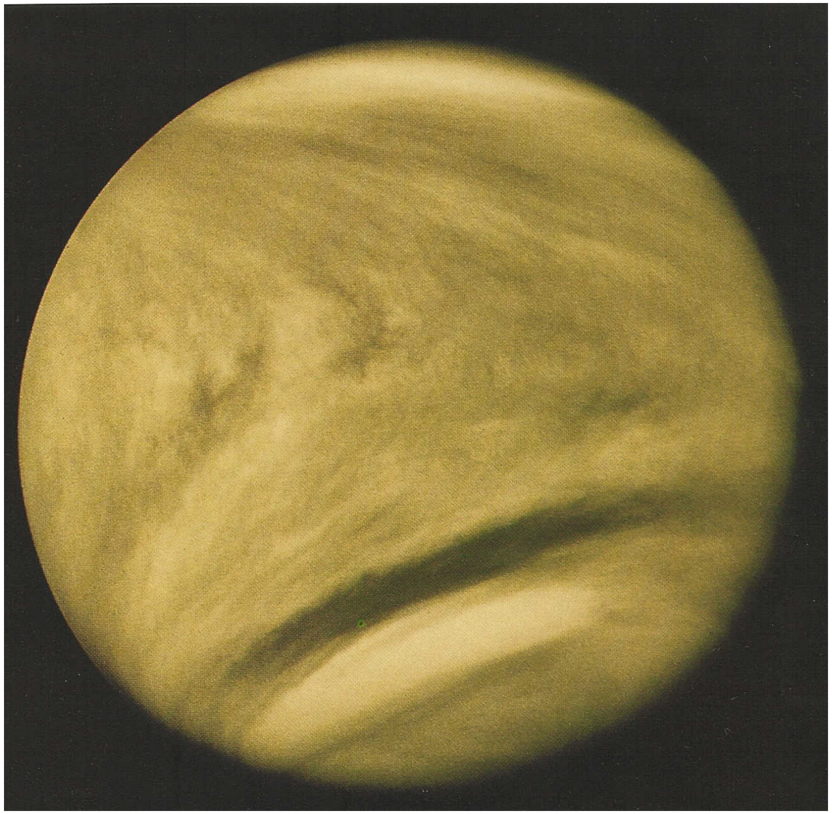

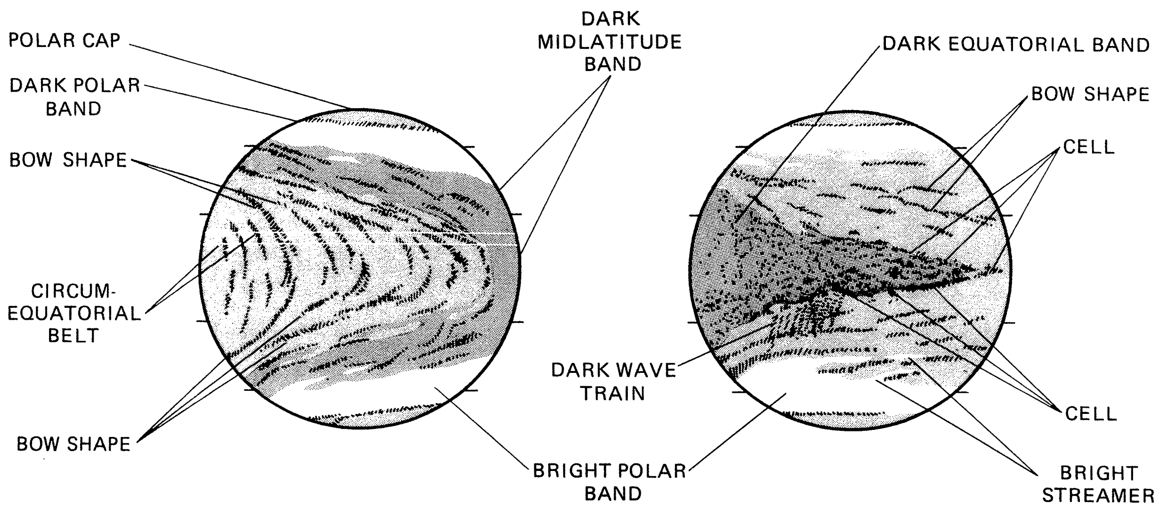

Figure 6-17. Basic types of cloud features observed in the UV images of Venus. The two views typically occur 2 days apart.

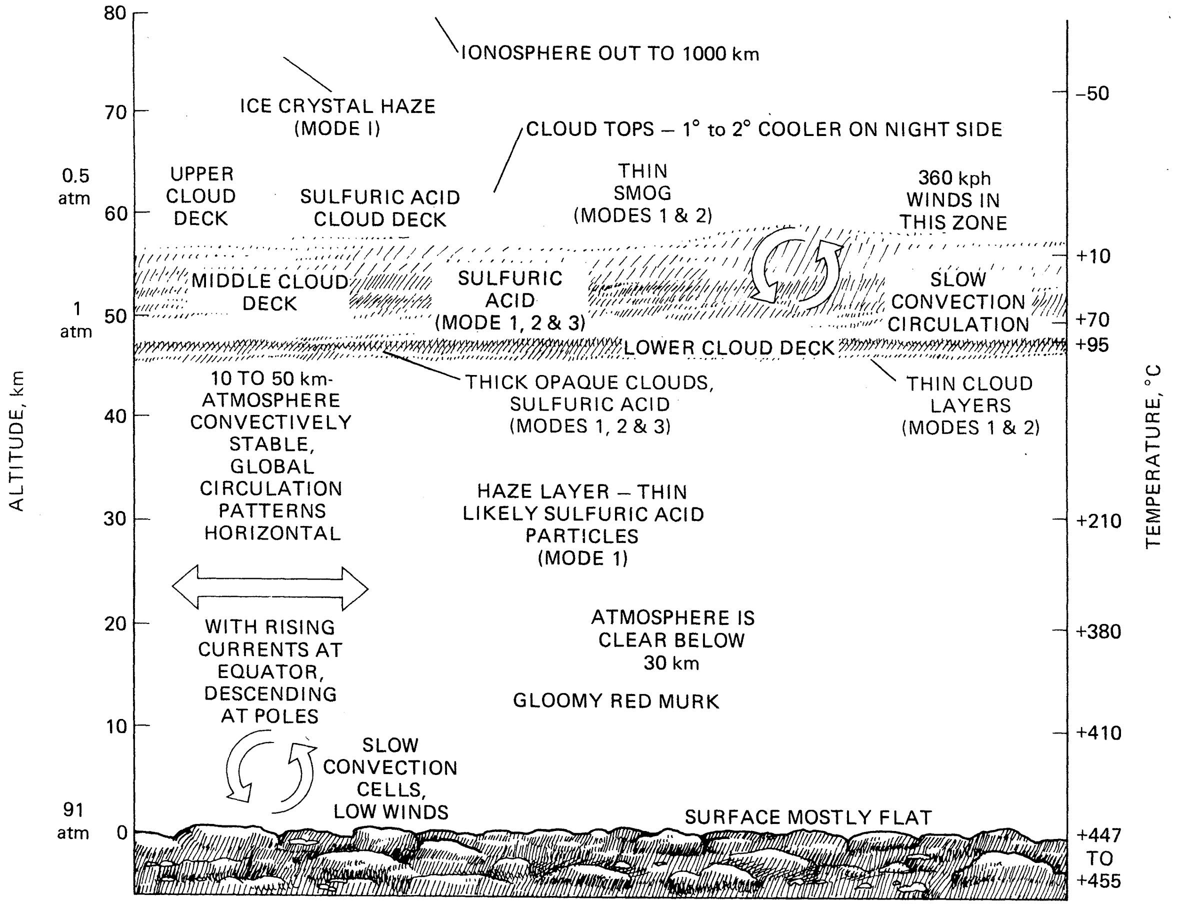

Figure 5-15. The Pioneer Venus mission provided a more detailed and accurate picture of the Venus atmosphere, its cloud layers, composition, and wind systems.

TABLE 6-3.– COMPARISON OF ATMOSPHERES OF VENUS AND EARTH

Gas	Venus at surface, % or ppm[a]	Earth at sea level, % or ppm[a]
Argon	70^{+50}_{-30}	0.93%
36	20^{+20}_{-10}	31
38	6[b]	6
40	31[b]	0.93%
Carbon dioxide	96%	0.02-0.04%
Carbonyl sulfide	<3	0.5
Chlorine	<10	
Hydrogen	<=500	
Krypton	0.05	0.5
Neon	10	18
20	9	16
22	1	2
Nitrogen	4%	78%
Oxygen	<30	21%
Sulfur dioxide[c]		

[a]1 ppm = 0.0001%
[b]Derived from ^{36}Ar
[c]<10 in clouds; <300 near surface

TABLE 6-4.– MIXING RATIOS IN THE LOWER ATMOSPHERE

Gas	Amount, ppm
Argon	40-120
40/36	1.03-1.19
38/36	0.18
Carbon dioxide	96%
Carbon monoxide	20-28
Krypton	0.05-0.5
Neon	4.3-15
Nitrogen	3.41% (at 24 km)[a]; 4%[b]
(percentages)	3.54% (at 44 km)[a]
	4.60% (at 54 km)[a]
Oxygen	16 (at 44 km)[a]; <30[b]
	43 (at 55 km)[a]
Sulfur dioxide	185 (at 24 km)
	<10 (at 55 km)
Water	20 (at surface)
	60-1350 (at 24 km)
	150-5200 (at 44 km)
	200-<600 (at 54 km)

[a]LGC
[b]LNMS

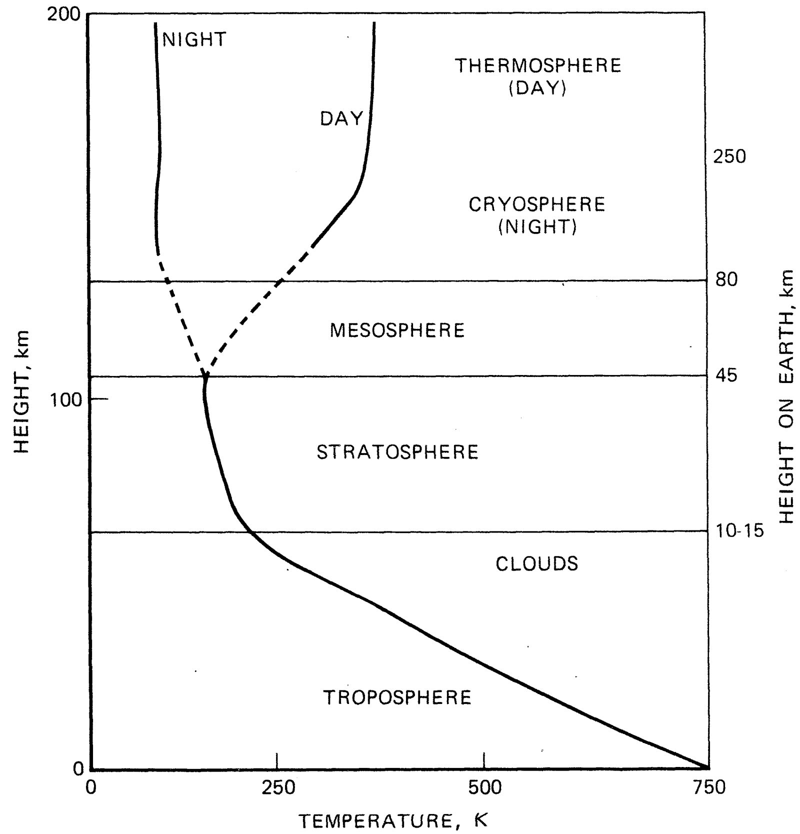

Figure 6-14. Typical temperatures for the Venus atmosphere and the corresponding regions. Heights for Earth are also shown for comparison.

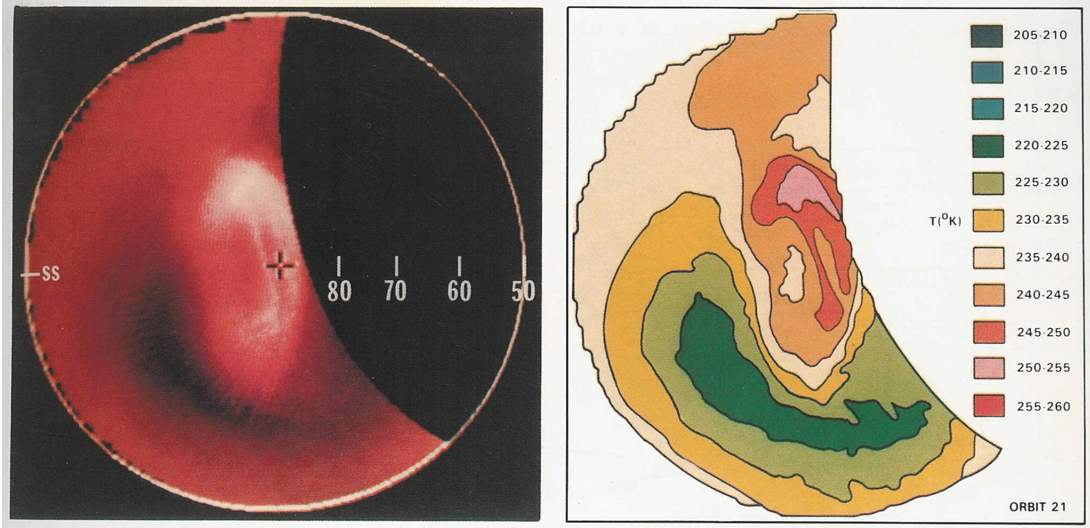

Figure 6-19(a). North polar infrared image and plot showing the temperatures. The north pole is in the center, the outer boundary is 50° north latitude, the noon point at SS at the left. The blacked out area is the region from which no data were obtained because of the geometry of the spacecraft's orbit. This image was obtained on December 26, 1978 during orbit 21.

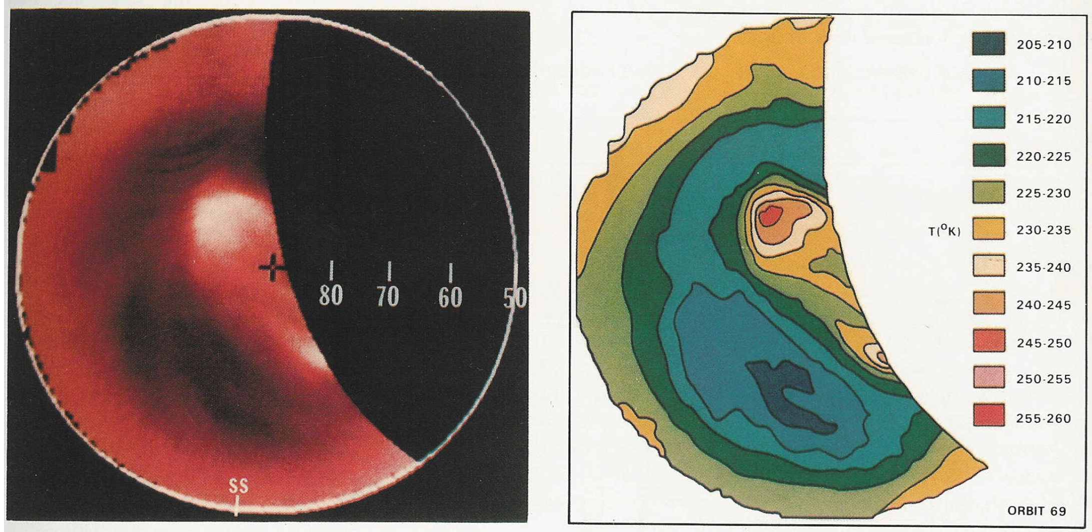

Figure 6-19(b). A similar image to (a) obtained February 11, 1979 on orbit 69.

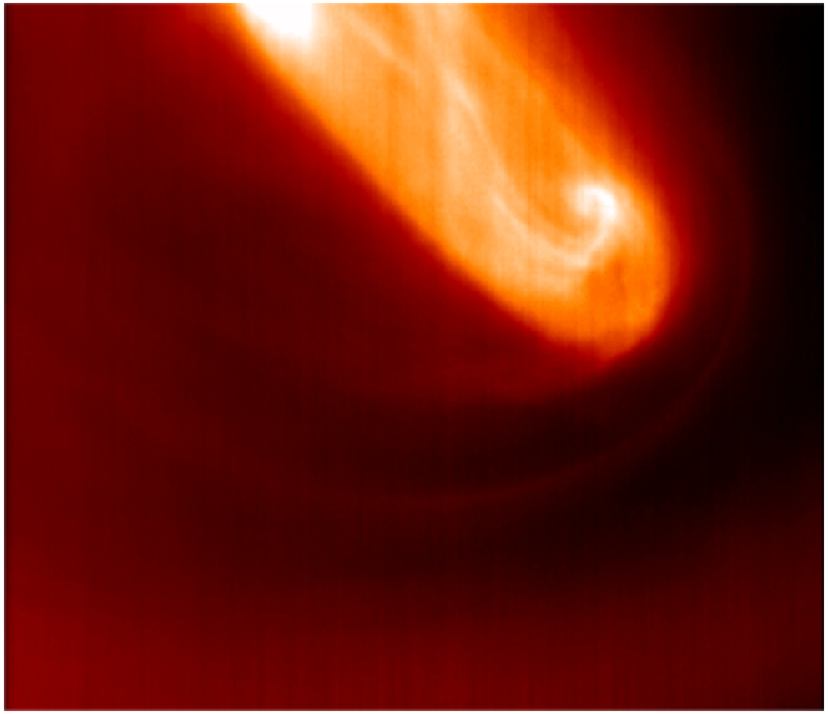

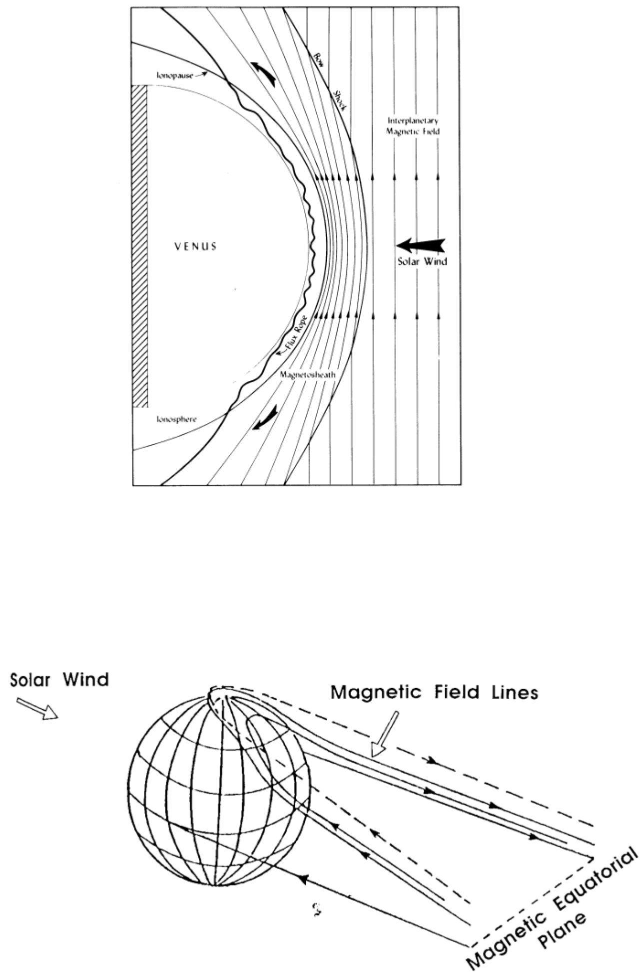

Fig. 1 – (upper panel) Accumulation of magnetic field fluxes around the ionosphere in the ecliptic plane [Russell and Vaisberg. 1983]. (lower panel) 3D geometry of draped magnetic field lines as they slide to the magnetic polar regions to enter the wake [Pérez-de-Tejada, 1986b].

PLASMA CHANNELS

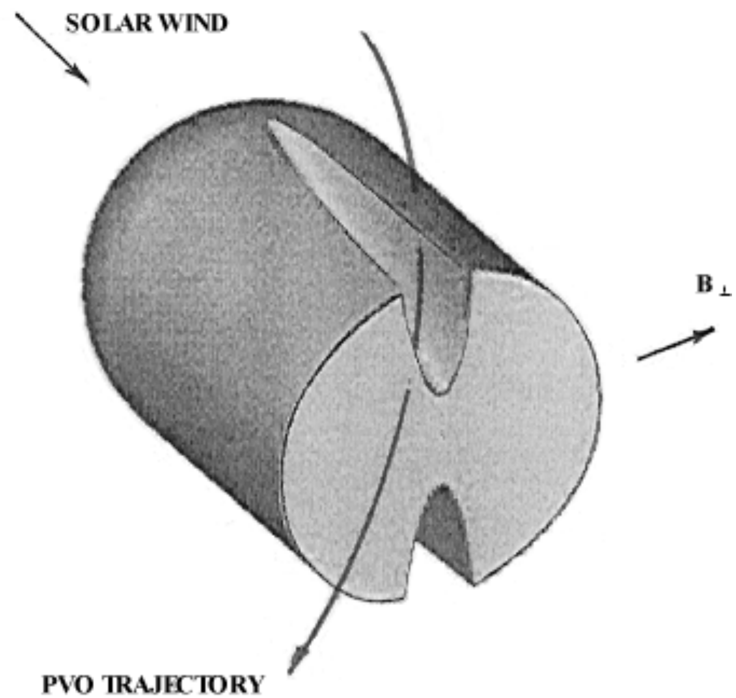

Schematic of the Venus nightside ionosphere with plasma channels that extend downstream from the magnetic polar regions. The trajectory of the PVO is traced for a situation in which the spacecraft traverses a plasma Channel across the nightside ionosphere (Pérez-de-Tejada, 2001).

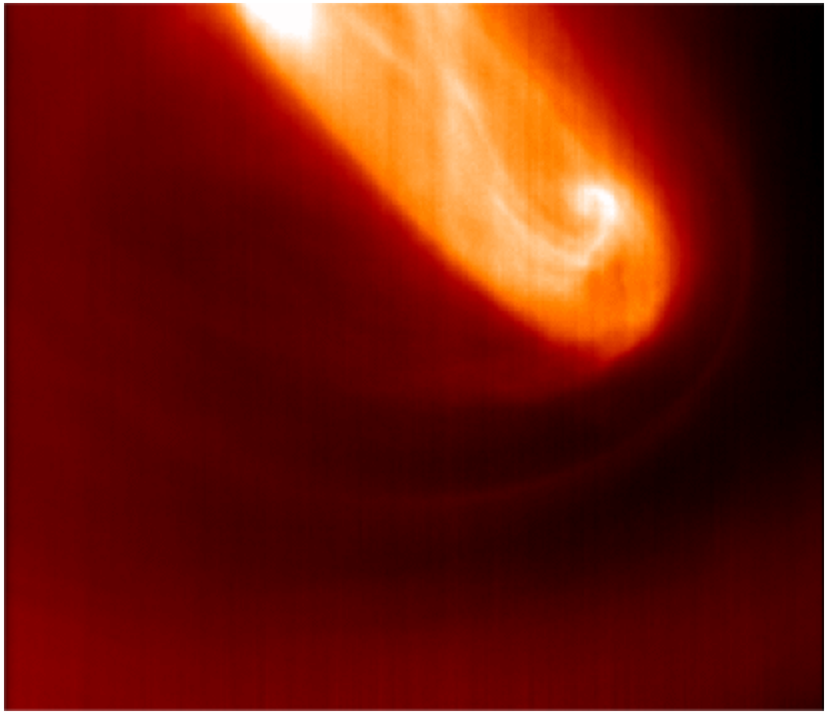

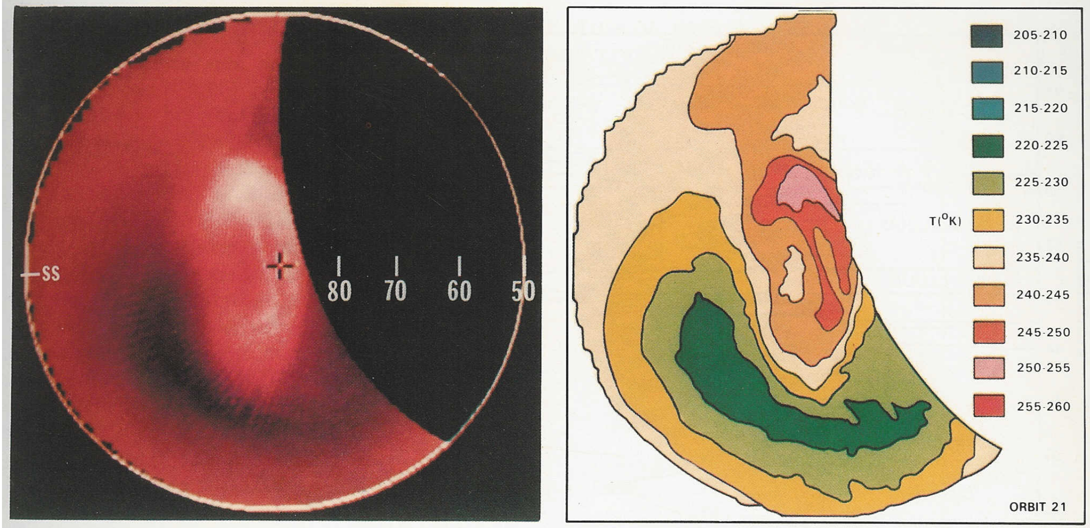

Figure 6-19(a). North polar infrared image and plot showing the temperatures. The north pole is in the center, the outer boundary is 50° north latitude, the noon point at SS at the left. The blacked out area is the region from which no data were obtained because of the geometry of the spacecraft's orbit. This image was obtained on December 26, 1978 during orbit 21.

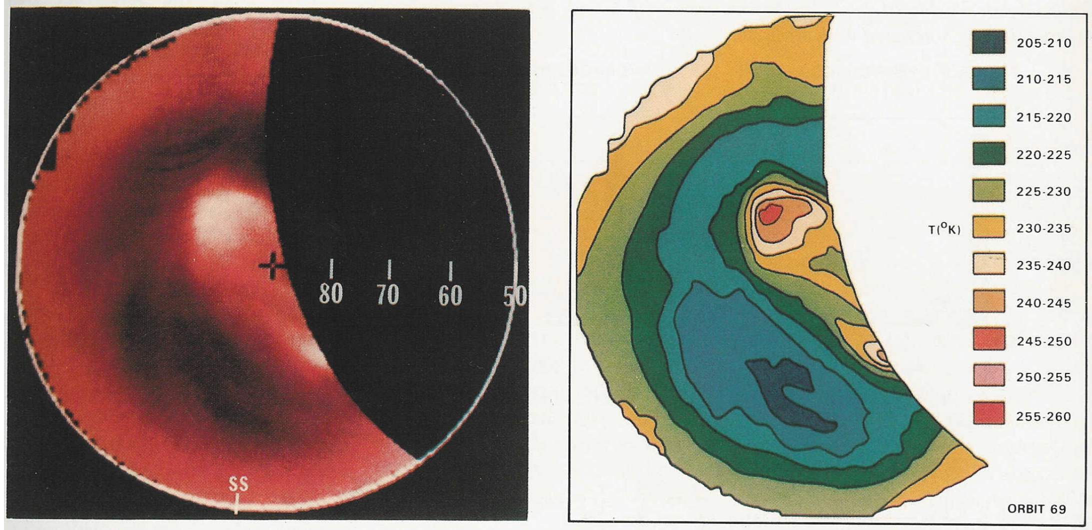

Figure 6-19(b). A similar image to (a) obtained February 11, 1979 on orbit 69.

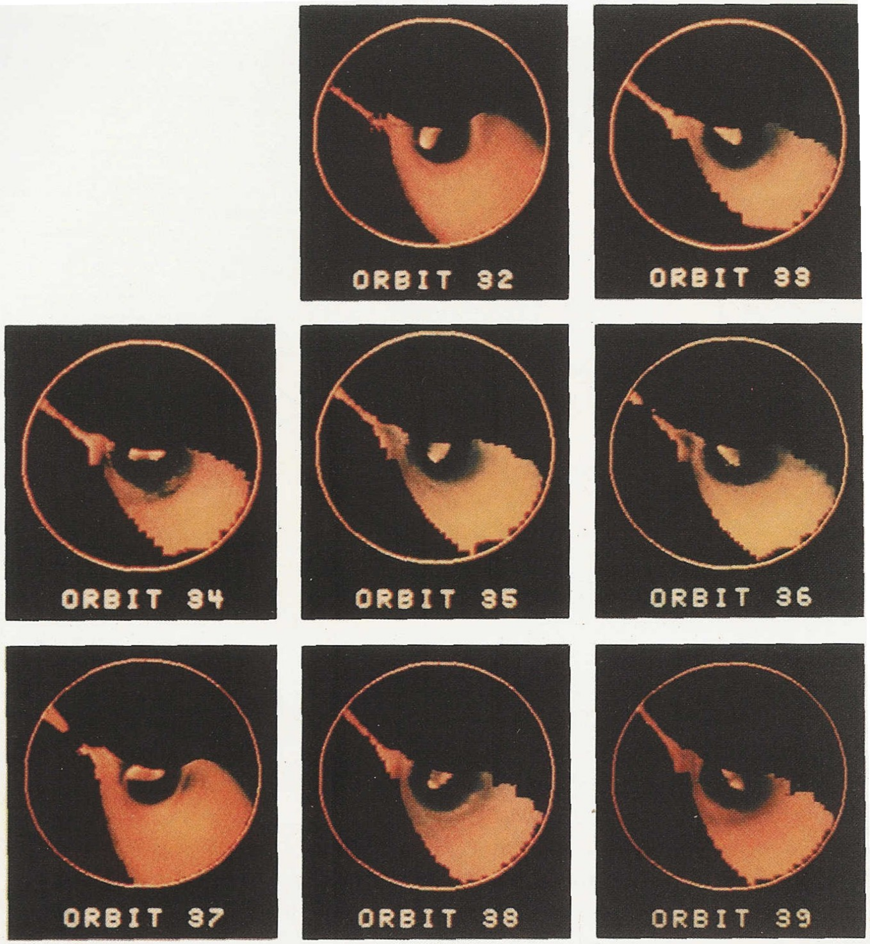

Figure 6-18. Eight consecutive polar stereographs of Venus' northern hemisphere taken at 11.5 μm. These images were taken one each day on orbits 32 through 39 (January 5 through 12, 1979). The north pole is at the center of each image and the equator is the outer boundary with the noon point at the bottom. Note that the polar dipole returns to approximately the same position in a period of three days.

K. Dennerl et al., 2006

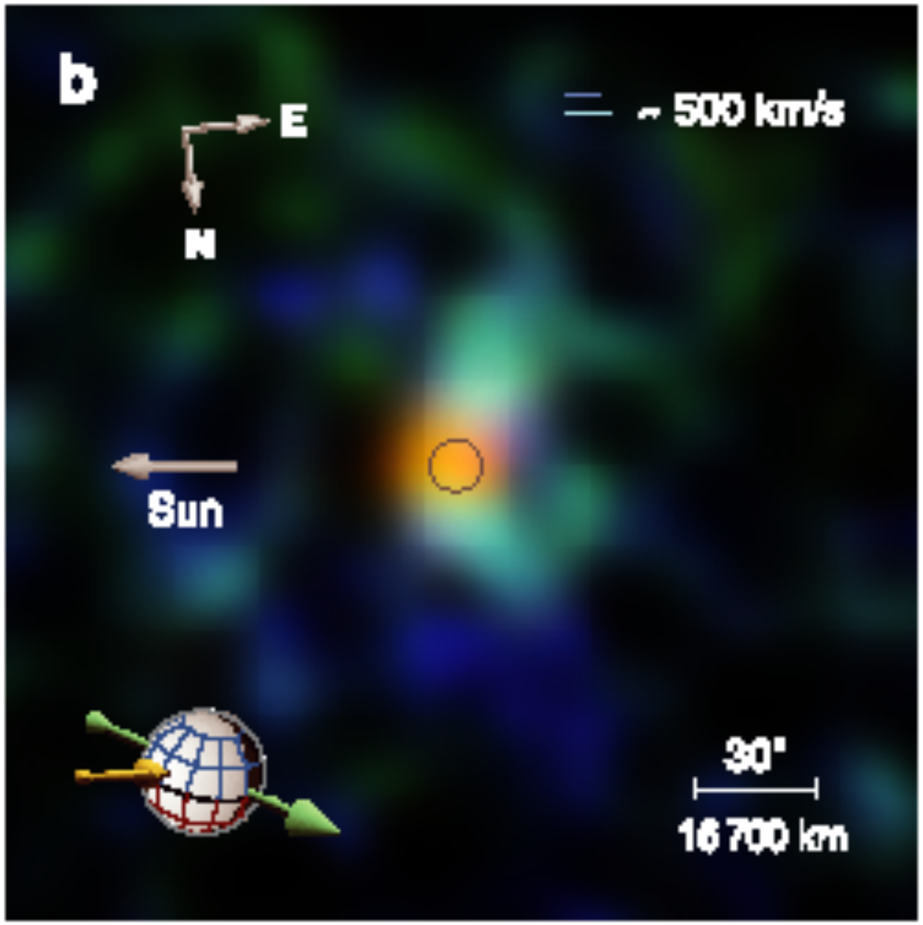

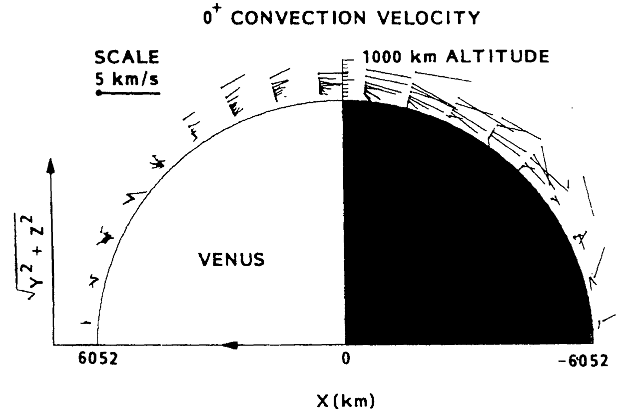

Fig. 5. Average ion velocities measured in the outbound leg of the orbit during the first 3.5 years of the Pioneer Venus mission (after Knudsen *et al.*, 1982a).

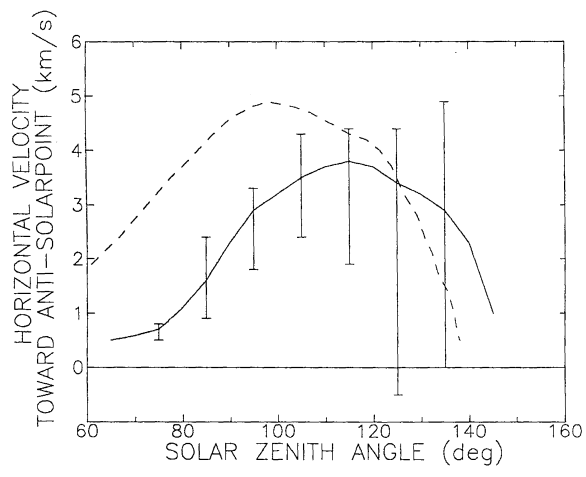

Fig. 6. Observed and calculated horizontal ion velocities toward the anti-solar point at 400 km altitude. The dashed curve was obtained with the simplified model of Singhal and Whitten (1987). The observed data (obtained from the ORPA experiment on PVO) are the average values, while the error bars show the standard deviation from the mean.

Shefer et al. 1979

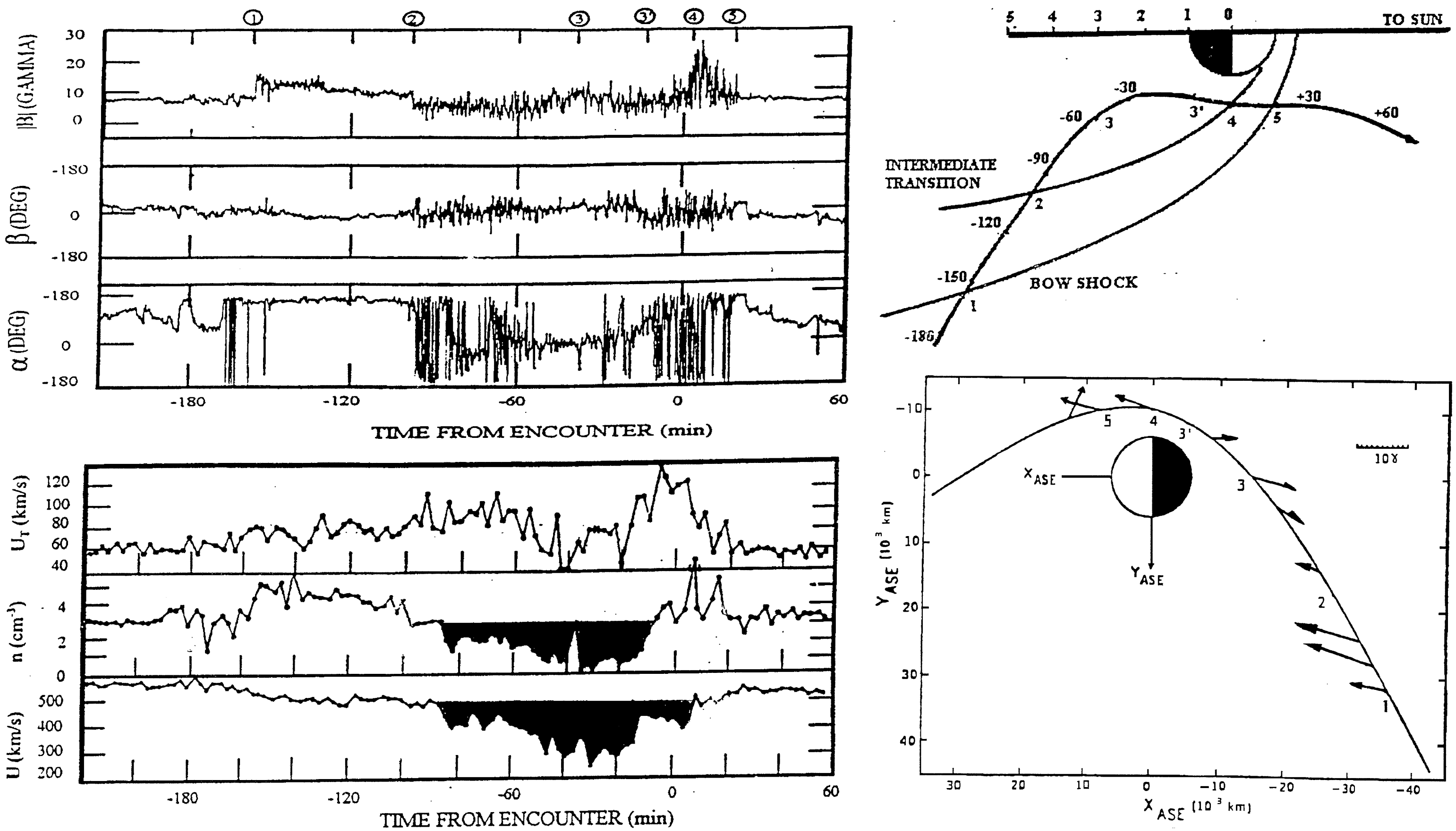

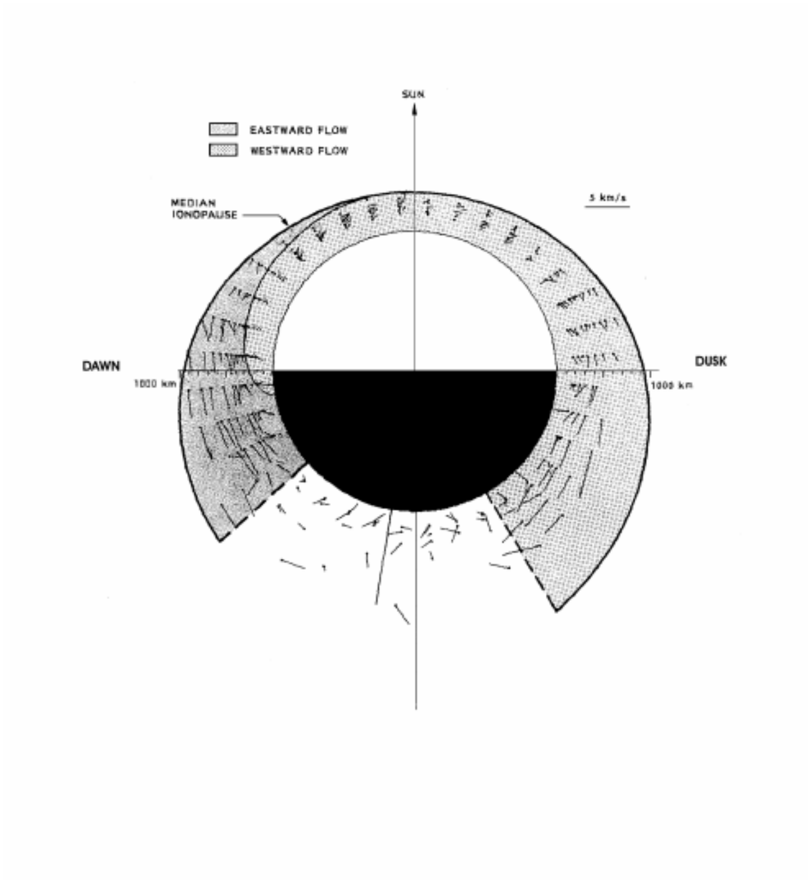

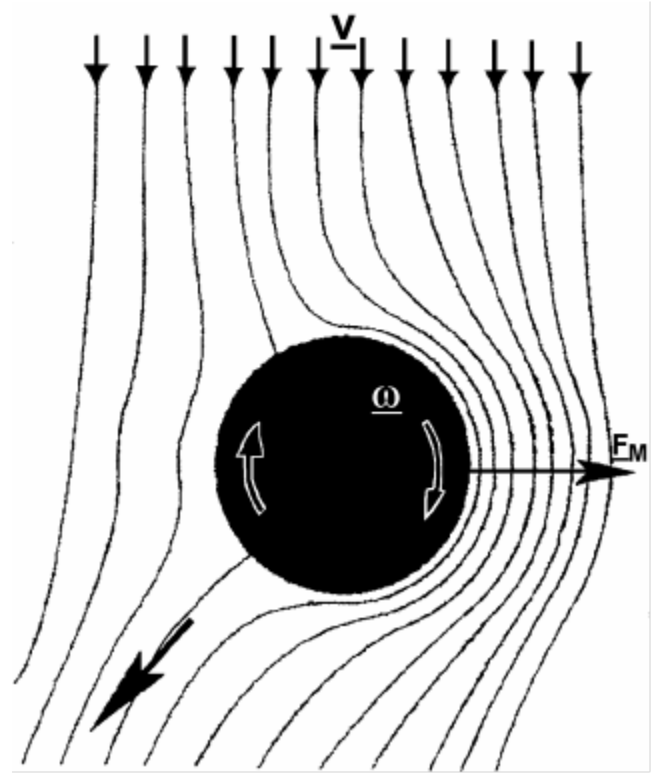

Magnus Force Eq: $F_M = C_M\,(r_2^{\,3} - r_1^{\,3})\,\rho\,V_i\,\omega$ **Bernoulli´s Eq:** $P + \rho V^2/2 = cst$

Dawn-Dusk Displacement: $D = A\,\zeta^2/2 = (F_M/M)[\pi\,r^2/2\,/V_i]^2/2$

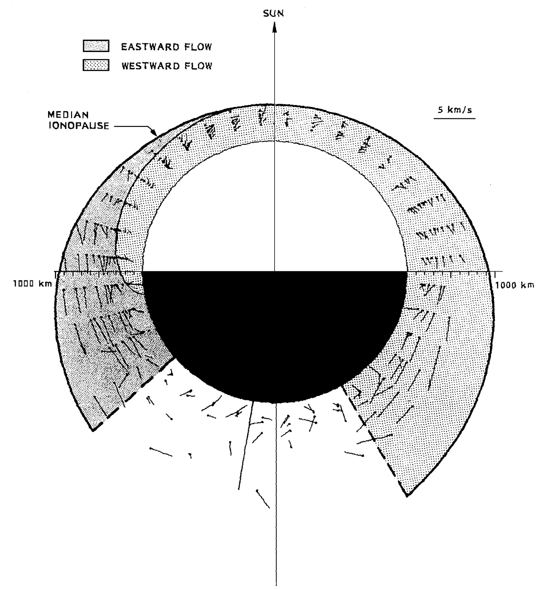

MAGNUS EFFECT

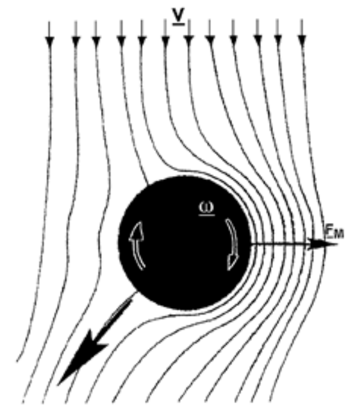

BERNOULLI'S EQ: $P + \rho V^2/2 = cst$

MAGNUS FORCE: $\underline{F}_M = C_M\, r^3\, \rho \underline{V} \times \underline{\omega}$

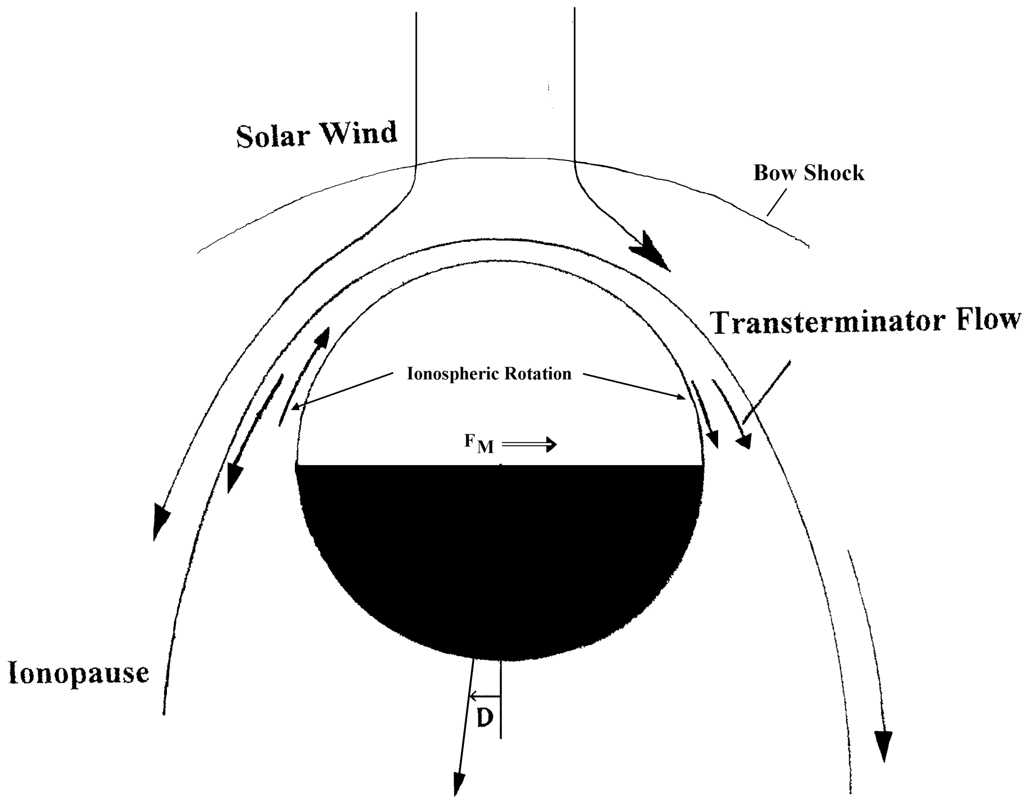

$F_M = C_M (r_2^{\,3} - r_1^{\,3})\, \rho\, V_i\, \omega$ $\qquad$ $D = (F_M/M)\, [(\pi\, r_2/2) / V_i]^2/2$

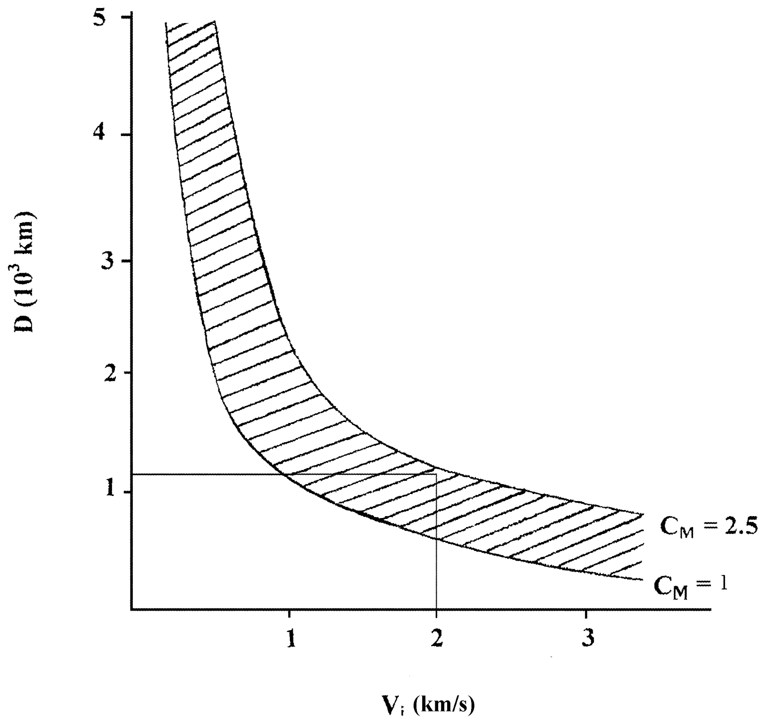

5
4
3
2
1
D (10^3 km)
1
2
3
Vi (km/s)
CM = 2.5
CM = 1

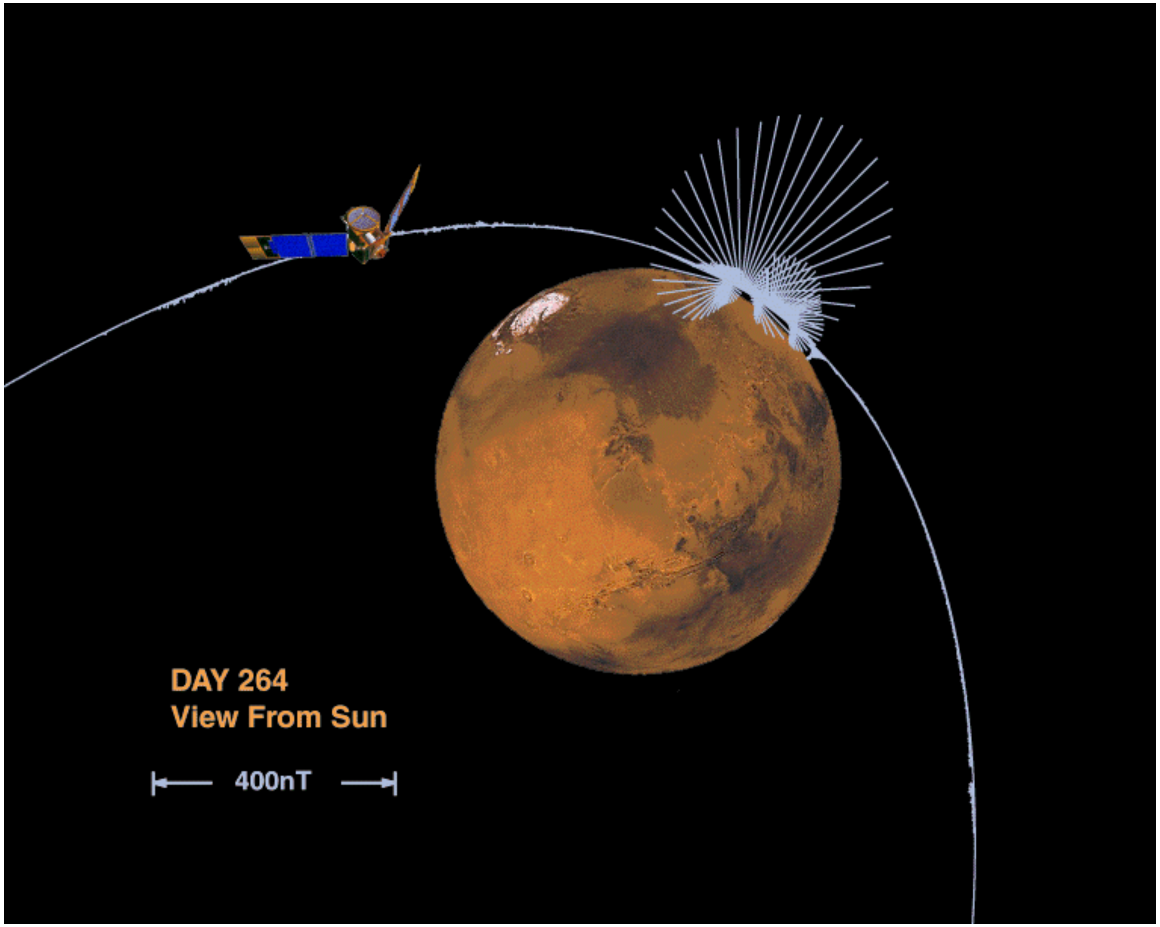
DAY 264
View From Sun
400nT

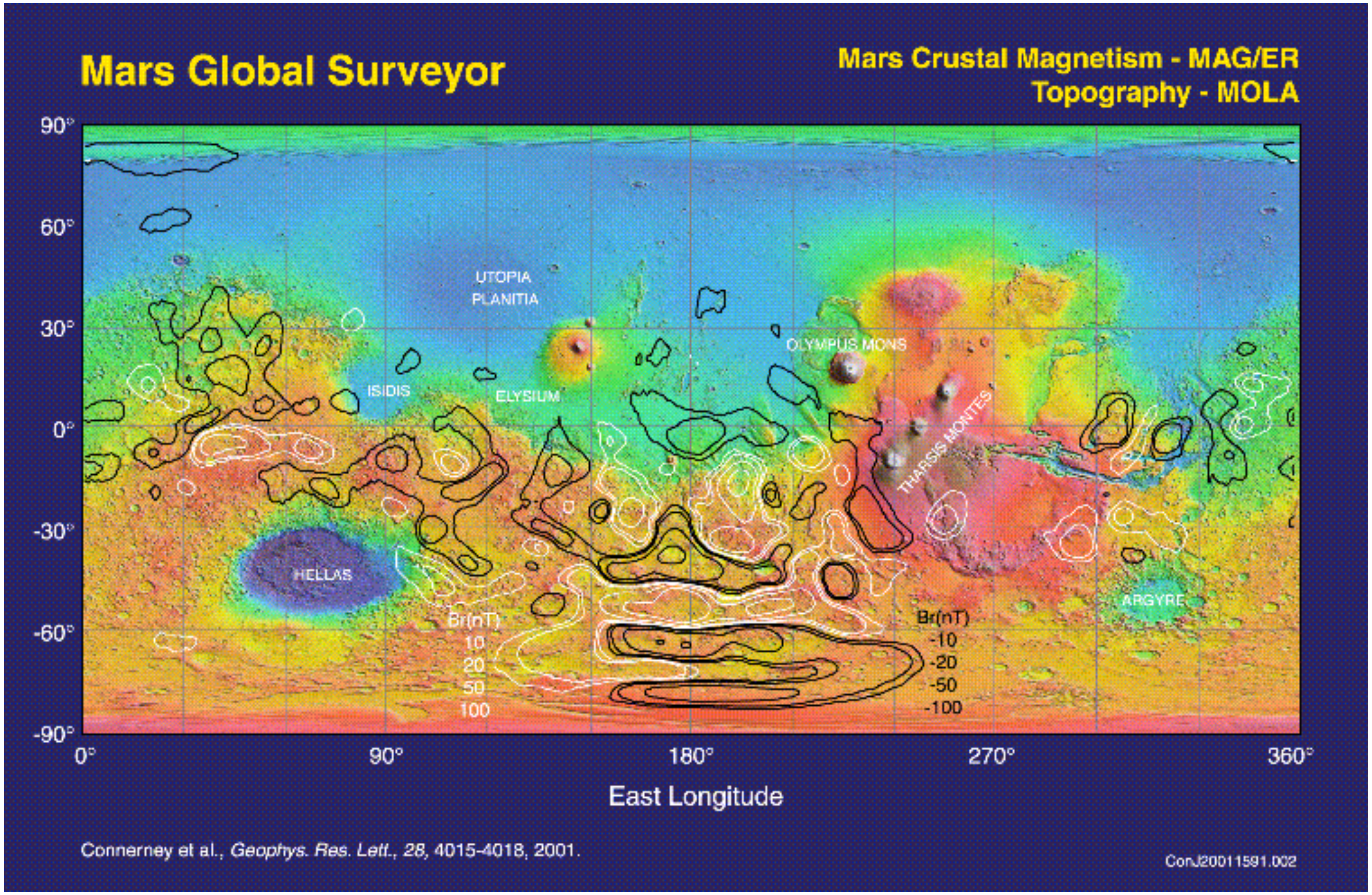

Topographic map of Mars from the MGS MOLA investigation with contours of constant radial magnetic field (black:negative, white: positive) as in Fig. 1. Elevation relative to a reference surface (yellow) range up to 8 km negative (yellow, green, light blue, dark blue) and 8 km positive (yellow, red, white). Crustal magnetization appears largely confined to the ancient southern highlands. Regions of extensive volcanism (e.g., Olympus Mons, Tharsis Montes) are non-magnetic as are regions surrounding the large impact basins Hellas and Argyre.

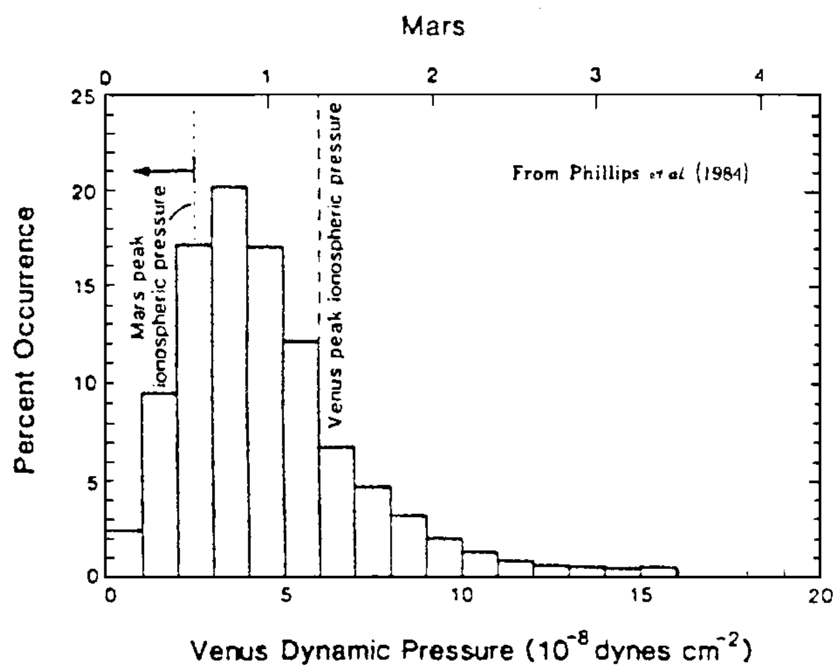

Mars
0
1
2
3
4
25
20
15
10
5
0
Percent Occurrence
Mars peak ionospheric pressure
Venus peak ionospheric pressure
From Phillips et al (1984)
0
5
10
15
20
Venus Dynamic Pressure (10^-8 dynes cm^-2)

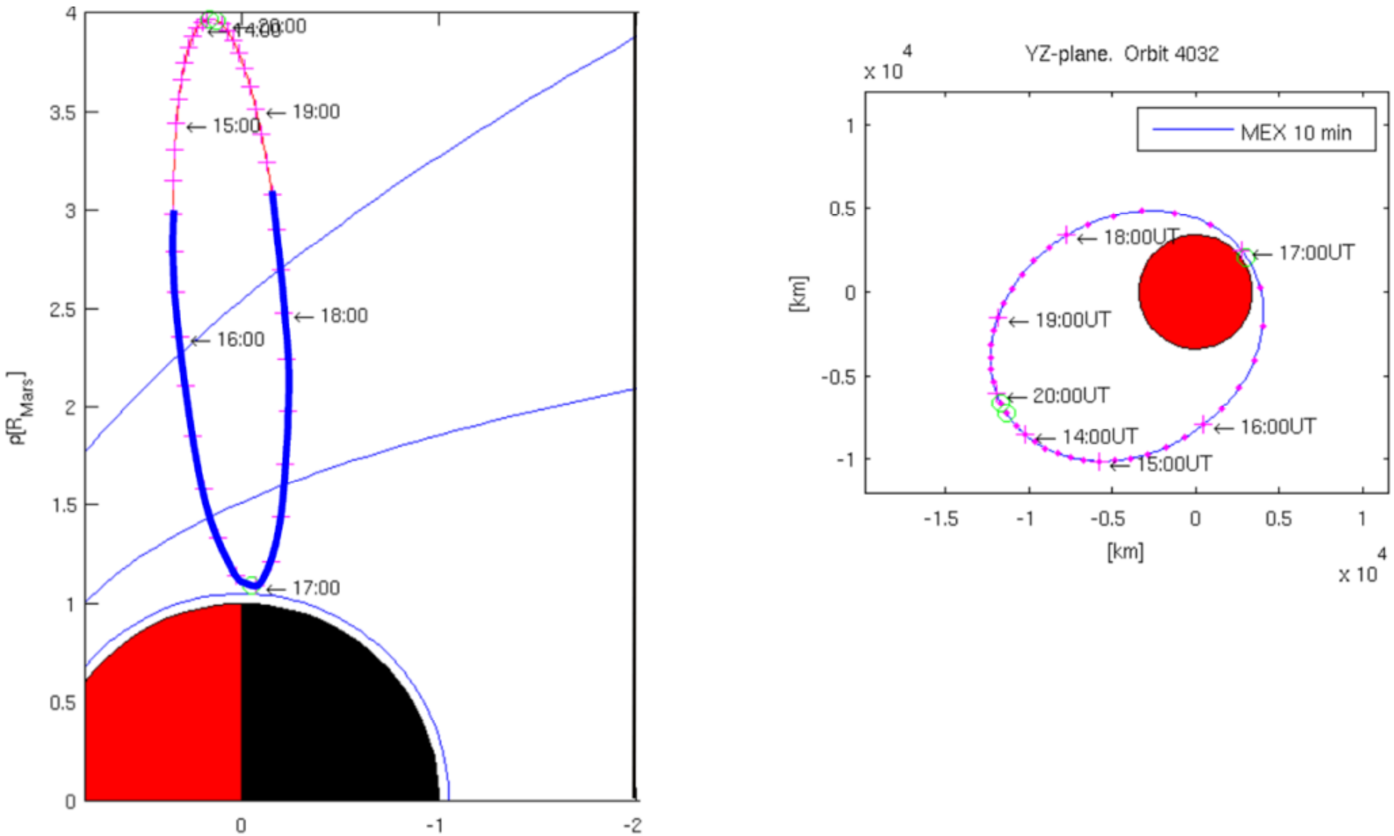

Trajectory of the Mars Express spacecraft in orbit 4032 by the north polar region of the Mars ionosphere traced in cylindrical coordinates (left panel) and on the plane transverse to the sun-Mars axis (right panel).

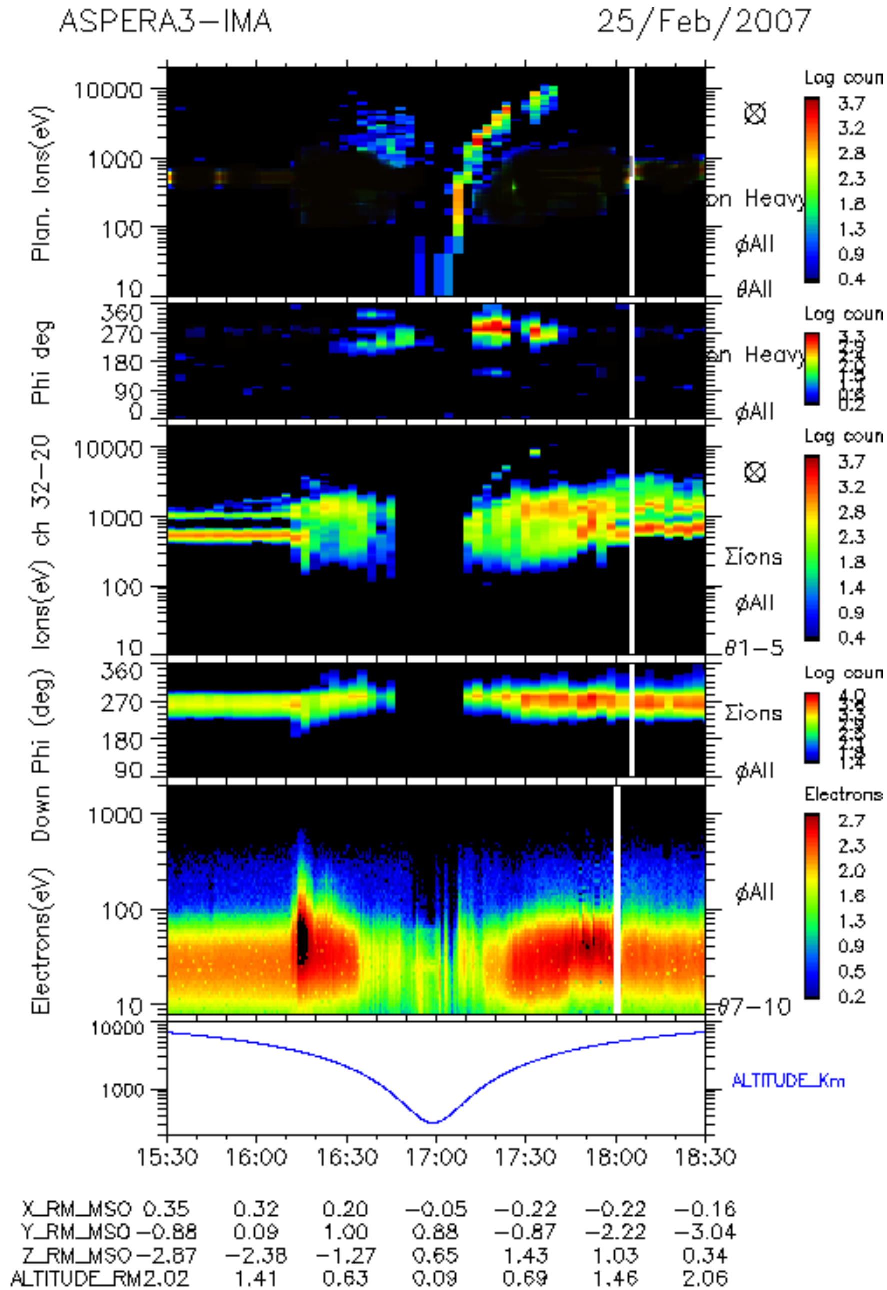

ASPERA3-IMA
25/Feb/2007
Plan. Ions(eV)
Phi deg
Ions(eV) ch 32-20
Down Phi (deg)
Electrons(eV)
Log coun
Electrons
on Heavy
φAll
θAll
Σions
θ1-5
θ7-10
ALTITUDE_Km
15:30
16:00
16:30
17:00
17:30
18:00
18:30
X_RM_MSO 0.35 0.32 0.20 −0.05 −0.22 −0.22 −0.16
Y_RM_MSO −0.88 0.09 1.00 0.88 −0.87 −2.22 −3.04
Z_RM_MSO −2.87 −2.38 −1.27 0.65 1.43 1.03 0.34
ALTITUDE_RM 2.02 1.41 0.63 0.09 0.69 1.46 2.06

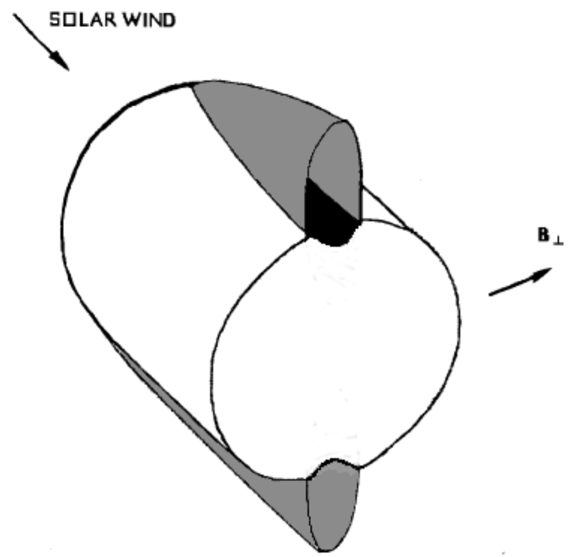

Schematic diagram representing a region around the Mars nightside ionosphere describing ionospheric plasma that has been eroded from the magnetic polar regions and is distributed with a velocity component directed away from the Mars wake

K. Dennerl et al., 2006

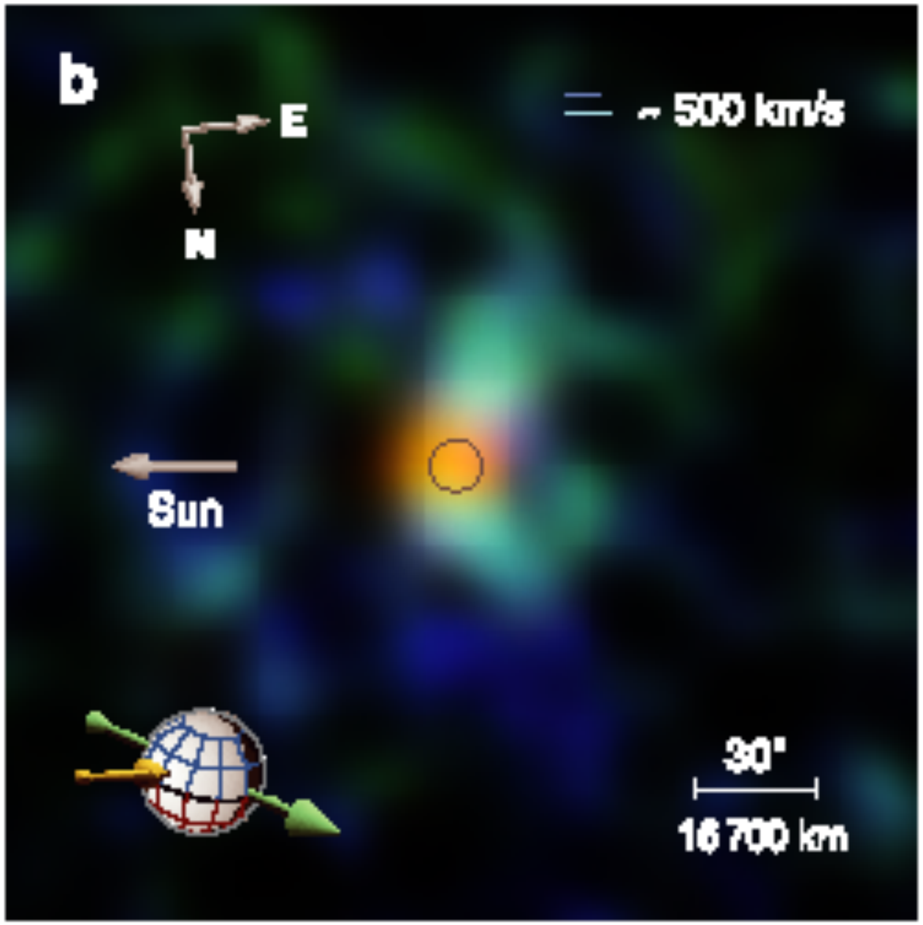

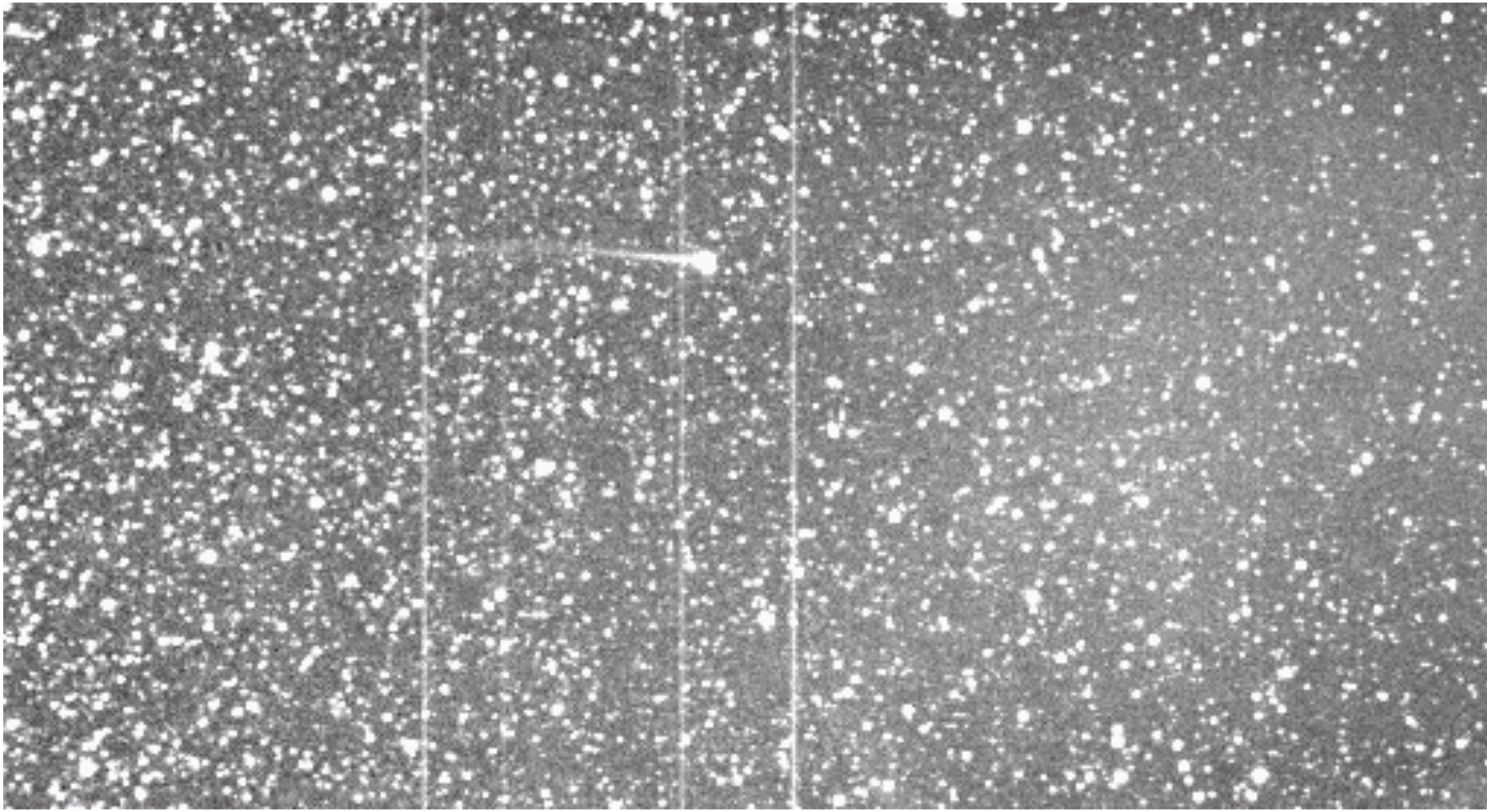

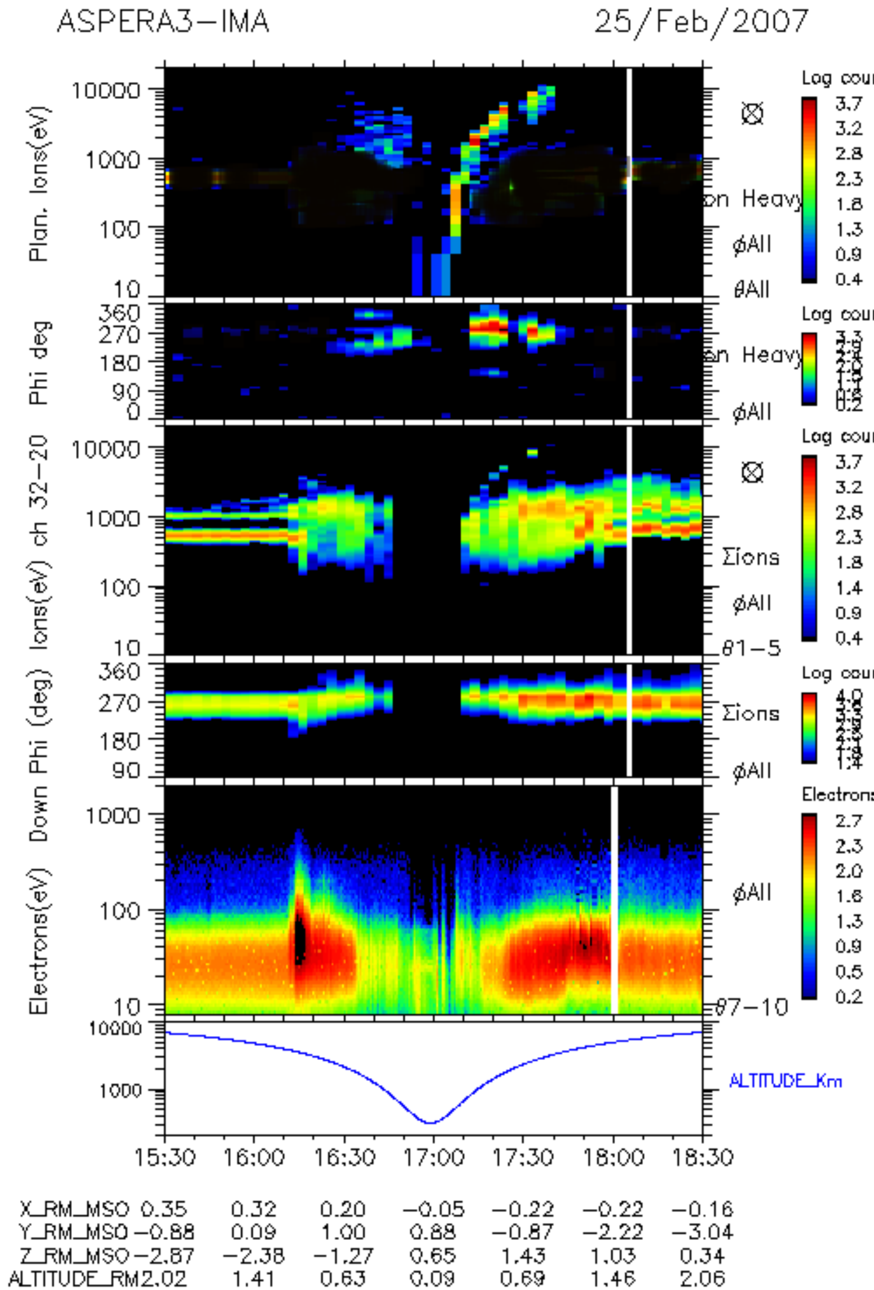
ASPERA3−IMA
25/Feb/2007
Plan. Ions(eV)
Phi deg
Ions(eV) ch 32−20
Down Phi (deg)
Electrons(eV)
Log coun
Electrons
on Heavy
ΦAll
θAll
Σions
θ1−5
θ7−10
ALTITUDE_Km
15:30
16:00
16:30
17:00
17:30
18:00
18:30
X_RM_MSO 0.35 0.32 0.20 −0.05 −0.22 −0.22 −0.16
Y_RM_MSO −0.88 0.09 1.00 0.88 −0.87 −2.22 −3.04
Z_RM_MSO −2.87 −2.38 −1.27 0.65 1.43 1.03 0.34
ALTITUDE_RM 2.02 1.41 0.63 0.09 0.69 1.46 2.06

MARS EXPRESS

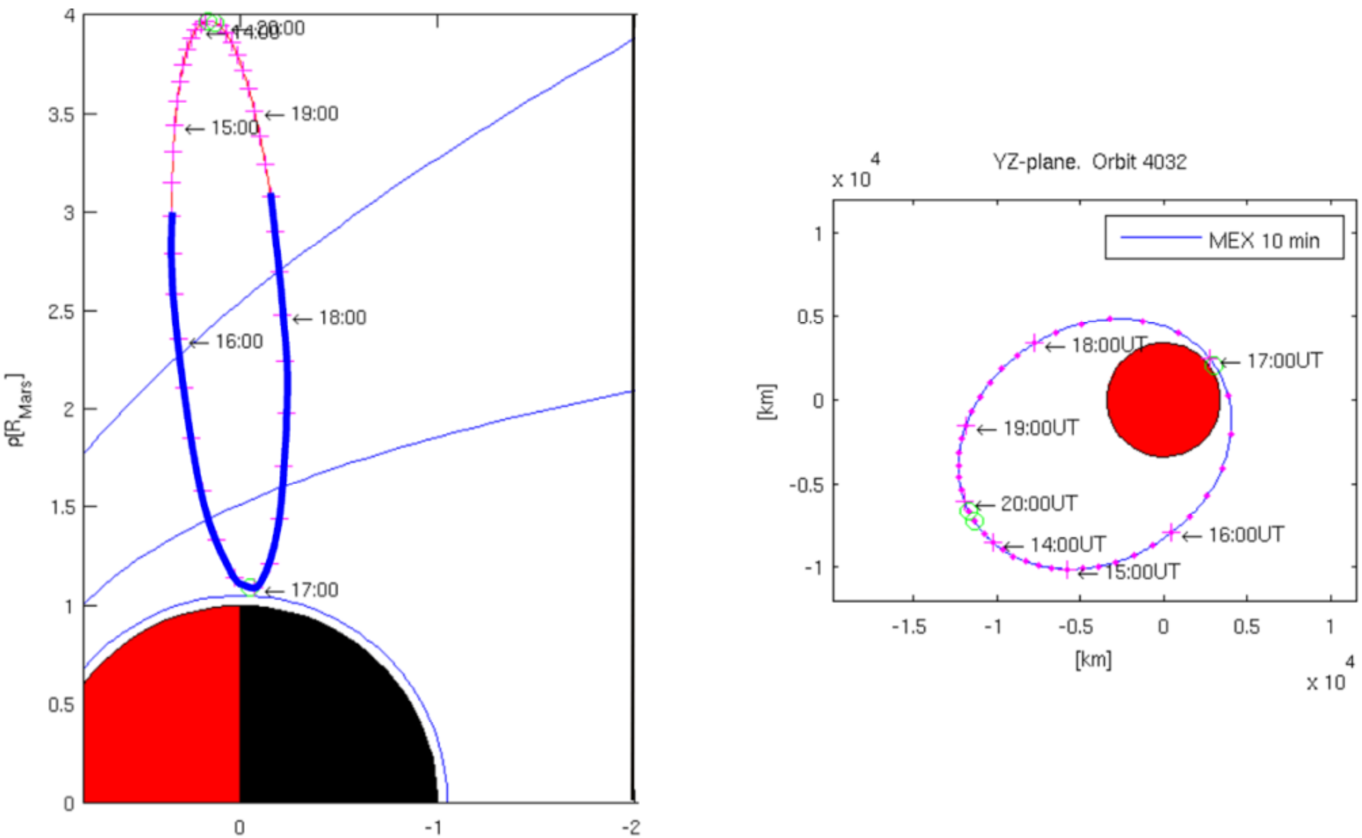

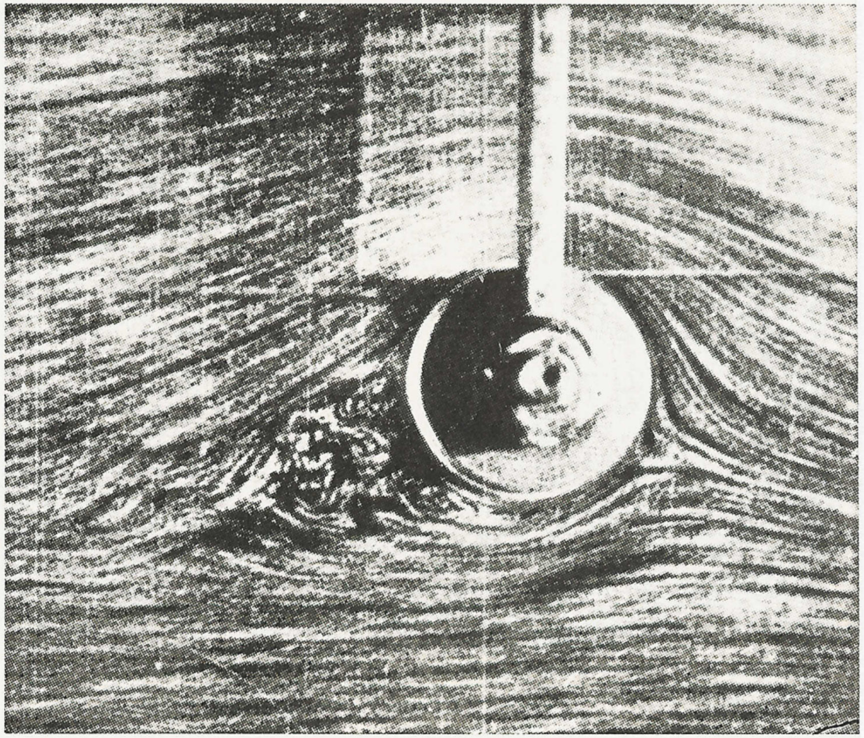

$a\Omega/U = 2$

Perfil de presión
(G. A. Landis, Jan. 2002)

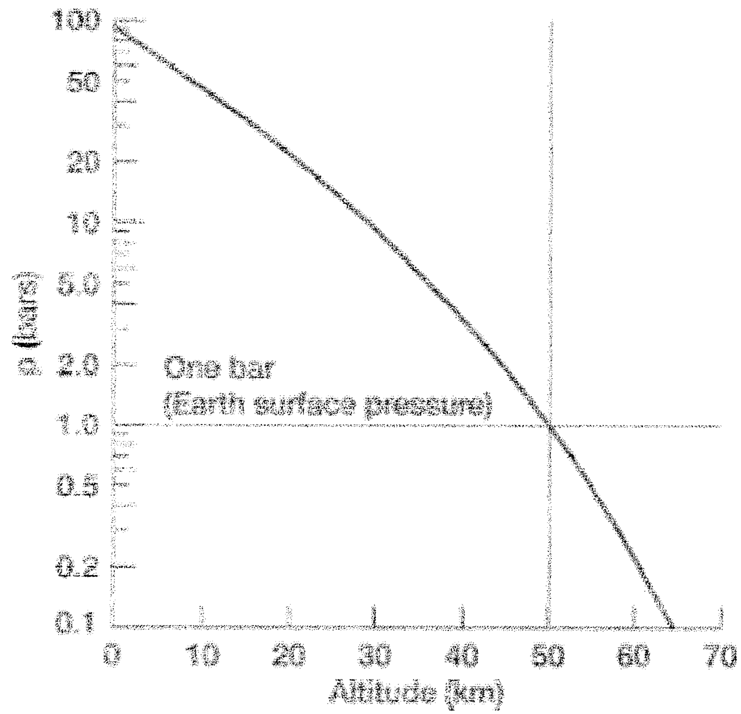

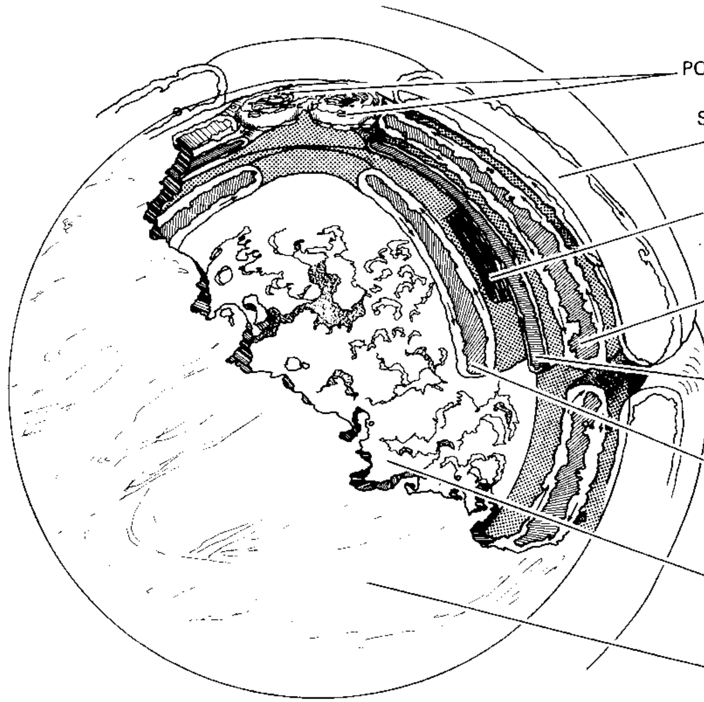

Figure 6-23. A possible pattern for the meridional circulation in the atmosphere of Venus.

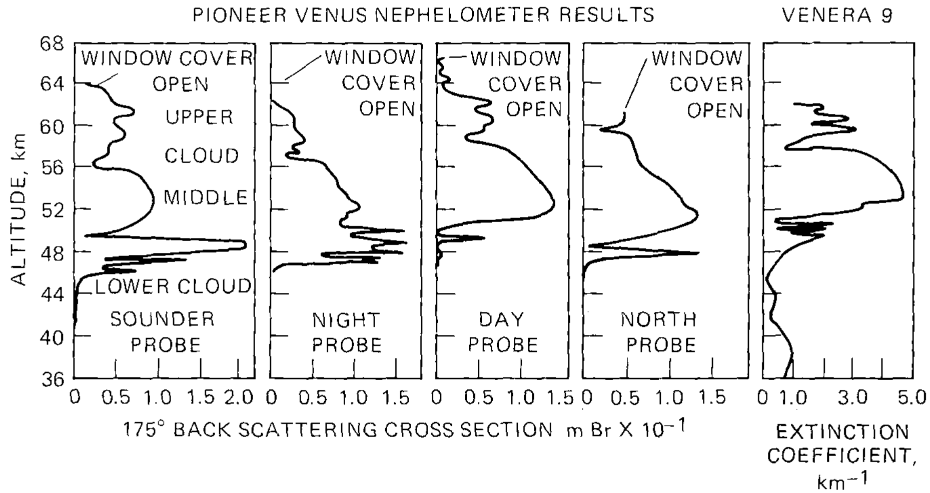

TABLE 6-1.– SUMMARY OF CHARACTERISTICS OF VENUS CLOUDS

Region	Altitude, km	Temperature, °C	Refraction index	Composition	Diameter, μm
Upper haze	90.0-70.0	-83 to -48	1.45	sulfuric acid + contaminants	0.4
Upper cloud	70.0-56.5	-48 to 13	1.44	sulfuric acid + contaminants	0.4, 2.0 (bimodal)
Middle cloud	56.5-50.5	13 to 72	1.42 1.38	sulfuric acid + contaminants + crystals	0.3, 2.5, 7.0 (trimodal)
Lower cloud	50.5-47.5	72 to 94	1.32	sulfuric acid + contaminants + crystals	0.4, 2.0, 8.0 (trimodal)
Layers	47.5-46.0	94 to 105	1.46 1.50	sulfuric acid + contaminants	0.3, 2.0 (bimodal)
Lower haze	47.5-31.0	94 to 209	---	sulfuric acid + contaminants	0.2

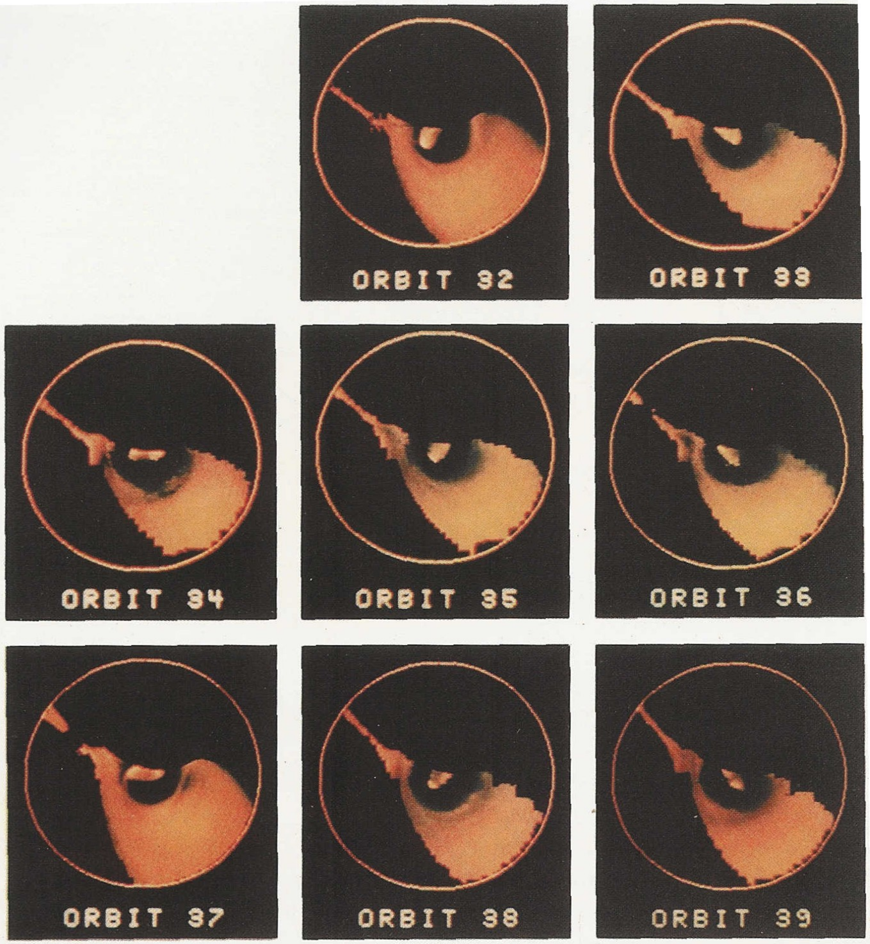

Figure 6-18. Eight consecutive polar stereographs of Venus' northern hemisphere taken at 11.5 μm. These images were taken one each day on orbits 32 through 39 (January 5 through 12, 1979). The north pole is at the center of each image and the equator is the outer boundary with the noon point at the bottom. Note that the polar dipole returns to approximately the same position in a period of three days.

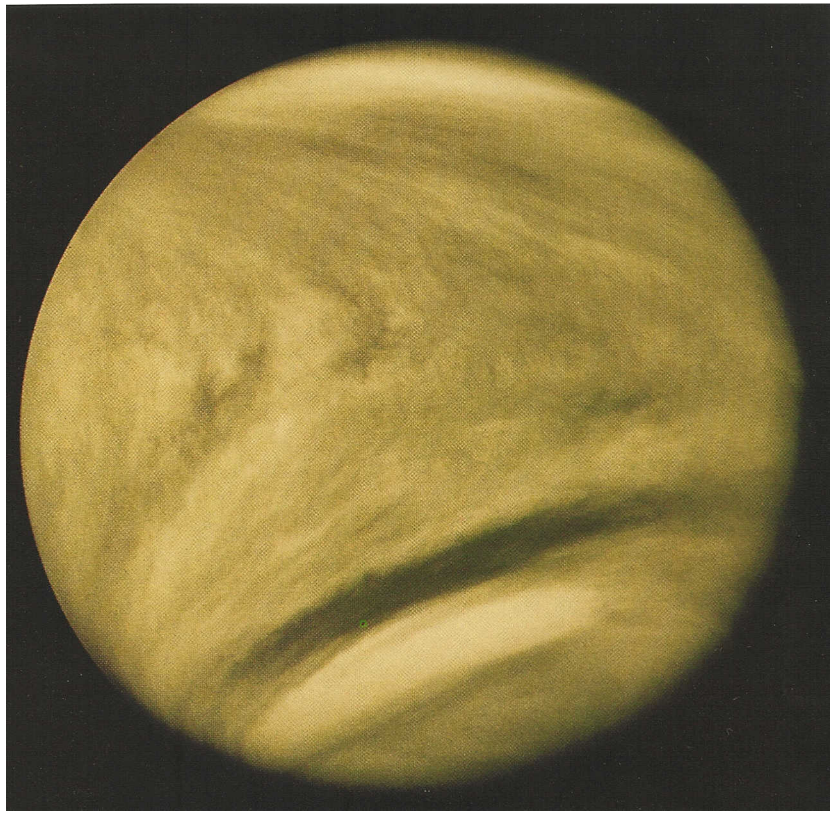

ANGULAR KINETIC ENERGY (~10^{30} Joules) = $Mv^2/2$

v = translational velocity (v = 30 km/s)
M = mass (if M = 5 10^{24} kg, $\rho^* \sim 10^{20}$ cm^{-3})

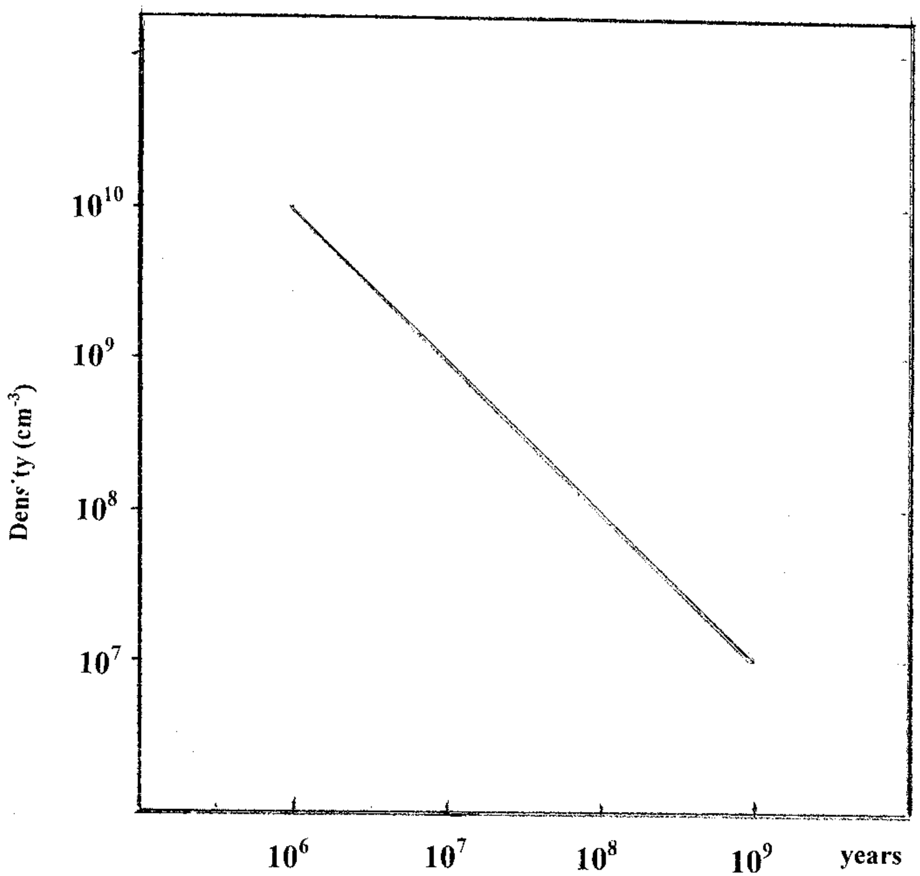

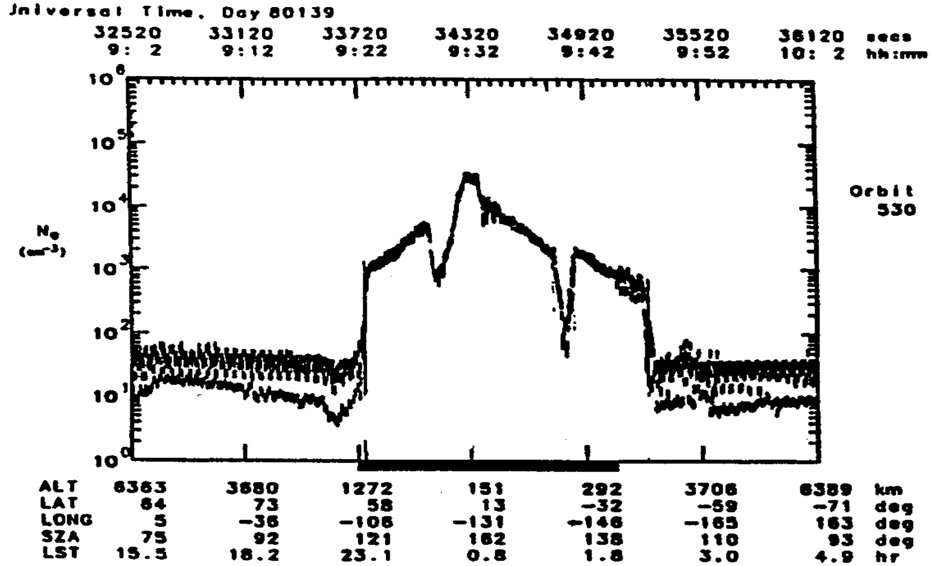
Universal Time, Day 80139
32520 33120 33720 34320 34920 35520 36120 secs
9: 2 9:12 9:22 9:32 9:42 9:52 10: 2 hh:mm
Ne (cm⁻³)
Orbit 530
ALT 6363 3680 1272 151 292 3706 6389 km
LAT 84 73 58 13 -32 -59 -71 deg
LONG 5 -36 -106 -131 -146 -165 163 deg
SZA 75 92 121 162 138 110 93 deg
LST 15.5 18.2 23.1 0.8 1.8 3.0 4.9 hr

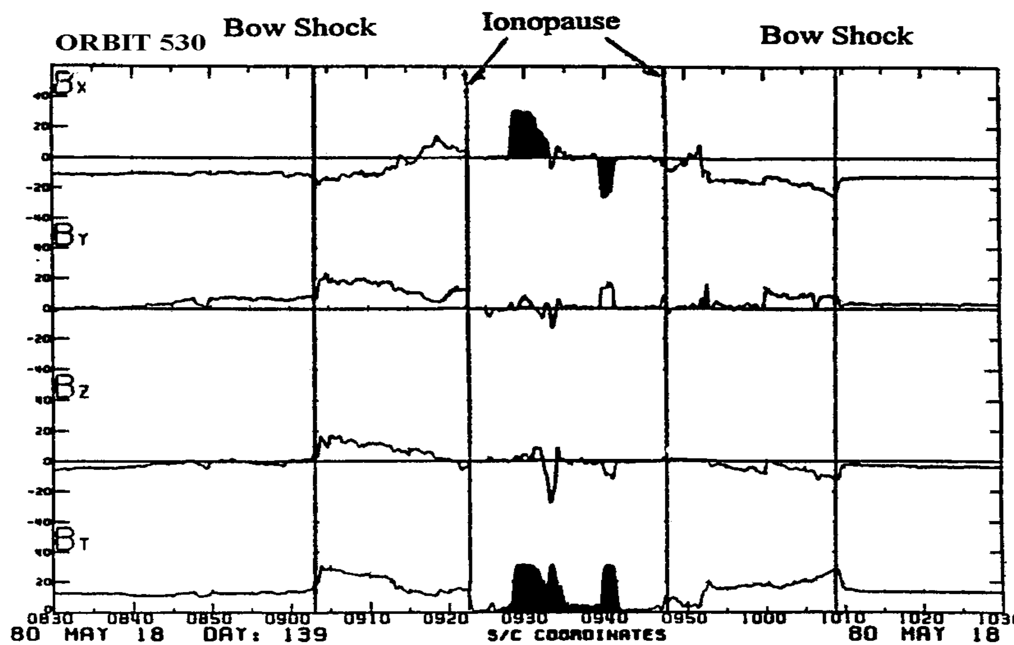
ORBIT 530
Bow Shock
Ionopause
Bow Shock
Bx
By
Bz
BT
0830 0840 0850 0900 0910 0920 0930 0940 0950 1000 1010 1020 1030
80 MAY 18 DAY: 139
S/C COORDINATES
80 MAY 18

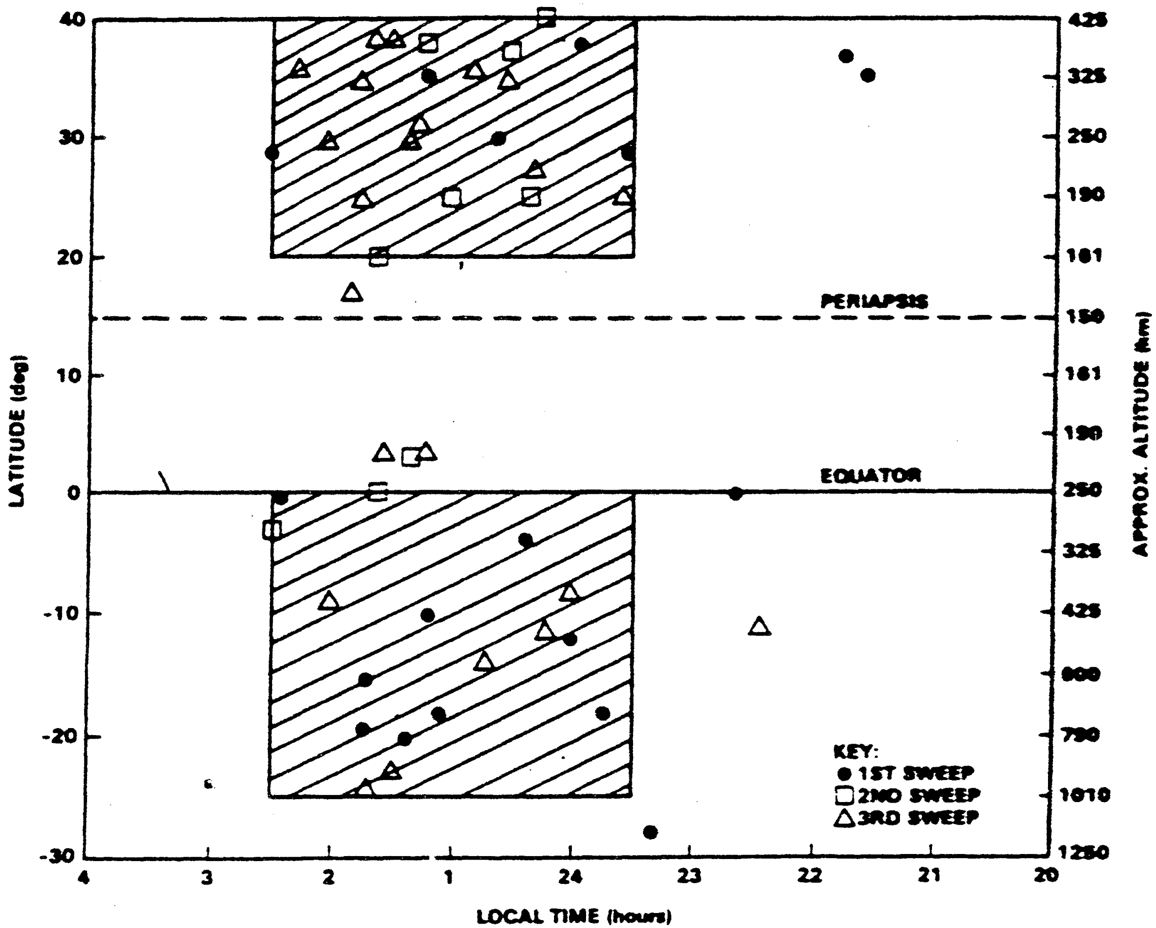
40
30
20
10
0
-10
-20
-30
LATITUDE (deg)
425
325
250
190
161
150
161
190
250
325
425
600
790
1010
1250
APPROX. ALTITUDE (km)
PERIAPSIS
EQUATOR
KEY:
1ST SWEEP
2ND SWEEP
3RD SWEEP
4
3
2
1
24
23
22
21
20
LOCAL TIME (hours)

DESPLAZAMIENTO DE LAS NUBES DE PLASMA

(Fuerzas de presión magnética y presión cinética)

Ec. de momento: $\rho_{sw}(U_{sw} \cdot \nabla)\ U_{sw} = (B_{sw} \cdot \nabla)\ B_{sw}/\mu_e - \nabla(B_{sw}^2/2\mu_e) + \rho_{sw}\ \nu\ \nabla^2\ U_{sw}$

Ec. de momento en forma no-dimensional: $\rho_{sw}\ U_{sw}^2 \sim \rho_{sw}\ U_{sw}^2\ [(V_A/U_{sw})^2/2 + (L/\delta)^2/R]$

$U_{sw}/V_A = M_A$ es el número de Mach de Alfven [$V_A = B_{sw}/(\mu_e\ \rho_{sw})^{1/2}$ es la velocidad de Alfven]
(M_A es el cociente de la densidad de energía cinética a la densidad de energía magnética)

$R = U_{sw}L/\nu$ es el número de Reynolds (L es la distancia efectiva de la región de flujo viscoso)
δ es el ancho de la capa límite de velocidad

Usando: $300\ km/s < U_{sw} < 500\ km/s$ $n_{sw} \sim 2\ cm^{-3}$ $B_{sw} \cong 10\ nT$

Se encuentra: $1 < M_A < 3$ (densidad de energía magnética < densidad de energía cinética)

MAGNUS EFFECT

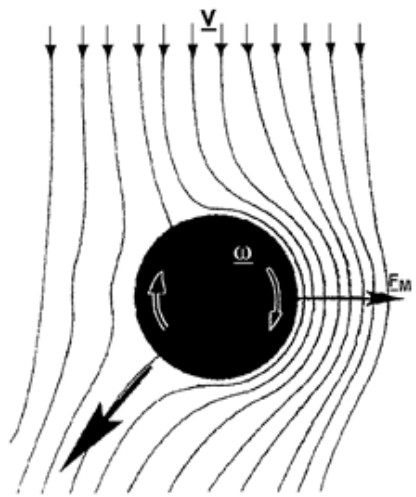

BERNOULLI'S EQ: $P + \rho V^2/2 = cst$

MAGNUS FORCE: $\underline{F}_M = C_M\, r^3\, \rho \underline{V} \times \underline{\omega}$

Shefer et al. 1979

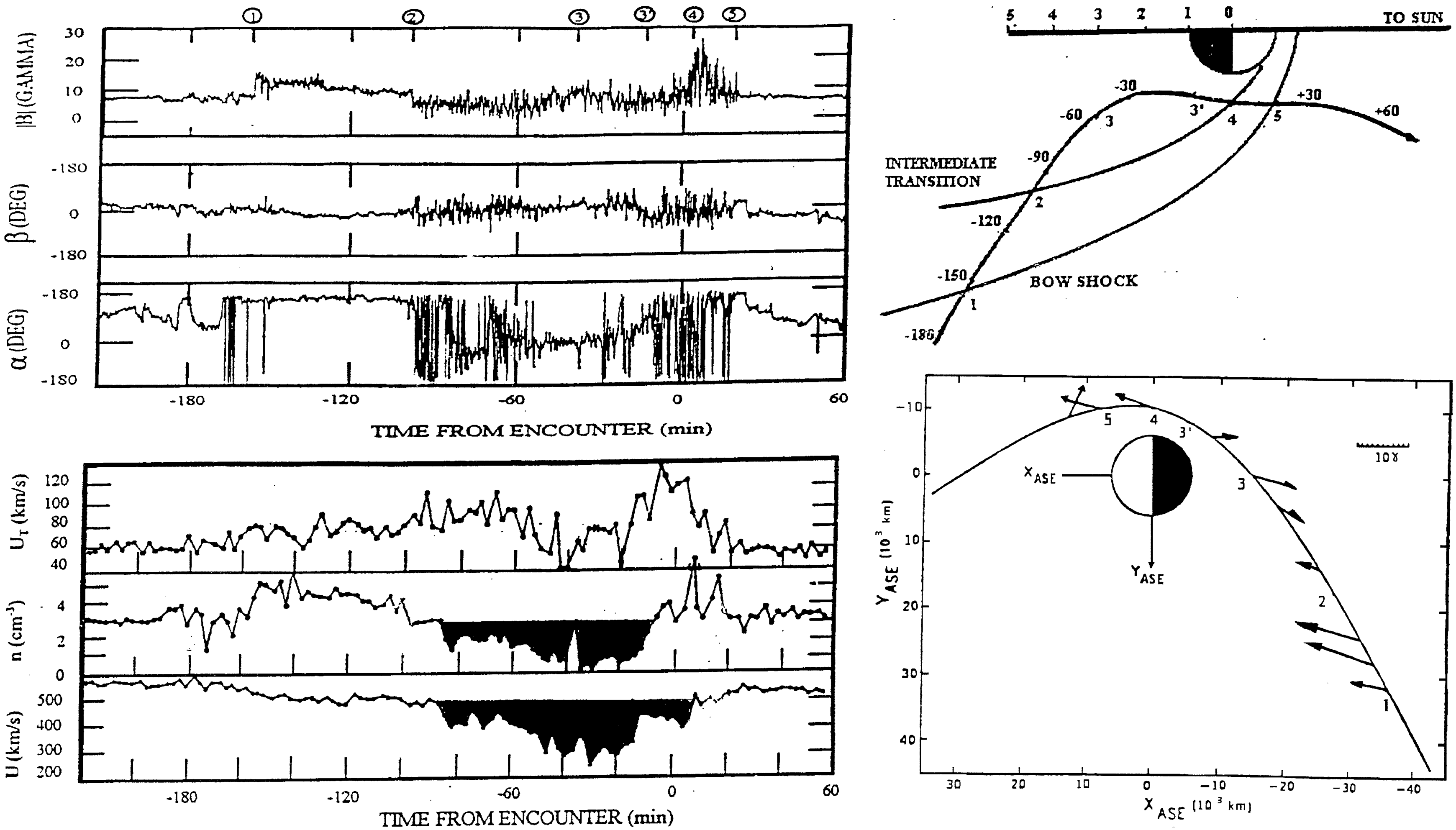

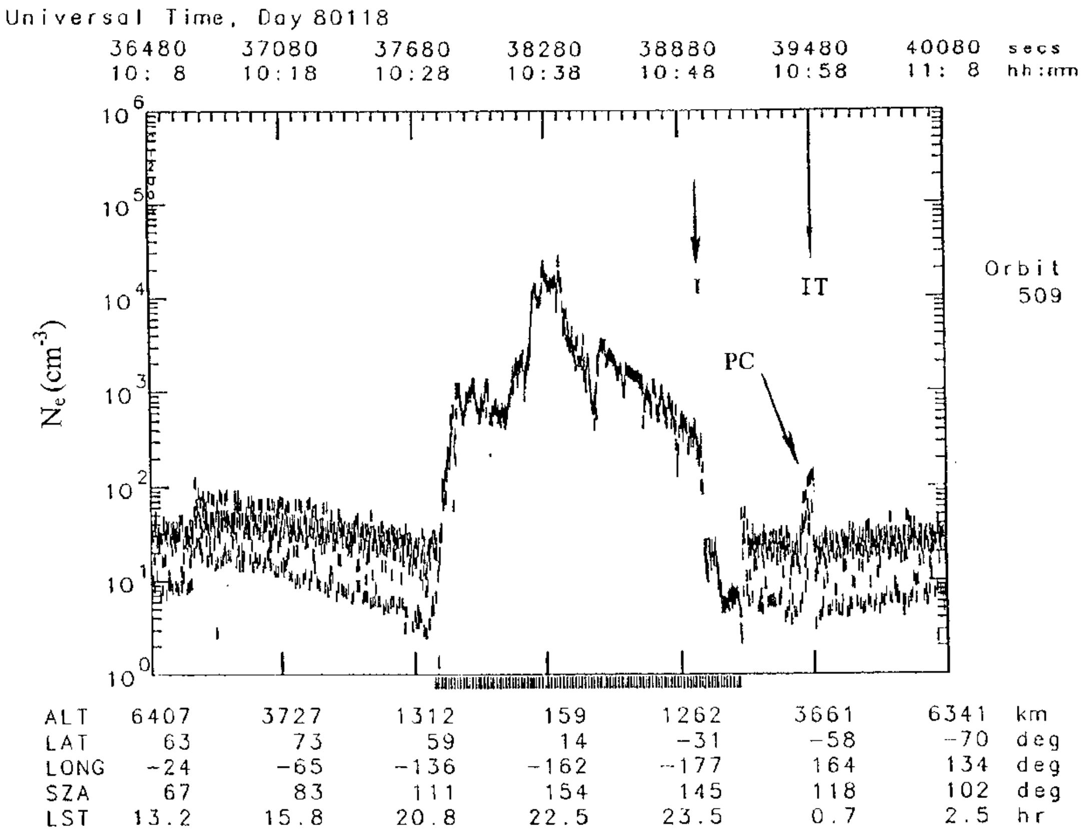

Universal Time, Day 80118
36480 37080 37680 38280 38880 39480 40080 secs
10: 8 10:18 10:28 10:38 10:48 10:58 11: 8 hh:mm
N_e (cm^{-3})
10^6
10^5
10^4
10^3
10^2
10^1
10^0
I
IT
PC
Orbit 509
ALT 6407 3727 1312 159 1262 3661 6341 km
LAT 63 73 59 14 -31 -58 -70 deg
LONG -24 -65 -136 -162 -177 164 134 deg
SZA 67 83 111 154 145 118 102 deg
LST 13.2 15.8 20.8 22.5 23.5 0.7 2.5 hr

Miller and Whitten, 1991

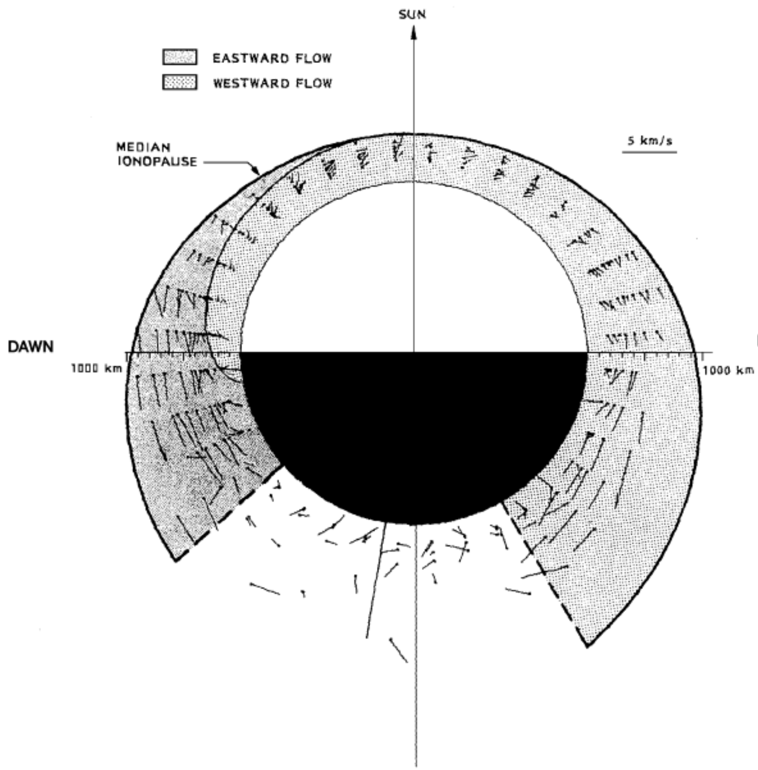

Pérez-de-Tejada, 2006

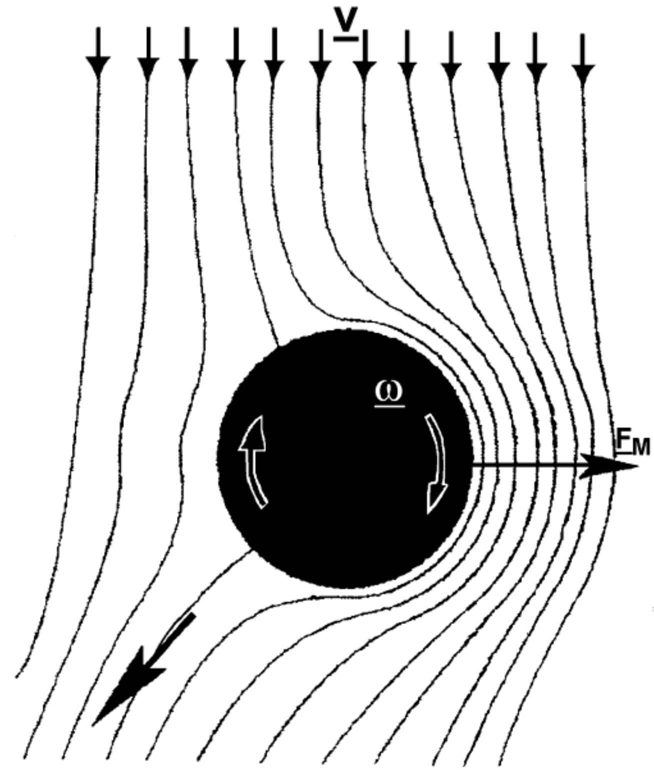

Magnus Force Eq: $F_M = C_M (r_2{}^3 - r_1{}^3)\, \rho\, V_i\, \omega$ **Bernoulli´s Eq:** $P + \rho V^2/2 = cst$

Dawn-Dusk Displacement: $D = A\, \zeta^2/2 = (F_M/M)[\pi\, r^2/2\, /V_i]^2/2$

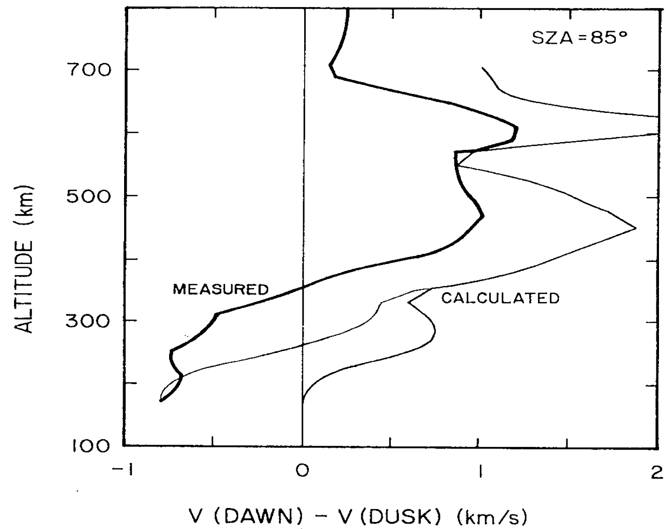

Fig. 16. Differences between average nightward velocity at the dawn and dust terminators. The heavy line is the measured difference at 85° SZA. The light line is the calculated difference based on the momentum equation. The line joining the two curves below 400 km altitude is the calculated difference assuming a 400 m s^{-1} superrotation of the neutral atmosphere (after Miller and Knudsen, 1987).

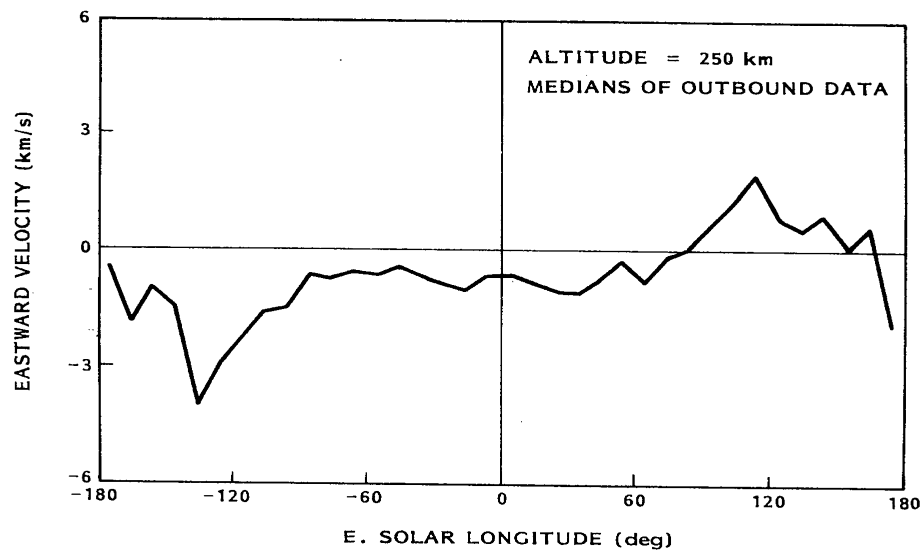

Fig. 14. Average eastward component of the O^+ velocity at 250 km altitude (after Miller and Knudsen, 1987).

ROTATIONAL ENERGY TRANSLATIONAL ENERGY

$$I\,\omega^2/2 = mv^2/2$$

I = moment of inertia
ω = angular velocity (T = 24 hours)
v = translational velocity (v = 30 km/s)
m = mass ($\rho^* \sim 10^{20}$ cm^{-3} if M = 5 10^{24} kg)

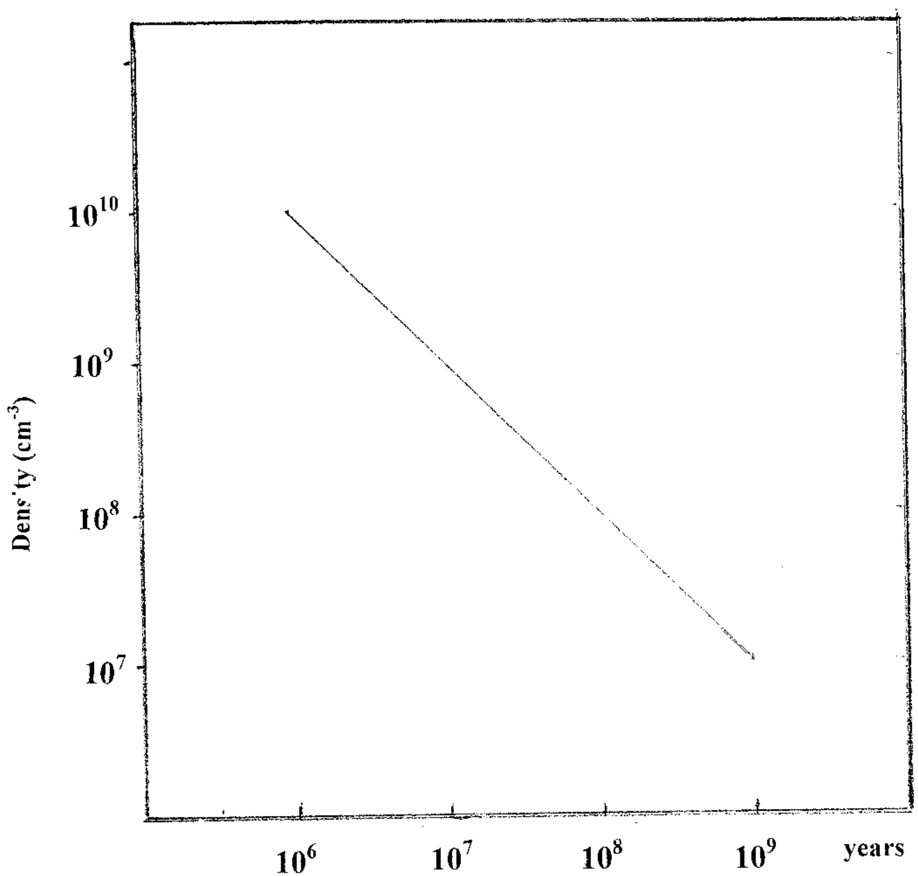

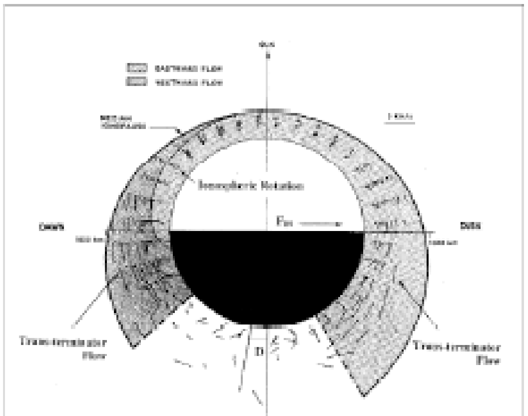

Figure 1: Anti -Sunward O^+ velocity averages in the trans-terminator flow measured in the Venus ionosphere with the ORPA instrument of the PVO. As a result of the super-rotation motion of the Venus atmosphere/ionosphere ¨dawn¨ occurs in the +Y solar ecliptic direction.

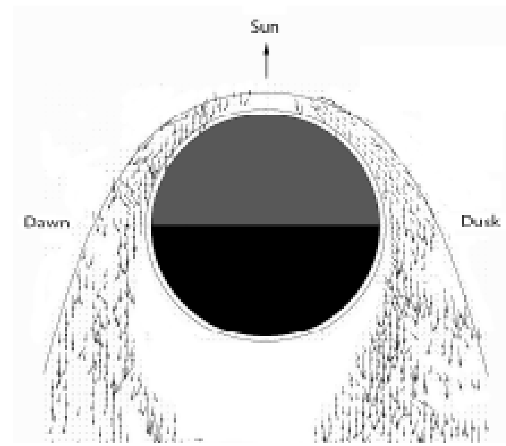

Figure 2: <200 eV O^+ flow near Mars measured by the ASPERA-3 experiment on MEX.